A CHEMICAL AND MECHANICAL EVALUATION OF INTERFACIAL FRACTURE IN DICYANDIAMIDE CURED EPOXY/STEEL ADHESIVE SYSTEMS

by

Mark A. Vrana

A dissertation in partial fulfillment of
the requirements for the degree of

DOCTOR OF PHILOSOPHY
IN
MATERIALS ENGINEERING SCIENCE

VIRGINIA POLYTECHNIC INSTITUTE &
STATE UNIVERSITY

APPROVED:

Dr. Thomas C. Ward, Chairman

Dr. David A. Dillard

Dr. John G. Dillard

Dr. Hervé Marand

Dr. James P. Wightman

July 1995
Blacksburg, Virginia

Key Words: Dicyandiamide, Epoxy, Interfacial Fracture, Double Cantilever Beam, XPS

c.2

A CHEMICAL AND MECHANICAL EVALUATION OF INTERFACIAL FRACTURE IN DICYANDIAMIDE CURED EPOXY/STEEL ADHESIVE SYSTEMS

by

Mark A. Vrana

Materials Engineering Science Program

Abstract

The interfacial fracture performance of dicyandiamide cured epoxy/steel adhesive systems was thoroughly investigated. Fracture mechanics based testing was utilized to study several variables which were believed to influence the epoxy/steel interphase region, specifically the elasomeric toughener concentration, the dicyandiamide concentration, and the cure temperature. Bulk mechanical measurements were conducted to provide background information for comparison with the fracture data, and surface analyses were carried out on the neat adhesives and failed fracture specimens to provide insight into the locus and causes of failure.

The addition of toughener drastically impacted the morphological, bulk mechanical, and adhesive properties in these latent cure systems. Modulus values decreased and bulk fracture toughness values increased with increasing toughener content. Static double cantilever beam (DCB), fatigue DCB, and notched coating adhesion (NCA) interfacial fracture performances all increased. X-ray photoelectron spectroscopy (XPS) and tunneling electron microscopy (TEM) analyses of the failed specimens revealed that chemical changes were more prominent at the epoxy/steel interphase than in the bulk of the materials. Morphological variations were also apparent with toughener level variations, but for a single formulation no differences between the bulk and intephase morphologies were seen.

Evaluations were conducted on a series of elastomer modified model epoxy formulations cured with varying amounts of dicyandiamide. The modulus and bulk fracture toughness values were shown to be independent of dicyandiamide concentration, whereas the adhesive performance was greatly influenced. For increases in the concentration of dicyandiamide, single lap shear (SLS) failure strength values increased while quasi-static DCB and NCA test performances decreased. Fatigue DCB results showed improved adhesive performance at both high and low levels of dicyandiamide content. The results of the failure surface evaluations suggest that dicyandiamide variations produce significant chemical changes only in the epoxy/steel interphase region, and not in the bulk.

Analyses were conducted on all of the above systems using two additional cure temperatures. The purpose of this work was to alter the dicyandiamide solubility, and possibly the dicy/epoxy reaction mechanisms, and to determine what influence these changes had on the interfacial fracture performance. In general it was found that performance increased as the cure temperature was increased.

Acknowledgments

There are many people whom I should acknowledge and thank for help with this research project. First and foremost, I thank my research advisor, Professor Thomas C. Ward, for his support and guidance. You are a truly impressive educator and scientist, and I am very proud to be able to say that I studied in your research group at VPI & SU.

I would like to thank my graduate committee, as well, for their generosity. Dr. David A. Dillard, Dr. John G. Dillard, Dr. Hervé Marand, and Dr. James P. Wightman, the sacrifice of your time is greatly appreciated.

Without financial support, none of this work would have been possible. I would like to give a special thank you to The Center for Adhesive and Sealant Science at VPI & SU, and to the Adhesive and Sealant Council, Inc., for nearly five years of graduate student support. The services you provide to both graduate students and the adhesion science community should be commended. Being involved with CASS greatly enhanced the quality of my experience at VPI.

Thanks are given to The Dow Chemical Company for partial financial support of this research, and for providing an internship opportunity. The time spent in Midland, MI, at the Central Research Advanced Polymeric Systems Laboratory, provided me with something most graduate students never get--a highly positive research experience in an industrial setting.

I would like to thank the staff of the Physics Shop in Robeson Hall; in particular Mr. Fred Blair, Mr. John Miller, and Mr. Melvin Shaver. Your expertise in the field of metals, and your tremendous generosity, have no doubt saved me much time (years?) in completing my studies. It was a real pleasure having the opportunity to work with you, and more importantly, to get to know you as friends. Your friendship (and comic relief) have, at times, been my only source of escape from the stresses of school.

There have been several graduate students directly involved in this work. In particular, thanks must be given to Mr. Dwayne Rakestraw and Mr. Tsunou Chang, both

with The Department of Engineering Science and Mechanics, for help on the mechanics portions of this work.

Thanks are given to the PolyPKem research group for providing such an enjoyable work atmosphere. I made a lot of good friends during my stay at VPI, and I probably had more good times than I should have. To my fellow graduate, Dan Hahn, good luck with your new job and your career. To the remaining students, Dave Porter, Tony Williams, Rob Jensen, Kermit Kwan, Ojin Kwon, and Mark Muggli, hang in there. Your day is approaching faster than you realize.

Finally, I wish to acknowledge my family, to whom this dissertation is dedicated. You have all done so much I wouldn't know where to begin thanking you.

Table of Contents

List of Figures

List of Tables

List of Acronyms and Symbols

Dicy - dicyandiamide (a curing agent)

DCB - double cantilever beam fracture specimen

PDMU - 3-phenyl-1,1 dimethyl urea (a cure accelerator)

SENB - single-edge-notch bend specimen

SERR - strain energy release rate

SLS - single lap shear specimen

a - crack length

A - parameter used to characterize quasi-static failure rates

b - y-intercept of DCB compliance-crack length experimental data

B - width of the DCB and SENB specimens

C - specimen compliance

E - Young's modulus

$(EI)_{eff}$ - effective flexural rigidity of DCB specimens

f - fatigue test frequency

G - applied strain energy release rate

G_a - interfacial fracture energy at crack arrest

G_c - interfacial fracture energy at the onset of crack growth

G_{Ic} - plane-strain critical fracture energy for bulk polymers

h - thickness of adherends

I - moment of inertia

K_{Ic} - plane-strain critical stress-intensity factor for bulk polymers

m - slope of DCB compliance-crack length experimental data

N - number of fatigue cycles

P - applied load

RH - relative humidity

r_y - plastic yield zone radius at crack tip

t - time

T - temperature

U - energy

W - height of the SENB specimens

x - apparent crack length offset in DCB specimens

z - parameter used to characterize quasi-static failure rates

Δ - opening displacement of the DCB specimens

$\dot{\Delta}$ - crosshead displacement rate

ε_y - yield strain

ε_u - ultimate strain

ϕ - energy calibration factor for SENB specimens

ν - Poisson's ratio

σ_y - yield stress

σ_u - ultimate stress

Subscripts

a - refers to adhesive

max - maximum

s - refers to substrate (adherend)

Dedication

In loving memory of my Grandparents,
Mr. Milton C. Fry and **Mrs. Helen E. (Betty) Fry**.
The boundless love and pride you had for all your grandchildren
has been a tremendous source of inspiration in my life. I only wish you were
here to share in this success.

To my parents,
Mr. Kenneth P. Vrana and **Mrs. Nancy L. Vrana**.
I am so thankful that I was fortunate enough to grow up in a home where the value of education was understood and emphasized. I realize the sacrifices you made for me, and I thank you for everything. Without your love, guidance, encouragement, and emotional and financial support, I know I never could have advanced my education to this level. I hope you are proud of this work, because it is as much yours as mine.

To my sister,
Mrs. Valerie S. Alford.
During my years in school you were always there when I needed advice or encouragement, or most importantly, friendship. Through all of your thoughtful and generous gestures, from calls to letters to gifts, you contributed
more to this work than you'll ever understand.

To the love of my life,
Dr. Lisa M. Vogler.
Since the moment I met you my life has continually improved. You've had a profound influence on every aspect, not the least of which has been my educational goals. I know how fortunate I was to have your help during the final stages of my research and writing. Without your love, support, and constant encouragement, I never could have realized this accomplishment.

Introduction

1.1 Adhesives and Adhesion: Practical Concepts

1.1.1 The Evolution of Adhesives

Adhesives have been in existence and use for thousands of years, and records indicate that they have been produced on an industrial scale for approximately 300 years.[1] Most significant advancements in the science of adhesion and adhesives, however, have come along only in the last fifty years. The predominate reason for this is the fact that nearly all adhesives utilized in technologically demanding applications have been based on advanced synthetic polymers.[2] The birth of the modern structural adhesive, for example, can be traced back to approximately 1910 when phenol-formaldehyde resins were first introduced. Yet it wasn't until the 1940s, after high-strength, polymer-modified phenolics became available, that there was a significant interest in using them as structural bonding materials. A basic outline of the historical development of structural adhesives, including the emergence of several advanced polymeric materials, is given in Table 1.1.[1]

Since the 1940s, the advantages of using adhesives in structural applications have provided the impetus for a substantial amount of research and development work (see Section 1.1.6). New and improved polymeric materials have been synthesized, and a plethora of ancillary products such as hardeners, toughenners, and fillers have been identified. A great deal of effort has been expended, as well, on studying the more fundamental aspects of adhesion. With this wide array of starting materials, and with recent advances in the scientific understanding of adhesion, the adhesives industry has seen tremendous success in a highly diverse market. As stated by Zalucha, "The growing availability of a variety of new materials and significant advances in bonding technology have allowed people to routinely trust their lives and fortunes to adhesively joined constructions. The study and understanding of adhesives and the art and science of using them has never been more pertinent."[3]

Table 1.1 The historical development of structural adhesives (Ref. 1).

Date of Commercial Availability	Adhesive (Polymer)
1910	Phenol-formaldehyde
1930	Urea-formaldehyde
1940	Nitrile-phenolic
	Vinyl-phenolic
	Acrylic
	Polyurethane
1950	Epoxies
	Cyanoacrylates
	Anaerobics
1960	Polyimide
	Polybenzimidazole
	Polyquinoxaline
1970	Second-generation acrylic

1.1.2 The Classification of Adhesives

Individual adhesive materials are classified in many different ways. Films, pastes, and liquid one-component adhesives are examples of materials classified by their physical state. Those classified by chemical functionality include epoxies, urethanes, acrylics, and silicones. Chemical composition is also used as a classification basis, with 100% solids, water-bornes, and solvent-based adhesives as examples. Other categories for adhesive materials include those based on cure conditions (room temperature, elevated temperature, ultra-violet), end uses (structural adhesives, pressure sensitive adhesives), and adherends (wood adhesives).

The most generalized, yet often most useful, classifications for adhesives are based on the final application of the material. This system gives rise to three main classes of adhesives: structural, laminating, and pressure sensitive. A structural adhesive is the type of adhesive used "to form a permanent, load-bearing, joint between rigid, high strength substrates."[4] For these materials, the bonded area is typically small compared to the total surface area of the structure. The epoxy resins utilized in this dissertation are typical of structural adhesives.

In some situations, adhesives must be classified by their performance characteristics. Hybrid adhesives, such as rubber-toughened epoxies, for example, are considered to be high-performance. High-performance adhesives are capable of withstanding elevated loadings and are often durable even under severely aggressive environments. In contrast, natural glues, such as hide and fish glues, are not high-performance. These can bear only low to moderate loads and environments.

1.1.3 Adhesive Attributes and Functions

An adhesive, as defined by ASTM, is "a substance capable of holding materials together by surface attachment."[5] Sharpe expands this definition to include the fact that an adhesive is a substance capable of holding materials together in a *functional manner*.[6] Since an adhesive does not perform its function independent of the context in which it is used, this is an important addition to the definition. Adhesives are typically application

specific, as is evidenced by the fact that there is not a universal adhesive which works equally well in all applications.

Adhesives serve a variety of functions in typical applications. The major function, of course, is *mechanical fastening*. When used in this capacity, adhesives offer many advantages over traditional fasteners such as bolts, rivets, and welds. Adhesives allow stresses to be transmitted from one member of the system to another, and this distributes the applied loads uniformly across the entire structure rather than concentrating them at one point. Thus, adhesives can be used to produce assemblies that are mechanically equivalent to, or superior than, conventional assemblies. This is often accompanied, as well, by cost and weight benefits.[6] For instance, consider an assembly prepared from one piece of thick metal and one piece of thin metal. With an adhesive the full strength of the thin sheet is utilized. In a welded structure, only the portions contacting the welds contribute to the strength of the system. Also, thin metals are often not amenable to welding and conventional fastening. The use of adhesives generally promotes high strength and rigidity and does not result in any substrate distortion.

Along with the other mechanical benefits mentioned above, adhesives also function to *dampen vibrations* and *resist fatigue* damage. Consider the fact that helicopter rotor blades are now held together solely by adhesives. These structures are much more durable, and possess a greater load bearing ability, than their mechanically fastened counterparts. Adhesives also function in a few less obvious ways. If used properly, an adhesive should provide full contact with the adherend surfaces. Thus, it has the potential to act in a *sealing capacity*, provided it is not susceptible to degradation by the environment. Also, if the adhesive contains the appropriate additives, it can function as a *thermal or electrical insulator*. This is extremely useful, for instance, in preventing the electrochemical corrosion of assemblies of dissimilar metals.

Although there is an extremely large number of different adhesives currently available, each with its own characteristics, properties, and uses, there are several important attributes shared by all of them. These are summarized below:[3]

By surface attachment only, they must possess the ability to transmit and distribute applied loads among the assembly components (from substrate to substrate).

They must behave as a liquid during some portion of the bonding process in order to adequately wet the substrate surfaces.

They must be capable of carrying some continuous, possibly variable, load throughout their intended service life.

They must work well with the other assembly components to provide a durable product suitable for the intended service environment.

Of these attributes, the load-bearing ability and substrate wetting ability, in particular, help determine if, and how, an adhesive can be used.

1.1.4 The Adhesively Bonded System

In the discussion of adhesion and adhesives, common words are often used to describe specific concepts that may not be equivalent to their common meaning.[3] Therefore, it is necessary at this time to define the terminology used in preparing this dissertation. Unless otherwise noted, all of the nomenclature on adhesion and adhesives comes from ASTM D907-89.[5] There is, however, one definition worth specifically mentioning. An *adhesive system*, in this text, will be taken to mean an adhesive/steel combination, including all variables which may influence the mechanical behavior of the adhesive joint being analyzed. A schematic of a typical adhesive system, along with the considerations which must be made for each of the individual components of the system, is given in Figure 1.1.

The concept of an adhesive system is important since adhesion, in a practical sense, is not an intrinsic property of the adhesive or polymer.[3] Rather, it refers to the response of an adhesively bonded structure to deformation. While the structure may be discussed in terms of the individual components, such as the adhesive, adherends, cure conditions, surface pretreatments, and so on, the overall structural response to a

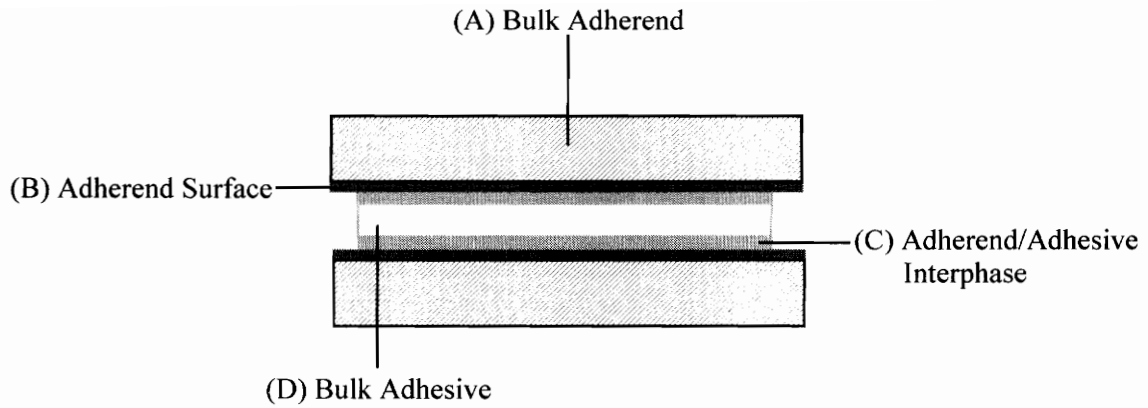

Considerations

(A) Composition, Chemical and Mechanical Properties, Environmental Conditions

(B) Composition, Contaminants, Chemical and Mechanical Properties, Structure

(C) Chemical/Mechanical Interactions (Mechanism of Adhesion), Voids and Residual Stresses, Energetics

(D) Chemical and Mechanical Properties, Cure Conditions, ,Environmental Conditions, Voids and Residual Stresses

Adhesive system performance is a function of A-D together with the details of structure geometry, fabrication, mechanical loading, and environmental conditions.

Figure 1.1 Schematic of a typical adhesive system with a summary of the general system considerations that should be included in any comprehensive adhesive performance evaluation.

deformation must be viewed in terms of the contributions made together by all of these components. In other words, adhesion science is a multidisciplinary effort which deals not only with the deformation and fracture of bulk materials and adhesive joints, but also with the chemistry and physics of surfaces and interfaces.[7]

1.1.5 The Adhesive Bonding Process

1.1.5.1 Adhesive Selection

With the variety of adhesives which are currently available, and considering the diversity of adhesive chemistries and forms, the process of selecting an adhesive for a specific application can seem overwhelming. According to Zalucha, the best approach is to start by considering what the material must do. Then work from that point.[3] By proceeding in this fashion, one is not limited to a specific chemistry or adhesive type and therefore has a better opportunity to select the most appropriate material for the application. Accordingly, this choice also includes consideration of the substrates and assembly process. To ensure selection of the appropriate adhesive, Sharpe suggests the use of a series of basic considerations, as shown below:

Specific Use and Function
What, specifically, will be done with the adhesive?
What is the intended function (fastening, insulating, etc.)?

Substrates and Joint Design
What are the substrates?
What is the specific geometry of the assembly?

Assembly Process
Exactly how will the system be assembled?
Specifically, how will the adhesive be applied?

Mechanical Requirements
What type and level of stresses (loads) will the assembly have to endure?
Will the adhesive have to hold permanently, or only temporarily?

Service Conditions

What are the maximum and minimum service temperatures?

What environments will the system be subjected to (water, solvents, etc.)?

1.1.5.2 Surface Considerations

Since adhesives function by surface attachment only, the properties of the substrate surfaces are of the utmost importance. The surface, unfortunately, often has a complex chemical composition which differs from the bulk substrate. In fact, if the surface has adsorbed environmental contamination, or if segregation of bulk constituents has occurred, it may have little in common with the bulk composition. These surface layers can be strongly or loosely bound, and can have cohesive strengths which range from low to high. They are not always homogeneous, and the inhomogeneities can lead to corrosion, weak bonds, and poor stress distributions. Due to this complex nature of the surface, it is often necessary to pretreat the substrates before the bonding process occurs. This pretreatment may be as simple as a solvent wipe or it may be a lengthy, complicated, chemical alteration. In either case, the surface pretreatment should remove adventitious surface layers and replace them with sound surface layers which are known to work well. Surface pretreatments for a variety of different substrates are discussed in the following paragraphs.

For *metals,* the minimum prebond treatment should be a solvent wipe or vapor degreasing. This treatment is also a prerequisite to more advanced surface preparations. It functions, generally, to remove surface contaminants such as grease and oil. It is an acceptable surface pretreatment only if the assembly is noncritical or will not be subjected to high stress levels or severe environmental conditions. It is important to understand, at this point, that initial joint strength is not an adequate indicator of joint durability. For example, joints which have received the minimal pretreatment described above often have equivalent initial breaking strengths when compared to joints which have received more advanced pretreatments. However, when exposed to severe service conditions they perform in an inferior fashion.

When necessary, metal surfaces can be significantly altered by immersion in one or more aqueous solutions, at room or elevated temperatures, after solvent degreasing. The aqueous solutions, typically, are strongly acidic and oxidizing, such as sulfuric acid/sodium dichromate, or strongly alkaline, like hypochlorite. The strongly acidic solutions are popular for altering the surface oxide structure of aluminum.

Ceramics and glasses are pretreated by immersion in a hot (60 °C) glass-cleaning solution. This is typically a mixture of aqueous sulfuric acid and sodium or potassium dichromate. After immersion, the parts are rinsed with water and dried. This pretreatment functions to remove organic contaminants.

Thermoplastic polymers are often very difficult to bond to. Thus, surface pretreatments are typically a necessity. One problem, however, is that the phenomena that inhibit adhesion also tend to inhibit the surface pretreatment. Some of these factors include migration of plasticizers, contamination by mold release agents, and the presence of antioxidants or other additives. For highly crystalline polyolefins, surface pretreatments include flaming the surface, subjecting it to "cold" plasma, subjecting it to a corona discharge, or immersing it in a glass-cleaning solution. These treatments alter both the chemical and mechanical properties of the polymer surface.

Thermoset polymers are much easier to pretreat and bond to than the thermoplastics. Usually all that is required is mechanical abrasion followed by a solvent wipe. The exceptions are silicone containing materials which require a "cold" plasma treatment. Sharpe reports that rather than using mechanical methods of abrasion, infrared and ultraviolet lasers have recently been utilized to ablate the thermoset surface.[6]

1.1.5.3 Joint Design

Joint design plays a major role in utilizing the advantages of adhesive bonding to the fullest extent. The basic principles are well-known and reported in the literature.[8-9] And although many standard configurations are available, the basic design criteria are the same regardless of the geometry.[10] These requirements are:

1. The bonded area should be maximized.
2. The bond should be stressed in its strongest direction (shear and tension).
3. Stresses in the weakest direction should be minimized (peel and cleavage).
4. Residual stresses, due to differential thermal coefficients of expansion, should be compensated for.

The initial design considerations require chemical and physical property information for the adhesive and adherends.[11] Furthermore, since the adhesively bonded structure is required to perform without failure, under the expected service conditions for the expected service lifetime, information on the long term chemical and physical properties is needed. This includes actual or predicted data such as environmental effects, fatigue performance, temperature and loading rate dependence, and aging effects.[11] Thus, an important part of the joint design effort is the test program. In an ideal situation, the adhesive system is first selected for its short term performance. Next, the program focuses on predictive methodologies to estimate the lifetime of the structure. Lastly, the entire product is assembled and tested, under the worst possible conditions, for the expected service lifetime. In most real development situations, the last stage is impractical since cost and speed are often major concerns.

To stay within the cost and time limitations, design engineers often utilize destructive testing methodologies. Unfortunately, these tests have the least predictive value. Consider, for example, the influence that creep can have on a system. This phenomenon would be overlooked in a typical destructive test. Also, combinations of low level stresses and environmental exposure can work synergistically. This is another phenomenon typically overlooked in standard destructive tests. For testing to be of any value in making predictions about assembly performance, it should mimic the real life conditions to the greatest possible extent. Cost/time considerations should be balanced carefully against the overall cost/liability considerations.

1.1.6 Advantages and Limitations of Adhesive Bonding

Many of the advantages, functions, and attributes associated with adhesives were briefly discussed in the previous sections of this dissertation. It is these factors, in general, that are responsible for the development and continual growth of the adhesives industry. Relatively little, however, was mentioned concerning the disadvantages of using adhesives. To ensure safe and effective adhesive bonding, serious consideration must be given to these limitations. A summary of the advantages and limitations of adhesive bonding is given in Table 1.2.

Table 1.2 The advantages and limitations of adhesive bonding (Ref. 6).

Advantages	Limitations
Ability to Join Dissimilar Materials	May Require Surface Pretreatments
Ability to Join Thin Sheet Materials	Upper Service Temperature Limited
Prevents Electrochemical Corrosion	Limited Ability to Join Thick Metals
More Uniform Distribution of Stresses	Few Non-Destructive Test Methods
Good Dynamic-Fatigue Resistance	May Require Heat/Pressure for Curing
Provides Smooth Contours	Rigid Process Control Often Necessary
Seals and Insulates	
Convenient, Cost-Effective	

1.2 Adhesives and Adhesion: Fundamental Concepts

1.2.1 Theories and Mechanisms of Adhesion

While the phenomenon of adhesion finds its main application in the area of bonding by adhesives, it is relevant as well in many other scientific disciplines. Adhesion is involved, in general, whenever solids are brought into contact.[12] Coatings, paints, varnishes, polymer blends, filled polymers, and composites are just a few examples. In all of these cases, material performance strongly depends on the quality of the interface, or interphase, formed between the components. Thus, the need to understand the adhesion phenomenon becomes apparent, even in practical applications.

If one works through a general description of the adhesive system, such as the one given in Section 1.1.4, it becomes obvious why basic studies of adhesion can quickly become confounded. The difficulties arise from the fact that adhesion can be approached with equal validity from molecular, microscopic, or macroscopic perspectives. In addition, it can be evaluated using macromolecular science, physical chemistry of surfaces and interphases, materials science, mechanics of fracture, and rheology. Therefore, depending on the discipline the scientist studies within, evaluation of the adhesion phenomenon can vary significantly. This becomes apparent when the theoretical models for adhesion are reviewed. Unfortunately, none of the individual theories can satisfactorily explain all aspects of the adhesion phenomenon.[13-15] Together they are both complementary and contradictory.[12] Six theories of adhesion are covered individually in Sections 1.2.1.1 through 1.2.1.6.:

1. Mechanical Interlocking
2. Electronic Theory
3. Theory of Boundary Layers and Interphases
4. Adsorption (Thermodynamic) Theory
5. Diffusion Theory
6. Chemical Bonding Theory

1.2.1.1 Mechanical Interlocking

Mechanical interlocking, unlike the other theories of adhesion, is based on the macroscopic scale. In fact, some argue that it is not a true theory of adhesion but simply a technological means of achieving adhesive bonding.[16] However, depending on the nature of the solids in contact, and depending on the conditions under which the bond is formed, the validity of this theory can be demonstrated.[12]

The mechanical interlocking theory, proposed by MacBain and Hopkins in 1925,[17] speculates that the most influential factor in determining adhesive bond strength is the mechanical keying of the adhesive into the cavities and pores of the solid surface. This was shown to be true by Borroff and Wake through their analysis of rubber and textile fabrics.[18] However, the fact that good adhesion can be established between two smooth surfaces leads researchers to the conclusion that mechanical interlocking cannot be universally true.

To address the inconsistencies in mechanical interlocking theory, Wake has proposed a model in which both interlocking and thermodynamics were accounted for.[19] In his model, the joint strength is given by G = (constant) x (mechanical keying) x (interfacial interactions). In practice, however, when the mechanical keying factor is improved, increases in adhesion are most often attributed simply to increases in the interfacial area due to surface roughness.[12]

Other scientists have investigated this concept as well and the conclusions remain generally consistent. Improved adhesion does not necessarily result from mechanical keying. Rather, it has been found that increases in surface roughness increase the ability of the system to viscoelastically or plastically dissipate energy around the crack tip and in the bulk of the material. This energy loss is often documented as the most significant component of adhesive system strength.[12]

1.2.1.2 Electronic Theory

Deryaguin and coworkers proposed the electronic theory of adhesion in 1948.[20] This work suggests that an electron transfer mechanism occurs between an adhesive and

substrate, differing in electronic band structures, to equalize the Fermi levels. A double electrical layer thus forms at the interface, and the resultant electrostatic forces contribute significantly to the adhesive bond strength. In essence, this theory views an adhesive/substrate interface as a capacitor that is charged due to the contact of two different materials. When the materials are separated, as happens during interfacial failure of the bond, the potential builds until a discharge occurs. The energy required to separate the interface, G_e, can therefore be related to the discharge potential, V_e, through the following expression:[20]

$$G_e = \frac{h\varepsilon_d}{8\pi}\left(\frac{\partial V_e}{\partial h}\right)^2 \qquad [1.1]$$

where h is the discharge distance and ε_d is the dielectric constant. And, except at very low pressures, this theory requires that the work of adhesion vary as a function of the pressure of the gas in which the fracture tests are conducted.

Deryaguin et al. measured the work of adhesion for several polymer/substrate interfaces, in argon and air, at various pressures.[20] Except at low pressures, they demonstrated a good correlation between the work of adhesion from theory and the experimental work of adhesion. There were, however, several major problems with this work. Firstly, when this work was repeated by Weidner, no correlation between peel strength of PSA tapes and the gas pressure was found.[21] Secondly, Wake has demonstrated that the determination of the parameters in the equation, and thus the determination of G_e, is circular.[22] And lastly, as with the studies of mechanical interlocking, this theory neglects to account for energy dissipated through the plastic and viscoelastic responses of the materials.[2]

1.2.1.3 Theory of Boundary Layers and Interphases

Bikerman is credited with introducing the theory of weak boundary layers (WBL). He has proposed that the cohesive strength of a WBL is always the controlling

factor in determining the adhesion of a system, even when the failure appears to be interfacial.[22] In other words, the adhesion energy, G, is always equal to the cohesive energy, G_c(WBL), of the weaker interfacial layer. Bikerman's theory is founded in the probability that fracture should never propagate only along the adhesive/substrate interface. Rather, it is more favorable for failure to occur within the weaker material near the interface.[12] Two main criticisms arise, however, concerning WBL theory. Firstly, it has been clearly shown that purely interfacial failure does occur in specific systems. Secondly, although cohesive failure occurs in the vicinity of the interface in at least one of the materials in contact, it is not always attributable to a WBL.[23-24]

This theory, while not demonstrating complete validity, did give rise to the concept of a thick interface, or *interphase*, a concept that has gained much attention in the field of adhesion science.[25] These interphases vary in thickness from a few angstroms to a few micrometers and are the result of various physical, physicochemical, and chemical phenomena. Several examples of the phenomena which result in interphase formation are given below:

1. Chemical groups and chain ends may orient, or overcrowd, to minimize the free energy of the interface.[26]

2. Additives and low molecular weight fractions may migrate to the interface.[27]

3. When the substrate can function as a nucleating agent, growth of a transcrystalline structure may occur.[28]

4. Through strong interactions with the substrate, chain mobility is lessened and a pseudoglassy zone forms.[29]

5. Thermodynamic or kinetic modification of polymerization, or cross-linking, at the interface occurs through adsorption or catalysis of reaction species.[30]

These interphases can have a profound effect on the strength of multicomponent systems. Thus, any truly comprehensive evaluation of adhesion performance must not neglect to compensate for their presence.

1.2.1.4 Adsorption (Thermodynamic) Theory

Sharpe and Schonhorn are generally credited with proposing the thermodynamic model of adhesion, and presently it is the most widely applicable theory in adhesion science.[31] It is based on the concept that adhesion occurs due to the establishment of interatomic and intermolecular forces at the interface, provided intimate contact between adhesive and adherend is achieved. These forces, typically, are van der Waals and Lewis acid-base interactions and their magnitude can usually be related to fundamental thermodynamic quantities such as the surface free energies of the adhesives and adherends.[12] The formation of an adhesively bonded system typically goes through a liquid-solid contact step, thus the criteria of good adhesion become the criteria of good wetting. However, as mentioned earlier, while this may be a necessary condition, it is not necessarily a sufficient one.

1.2.1.4.1 Wetting

For a solid-liquid system, wetting equilibrium can be quantitatively defined using the profile of a sessile drop on a planar solid surface.[12] This is represented schematically in Figure 1.2.

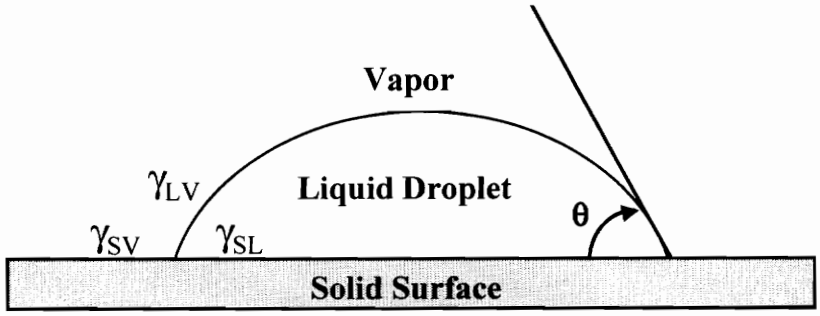

Figure 1.2 A sessile liquid droplet on a solid surface (Ref. 2).

Young's equation can be used to relate the surface tension, γ, to the equilibrium contact angle, θ, at the three-phase contact point. It is given by:[12]

$$\gamma_{SV} = \gamma_{SL} + \cos\theta\, \gamma_{LV} \qquad [1.2]$$

The subscripts S, L, and V refer, respectively, to the solid, liquid, and vapor phases. SV refers to the solid-vapor interface, SL refers to the solid-liquid interface, and LV refers to the liquid-vapor interface. The term γ_{SV} is used to represent the surface free energy of the substrate after equilibrium adsorption of vapor from the liquid. It is sometimes lower than the surface free energy of the solid, γ_S, in vacuum, and the difference in these values is the spreading pressure, Π_S, of the vapor onto the solid.[12] When the vapor obeys the ideal gas law, Π_S can be represented as follows:

$$\Pi_S = \gamma_S - \gamma_{SV} = RT \int_0^{P'} \Gamma\, d(\ln P) \qquad [1.3]$$

where P is the vapor pressure, P' is the equilibrium vapor pressure, R is the gas constant, T is the absolute temperature, and Γ is the surface concentration of adsorbed vapor. Thus, γ_S can be expressed as:[12]

$$\gamma_{SL} = \gamma_{SL} + \gamma_{LV} \cos\theta + \Pi_S \qquad [1.4]$$

When $\theta > 0$, the liquid does not spread onto the solid surface, but when $\theta = 0$, the liquid wets the solid completely and spreads spontaneously over the surface. Thus, the criteria for spontaneous wetting are:

$$\gamma_{SV} \geq \gamma_{SL} + \gamma_{LV} \qquad [1.5]$$

$$\gamma_S \geq \gamma_{SL} + \gamma_{LV} + \Pi_S \qquad [1.6]$$

These criteria may also be expressed using a parameter termed the equilibrium spreading coefficient, S, where:[12]

$$S = \gamma_{SV} - \gamma_{SL} - \gamma_{LV} \qquad [1.7]$$

$$S = \gamma_S - \gamma_{SL} - \gamma_{LV} - \Pi_S \qquad [1.8]$$

However, it should be noted that geometrical aspects or processing conditions, such as applied external pressure or surface roughness, are capable of restricting the validity of these criteria.

A more fundamental approach, leading to the other wetting criteria, is based on the analysis of the nature of the forces involved at the interface.[12] For low surface energy solids such as polymers, the thermodynamic surface free energy has been estimated from contact angle data. Zisman is credited with developing the first approach. He and his coworkers found that a linear relationship often exists between the surface tension, γ_{LV}, and the cosine of the contact angle, cos θ, of several liquids.[32] From this, Zisman has suggested the concept of the critical surface tension, γ_c. This value corresponds to the surface energy of an actual or hypothetical liquid that will spread on the solid surface to yield a contact angle of zero.

For solid-liquid systems, and accounting for Dupré's relationship, the adhesion energy, W_{SL}, can be defined as:

$$W_{SL} = \gamma_S + \gamma_{LV} - \gamma_{SL} = \gamma_{LV}(1 + \cos\theta) \qquad [1.9]$$

in agreement with Young's equation and neglecting the spreading pressure.[33] Fowkes has suggested that the surface free energy can be represented by the sum of the different

types of interactions, and Schultz has proposed that it is the sum of only two components, dispersive (London's interactions) and polar.[35-35] The equation , then, is:

$$\gamma = \gamma^D + \gamma^P \qquad [1.10]$$

where the superscripts D and P refer to dispersive and polar components, respectively. The polar term corresponds to the nondispersion forces such as Debeye and Keesom interactions and hydrogen bonding. Fowkes has proposed, as well, that the dispersive part of these interactions between two solids can be quantified as twice the geometric mean of the dispersive component of the surface energy of both solids.[36] Thus, the adhesion energy, W_{12}, is defined for the interaction of two solids (dispersion forces, only):

$$W_{12} = 2\,(\gamma^D\,\gamma^D)^{1/2} \qquad [1.11]$$

By analogy, Owens and Wendt[37] have proposed that the nondispersive part on the interactions can be expressed in a similar geometric fashion. Thus, the equation for the work of adhesion becomes:

$$W_{12} = 2\,(\gamma^D\,\gamma^D)^{1/2} + 2\,(\gamma^P\,\gamma^P)^{1/2} \qquad [1.12]$$

For solid-liquid equilibrium, a relationship between θ and the surface properties of both products is obtained from equations 1.9 and 1.12. By making contact angle measurements with different liquids of known surface properties, the components γ_S^D and γ_S^P of the surface free energy of the substrate can be obtained.[12]

Fowkes and coworkers have demonstrated, more recently, that electron acceptor and donor interactions, according to Lewis acid-base concepts, are a significant interfacial force between the adhesive and substrate.[38] This approach, unlike the others, can account for hydrogen bonding. Moreover, Fowkes has proposed that the contribution

of polar (dipole-dipole) interactions to the thermodynamic work of adhesion is negligible by comparison to the dispersive and acid-base contributions.[39] Also, to establish a relationship for acid-base interactions at the interface, he has related the acid-base component of the adhesion energy, W^{ab}, to the variation in enthalpy, $-\Delta H^{ab}$, such that:

$$W^{ab} = f\,(-\Delta H^{ab})\,n^{ab} \qquad [1.13]$$

where f is a conversion factor, taken equal to unity, that converts enthalpy into free energy, and n^{ab} is the number of acid-base bonds per unit interfacial area (approximately 6 $\mu mol/m^2$). Thus, from equations 1.11 and 1.13, the total work of adhesion becomes:

$$W_{12} = 2\,(\gamma^D\,\gamma^D)^{1/2} + f\,(-\Delta H^{ab})\,n^{ab} \qquad [1.14]$$

Experimental values of $-\Delta H^{ab}$ can be estimated from the work of Drago according to the following expression:[40]

$$-\Delta H^{ab} = C^A\,C^B + E^A\,E^B \qquad [1.15]$$

where C^A and E^A are two quantities that characterize the acidic material at the interface, and C^B and E^B characterize the basic material. The validity of this expression has been proven for the adsorption of polymer on various substrates.[41]

Another approach to estimating $-\Delta H^{ab}$ has been proposed by Gutmann.[42] It suggests the use of two constants, an electron acceptor number, AN, and an electron donor number, DN, to characterize each material. For solids, K_A and K_D have been similarly defined and measured by inverse gas chromatography.[43] Thus, the expression for $-\Delta H^{ab}$ is given as:

$$-\Delta H^{ab} = K_{A1}\,K_{D2} + K_{A2}\,K_{D1} \qquad [1.16]$$

1.2.1.4.2 Relation of Adhesion Strength and Adhesion Energy

It is a common hypothesis in the scientific literature that it should be quite feasible to relate the thermodynamic work of adhesion, W_A, to the measured strength of an adhesive bond. In fact, after Zisman's introduction of the critical surface tension, γ_c, Levine and coworkers demonstrated a correlation between bond strength and γ_c.[44] These analyses were carried out using an epoxy adhesive and various polymeric substrates. Replication of this work by other scientists, however, leads to conflicting results. In his analysis of the theory and of the individual studies, Kinloch suggests several reasons for the conflict.[2] Firstly, the test methods used to measure the strengths of the adhesive joints are not well suited to theoretical analysis, especially concerning isolation of the viscoelastic and plastic energy losses. Secondly, the proposed correlation is only expected when the joint failure occurs at the interface.

To address these problems, Andrews and Kinloch have utilized continuum fracture mechanics to define a geometry independent measure of joint strength, the adhesive fracture energy, G_c.[45] From both experimental and theoretical considerations, they have demonstrated that this adhesive fracture energy, for a cross-linked rubber adhesive/rigid plastic interface, can be divided into two major components:

> The energy necessary to propagate a crack through a unit area of interface, absent viscoelastic energy losses, such as an intrinsic adhesive fracture energy, G_0, or
>
> The energy, ψ, dissipated viscoelastically within the rubbery adhesive at the propagating crack.

The energy dissipated viscoelastically, ψ, is typically the major contribution to the measured adhesive fracture energy, G_c. Thus, G_c is often much greater than G_0, and G_c is greatly dependent on temperature and rate. The relationship between these terms is given as follows:[45]

$$G_c = G_0 + \psi \qquad [1.17]$$

But it is known that:

$$\psi = G_0 f(a^{\cdot}, T, \epsilon) \qquad [1.18]$$

where f is a function, the value of which depends on the crack growth rate, $a^{\cdot}$, the temperature, T, and the level of strain, ϵ. Now, let:

$$\Phi_V(a^{\cdot}, T, \epsilon) = 1 + f(a^{\cdot}, T, \epsilon) \qquad [1.19]$$

The combination of equations 1.17 through 1.19 yields:

$$G_c = G_0 \Phi_V(a^{\cdot}, T, \epsilon) \qquad [1.20]$$

where Φ_V is the mechanical loss function. The dependence of the energy dissipation term, ψ, on the intrinsic adhesive fracture energy is rather interesting. It arises because the material around the crack tip can only be subjected to stress, and thus energy losses, while the chemical and physical bonds ahead of the crack tip are unbroken.[12] When viscoelastic and plastic energy losses are negligible ($\Phi_V(a^{\cdot}, T, \epsilon) \rightarrow 1$, $f(a^{\cdot}, T, \epsilon) \rightarrow 0$), the measured adhesive fracture energy equals G_0. Therefore, interatomic and intermolecular bonding forces across the interface can be directly measured. Since the failures are not typically 100% interfacial, the intrinsic adhesive fracture energy can be expressed through a weighted average of the various failure modes:[12]

$$G_0 = iG_0 \text{ (interfacial)} + b'G_0 \text{ (adhesive)} + sG_0 \text{ (substrate)} \qquad [1.21]$$

where G_0 (interfacial), G_0 (adhesive), and G_0 (substrate) are the fracture energies for interfacial, cohesive in the adhesive, and cohesive in the substrate failures, respectively, and i, b', and s are the respective area fractions. In the case of a solely interfacial failure

in which there is only secondary bonding, i = 1, G_0 (interfacial) = W_A, and the measured value of G_0 should equal the thermodynamic work of adhesion, W_A.[12]

Through the above work, a very important point comes to light. Specifically, the energy dissipated viscoelastically and plastically is dependent on the value of W_A.[12] Thus, designing an interphase which maximizes interfacial bonding forces, and recognizing the possibly conflicting need to attain good interfacial contact, is not a simple matter.

1.2.1.5 Diffusion Theory

Voyutskii is the primary supporter of the diffusion theory of adhesion.[46] This theory states that the intrinsic adhesion of polymers to themselves (autohesion) and to each other is due to mutual diffusion of polymer molecules across the interface to form an interphase. Such a mechanism implies that the macromolecular chains or chain segments are sufficiently mobile and mutually soluble.[12] If the concept of interdiffusion is valid, then the adhesive strength of a system should depend on different factors such as contact time, temperature, and the nature and molecular weight of the polymers. Voyutskii has experimentally verified this.

As added support for the diffusion theory, Vasenin has developed a quantitative model.[47] Starting with Fick's first law, he correlates the amount of material diffusing (w) in a given direction (x) across a plane of unit area to the concentration gradient ($\partial c/\partial x$) and the time (t):

$$\partial w = -D_f \, \partial t \, (\partial c/\partial x) \qquad [1.22]$$

where D_f is the diffusion coefficient. This equation, however, can be applied directly only to steady-state diffusion, where concentrations at points within the system do not vary with time. Clearly, penetration of a polymer chain into the surface of a polymeric substrate does not meet this criterion.

The build-up or decay of a diffusing species is better represented by Fick's second law (which can be derived from Fick's first law).[12] Utilizing these equations, Vasenin has modeled the depth of penetration of the diffusing molecule. First, he assumes that as the molecules interdiffuse into the surface regions, during the contact time, t_c, the diffusion constant decreases with time according to the following:

$$D_f = D_d \, t_c^{-\beta} \qquad [1.23]$$

where D_d is a constant which characterizes the mobility of the molecules and β is a constant which determines the rate of change of the coefficient of diffusion, D_f. Next, he calculates that the depth of penetration, l_p, can be expressed by the following:[47]

$$l_p = [(\pi \, D_d \, t_c^{1/2})^{1/2}] / k_3 \qquad [1.24]$$

where k_3 is a constant which characterizes the stiffness, bond length, and the valency angles along the polymeric molecules. Vasenin also calculates the number of molecular chains crossing the interface, N_c, such that:

$$N_c = [(2 \, N \, \rho) / M]^{2/3} \qquad [1.25]$$

where N is Avogadro's number, ρ is the density, and M is the molecular weight of the polymer. Finally, Vasenin assumes that the peel energy, G, is proportional to both the number of chains crossing the interface and the depth of penetration. Thus, G can be expressed in the following manner:[47]

$$G \sim K \, [(2 \, N \, \rho) / M]^{2/3} \, D_d^{1/2} \, t_c^{1/4} \qquad [1.26]$$

where K is a constant that depends on the molecular characteristics of the polymers

involved. It relates the peel energy to the time of contact allowed between the polymers and to the molecular weight of the polymers. It has been used successfully to predict autohesion of polyisobutylene.[47]

One criticism of Vasenin's model is that, not unlike other theories of adhesion, it does not compensate for viscoelastic and plastic energy dissipation. Vasenin recognized this and he has stated that the model is only an approximation. However, since the constants are obtained by fitting the equation to the data, it is likely that the hysteretic losses to the peel energy are implicitly included in them.[12]

Another more basic criticism of diffusion theory has been raised by Anand.[48] It states that the dependence of joint strength on time of contact and polymer molecular weight can be readily explained by the kinetics of wetting. Increases in joint strength actually arise from an increased degree of interfacial contact, and the actual mechanism of adhesion is the formation of secondary (van der Waals) forces across the interface. In the cases where interdiffusion is proven, Anand believes that the contribution to joint strength by intrinsic adhesion is minimal when compared with the contribution made by the formation of interfacial secondary bonds.[48] Since quantitative determination and separation of these contributions is extremely difficult, this conflict has not yet been resolved.[12]

In summary, the validity of diffusion theory has been demonstrated under specific circumstances. For polymer/polymer interfaces, the polymer chains must be mutually soluble and have sufficient mobility. If these conditions are met, as in autohesion and solvent welding, interdiffusion does contribute to intrinsic adhesion. However, if the solubility parameters of the materials are dissimilar, or if one or both of the materials is crystalline or glassy, then interdiffusion is unlikely. For polymer/metal interfaces, it appears that interdiffusion does occur, but increases in adhesion arise mainly from increased adsorption of the polymer.

1.2.1.6 Chemical Bonding Theory

It is logical that chemical bonds that form across an adhesive/substrate interface may dramatically contribute to the level of adhesion. These bonds are considered primary bonds in contrast to physical interactions, such as van der Waals, which are often termed secondary force interactions.[12] The designations of primary and secondary arise from the relative strength of each type of interaction. Primary bonds typically have strengths on the order of 100 to 1000 kJ/mol while secondary force interactions are generally not more than 50 kJ/mol.

The formation of primary bonds at the interface depends on the chemical reactivities of both the adhesive and substrate. Different types of primary bonds, such as ionic and covalent, have been detected in various interfaces and reported in the literature. One famous example discusses the formation of polysulfide bonds when brass and vulcanized rubber are attached.[49] In another practical situation, the concept of chemical bonding is realized through the application of coupling agents. These materials contain multiple reactive sites which enable them to chemically bond with both the adhesive and substrate. The result is formation of a bridge across the interface and thus improvements in joint strength and durability. Silanes are a typical form of adhesion promoter.[50]

The influence of primary bonding on the joint strength, G, and more specifically on the intrinsic adhesion fracture energy, G_0, has been studied. Gent and Ahagon, in the most relevant work in this field, have evaluated the influence of interfacial chemical bonds on the adhesion of polybutadiene to glass.[51] This was accomplished using a combination of silanes, both of which reacted with glass, but only one of which would react with the elastomer. Their results indicate that intrinsic peel energy, G_0, increases linearly with increases in primary bonding, thus the effect of primary bonds on adhesion strength is validated.

1.3 Epoxy Adhesives

Epoxy resins are a class of thermosetting materials characterized by the presence of the epoxide or oxirane group.[52] They are capable of reacting with a multitude of materials, at room temperature or elevated temperatures, to form three-dimensional cross-linked structures. Epoxies possess great strength and excellent adhesion on a wide array of substrates and are relatively insensitive to moisture. Thus, they are perfectly suited for many high performance structural applications. Epoxies also possess the unique characteristics of excellent chemical resistance, limited shrinkage during cure, and the ability to bond nonporous substrates. Due to these characteristics, epoxy resin systems have become the most versatile, and widely accepted and used, of all the structural adhesives. It has been reported that, overall, they account for nearly 50% of the structural adhesives market.[53] This is not surprising since epoxies are utilized in, and provide a unique, distinctive advantage to, a multitude of applications. These include, but are not limited to: building and construction, metal bonding, road making, wood bonding, and electrical.

Research studies dealing with epoxy resins were initiated in the 1920s. Commercially available systems, however, did not appear until approximately 1946, when first introduced by Ciba-Geigey.[52-53] These systems were based on the diglycidyl ether of bisphenol A (DGEBA, see section 1.3.2). DGEBA is still the main constituent of modern epoxy resin systems, but it is now available in a wider variety of molecular weights. Depending on the application requirements, it can be combined with any of a multitude of commercially available hardeners. Unlike the DGEBA constituent, the numbers and types of hardeners have grown and changed tremendously. Choices include, to mention only a few, amines, anhydrides, amides, mercaptans, and Lewis acids and bases. Each of these materials combines with DGEBA to yield a unique final product, thus the versatility of epoxy resin systems is apparent.[52]

1.3.1 Formulation of Epoxy Resins

While the adhesives industry has seen tremendous growth due to the synthesis of new polymeric materials, it should be noted that most commercial adhesives are not just simple polymers. Rather, they are typically a complex mixture of the polymer together with multiple other additives.[19] The following section of this dissertation describes the process by which this complex mixture is derived and assembled. Details are given, as well, on the purpose of each individual component.

Most epoxy adhesive systems begin with bisphenol A and epichlorohydrin. These materials are reacted to give a linear, epoxy terminated, moderate molecular weight liquid resin (DGEBA). An example of such a structure is shown in Section 1.3.2, along with additional details on the various epoxy reactions that may occur. DGEBA resins provide the backbone for most epoxy systems but are sometimes blended with other types of epoxy resins, such as epoxy novolacs, to optimize a particular property. Epoxy novolacs, for example, are higher in functionality than DGEBA and are therefore added to provide greater cross-linking. The result is a material with better heat resistance.

A second component, the curing agent or hardener, is added to this epoxy resin starting material. The purpose of the curing agent is to react with the epoxide end groups to form a three-dimensional, thermoset structure. The most frequently used curing agents are polyfunctional, the reactive groups of which are typically primary amines. However, as mentioned previously, a wide variety of curing agents are commercially available, including such materials as aliphatic or aromatic amines, amine adducts, tertiary amines, amides, mercaptans, acids, and anhydrides. Since the rate of curing and final material properties depend on the cross-linking agent used, very often a specific material is used for a specific application. For example, dicyandiamide (dicy, see Fig. 2.1) is used in metal bonding. Accordingly, dicyandiamide is the hardener chosen for this dissertation research.

Epoxy resins can be formulated as 1-part or 2-part materials. In 2-part materials, the curing agent and resin are not mixed until the adhesive is ready to be used. After

mixing the adhesive lifetime is limited. In 1-part materials, on the other hand, the curing agent is generally non-reactive at room temperature and thus provides the advantage of a longer shelf life. However, because latent-cure systems require elevated temperatures to cure, a third resin component is sometimes needed. This component is called a catalyst or cure accelerator. Ureas, such as the 3-phenyl-1,1-dimethyl urea that is employed in this dissertation research, are common accelerators. Reactions involving dicyandiamide, epoxy and urea, not unlike the uncatalyzed dicy/epoxy reactions, remain the subject of considerable controversy.[54, 56-62]

A fourth component often found in epoxy adhesives is a toughener, added since most cured epoxies are inherently brittle. This material is usually a rubber which precipitates as a separated, micro-dispersed phase when the resin hardens.[19] A common toughener is the copolymer of butadiene and acrylonitrile, and it is often reacted into an epoxy backbone to give a reactive block copolymer. This advancement in epoxy technology was developed in the 1960s, and even after approximately thirty years, the combination of dicyandiamide, epoxy, and toughener remains the basis for many 1-part structural adhesives.

While these four components are the basis for most epoxy adhesive resins, a multitude of other additives are frequently utilized. Chemically inert fillers (non-reactive) are most commonly used. For instance, aluminum powder may be added as a reinforcing agent or carbon black may be added to deter the harmful effects of ultraviolet radiation. Sometimes fillers are added to promote a specific type of failure in a bonded joint. Since interfacial failures are usually unacceptable in commercial applications, a filler such as talcum powder may be added to the resin to promote cohesive failures. The filler functions by reducing the bulk strength of the adhesive to a level that is lower than the interfacial strength, and failures therefore occur in the bulk of the material rather than at the interface.

The adhesives formulated for this dissertation research are typical of 1-part, heat cured, structural epoxy adhesives. They consist of a liquid epoxy resin, a latent curing agent (dicyandiamide), a cure accelerator (3-phenyl-1,1-dimethyl urea), a reactive

(epoxide terminated) rubber toughener, and a flow control agent (fumed silica). There are, however, no other additives. Thus, these adhesives are somewhat more simple, and therefore more amenable to evaluation, than commercially available systems. They are well suited for this dissertation research.

1.3.2 Mechanistic Features of Epoxy Curing

1.3.2.1 The Dicy/Epoxy Reaction

The curing of a thermosetting resin is typically a highly complex process involving multiple reactions, byproducts, and final products. Curing begins with the formation and linear growth of the chains, followed by branching and the formation of a final cross-linked matrix. At the gel point, the material transforms from a viscous liquid into an elastic gel. This is caused by a rapid increase in the molecular weight (i.e., the network becomes essentially infinite in length). As curing reactions proceed beyond the gel point, there is a substantial increase in the cross-link density, glass transition temperature, and the overall mechanical properties of the material, in general.[67] A typical thermosetting reaction, the reaction of an epoxy resin and amine, is shown below:

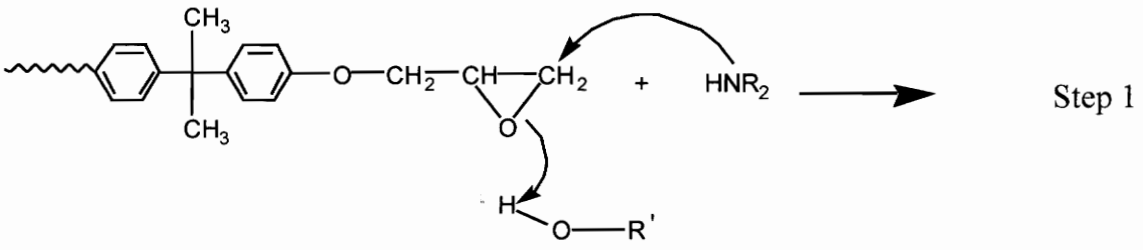

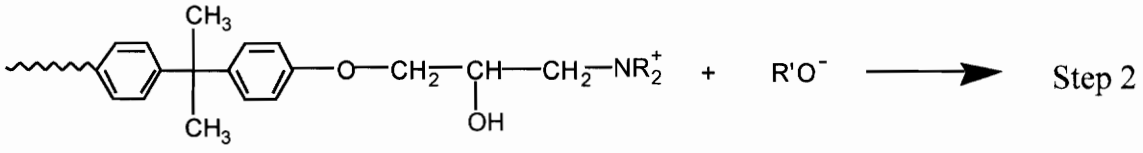

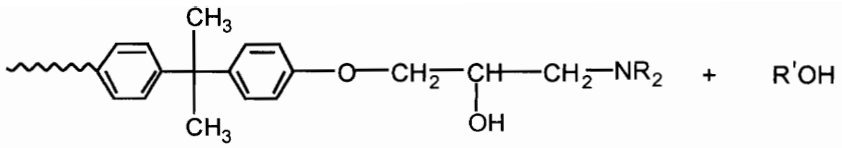

Step 3

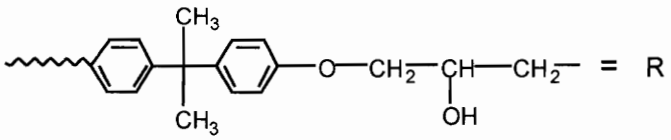

The epoxide end groups of the chains in this reaction are highly electrophilic and can react with a variety of nucleophilic curing agents. Substituted amines and their derivatives are commonly utilized in this manner. In the most straightforward scenario, the amine reacts with and opens the terminal epoxy group resulting in the formation of an aminoalcohol. This is followed by the intermolecular reaction of the terminal amine with an epoxide end group of another chain. As this process continues, a cross-linked matrix is formed.[63] However, depending upon the cure temperature and conditions utilized, there may also be side reactions. One such situation involves the pendant hydroxyls acting as nucleophilic centers, or hydrogen bonding donors, to accelerate the amine reaction. In addition, nucleophilic attack of the epoxide ring by the alkoxide, formed in Step 2 of the above reaction, can result in the subsequent formation of an ether linkage. A schematic of this reaction is shown below:

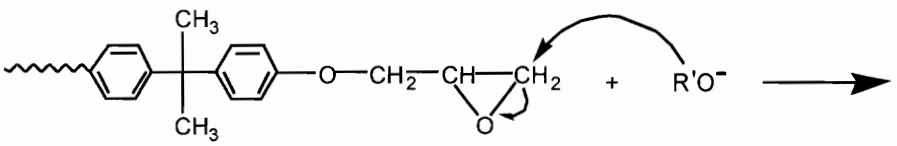

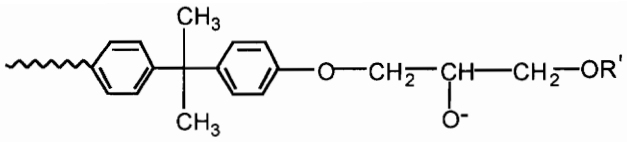

A great deal of effort has been exerted to elucidate the mechanism of the dicy/epoxy reaction. In most cases it has been suggested that multiple, competing reactions are present, and that these are highly dependent on the stoichiometry, the absence or presence of an accelerator, the type of accelerator if present, and the cure temperature.[56-71] Many difficulties, however, were encountered reaching these conclusions. Firstly, the network formed in the dicy/epoxy reaction does not allow for separation of the different reaction products. Secondly, dicyandiamide is highly insoluble in epoxy resins. Thus, the uncured resins possess two phases, and the dicyandiamide has a tendency to settle as the resin is heated and the viscosity drops.

The initial research in this area utilized model systems, in particular the base-catalyzed reaction of a monofunctional epoxy, phenyl glycidyl ether (PGE), with both dicyandiamide and cyanamide. In these reactions, the rate determining step is considered to be the initial dicy to epoxide addition, followed by a rapid cyclization. The net result is cyanamide and 2-iminooxazolidine, as shown in the schematic below. The 2-iminooxazolidines are reactive with epoxies and act as trifunctional cross-linking agents, while the cyanamide is difunctional and reacts to form dialkylcyanamides.[56, 72]

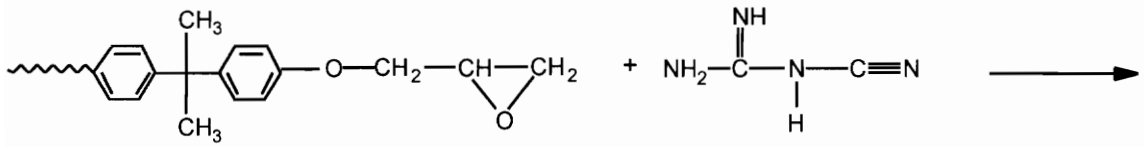

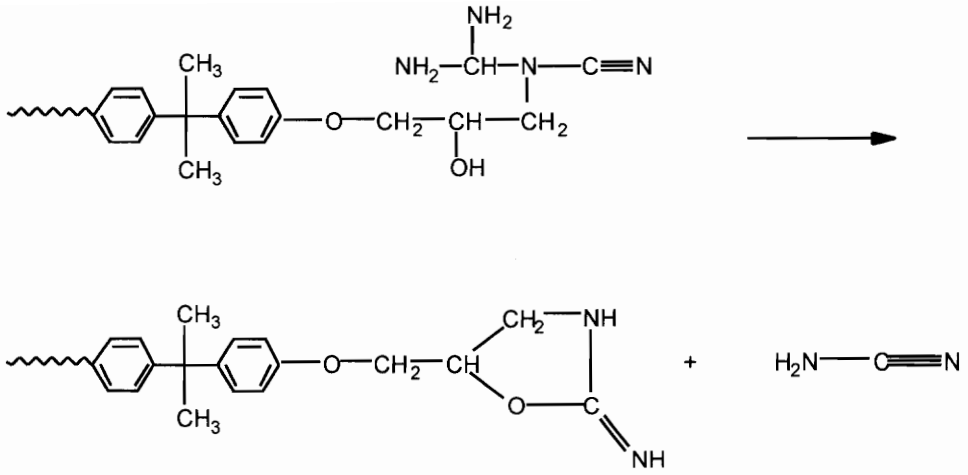

Gilbert and coworkers recently evaluated the reaction of dicyandiamide and methyl glycidyl ether of bisphenol A.[61] From the results of this study, they have suggested an alternative mechanism for the dicy/epoxy reaction. The initial products are proposed to be the 1:1 adduct product and the 2:1 adduct product. These are shown in the following schematic as product I and product II, respectively.

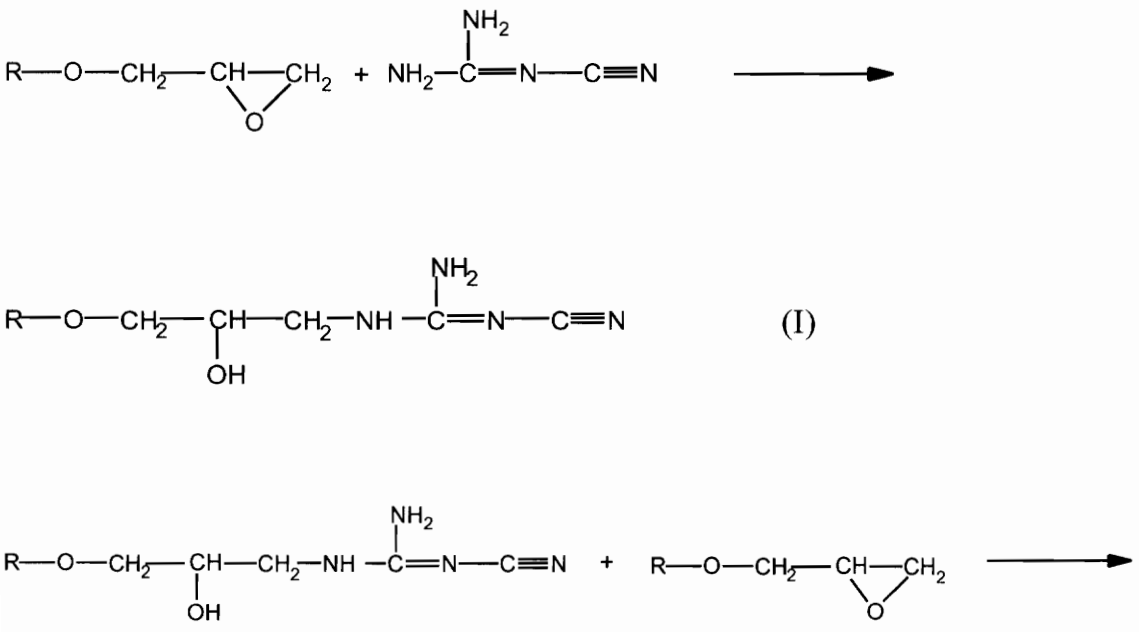

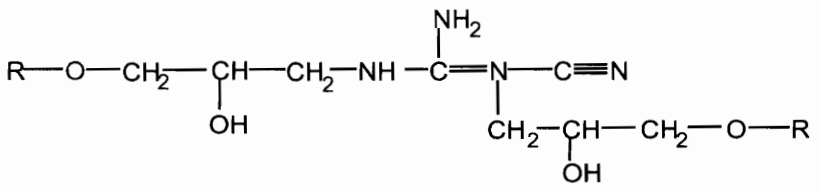

(II)

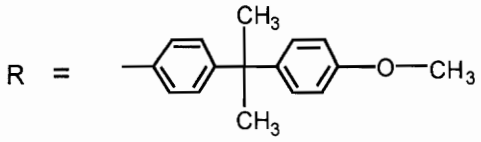

As discussed earlier, Zeppenfeld et al. proposed that cyclization of alkylated dicyandiamide molecules occurs through intramolecular nucleophilic attack of the cyano group by the hydroxyl group.[72] Gilbert and coworkers, however, have found that attack actually occurs on the imide carbon atom.[61] According to this scenario, 2-cyanimidooxazolidine is formed and ammonia or alkylamine is eliminated. A schematic of the reaction is given below:

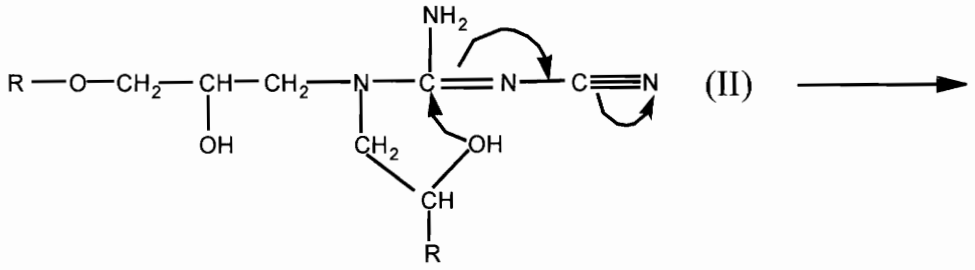

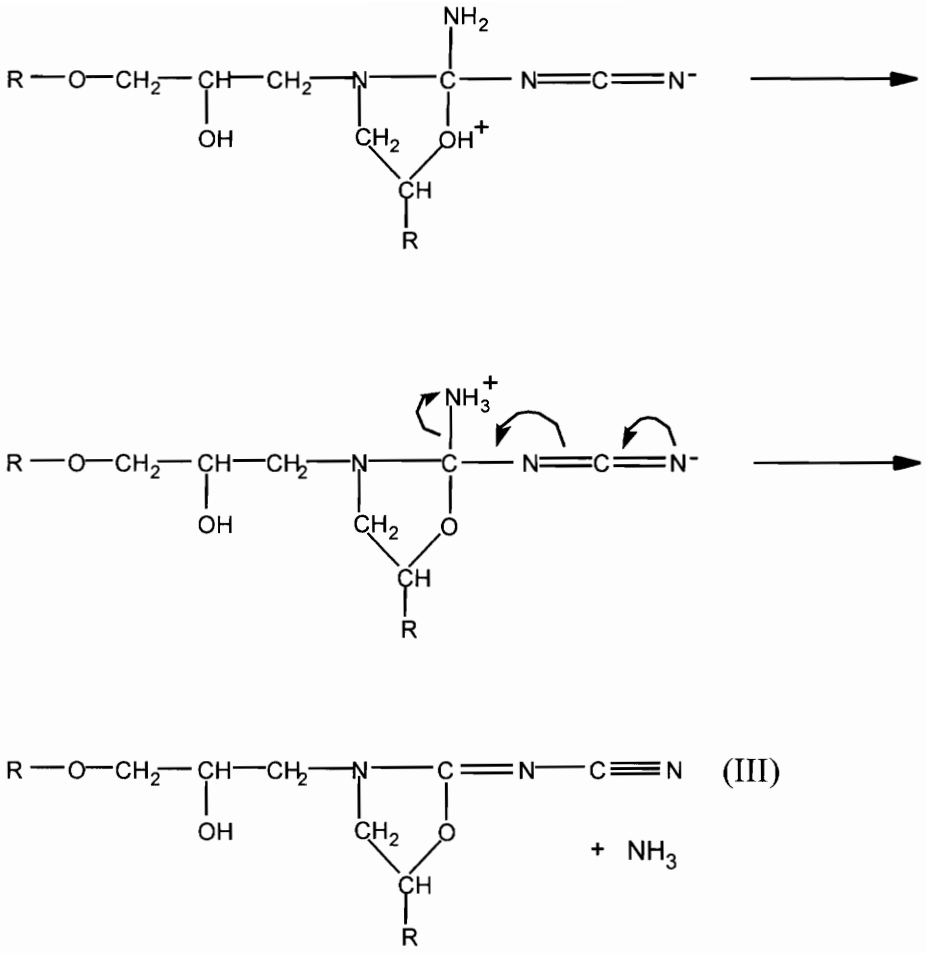

(III)

Formation of ammonia, or alkylamine, then leads to rapid reaction with an epoxy end group. The 1:1 dicy/epoxy adduct, (I) and the 2:1 adduct (II) are not observed at the temperature required for uncatalyzed reactions (160°C).[61] This is most likely due to the fact that they very readily react at these temperatures. On the other hand, in benzyldimethylamine catalyzed cures conducted at lower temperatures (100°C), both adduct products can be detected. For cross-linking systems, product III, the 2-cyanimidooxazolidine, functions as a difunctional chain extender. Ammonia acts as a trifunctional cross-linking agent.[61]

If an excess of epoxy functionality is present in the cross-linking system, such as in the case of the model systems studied in this dissertation, dicy/epoxy addition and etherification are most likely both present as competing pathways. A low dicyandiamide

content favors etherification, resulting in both a decrease in pendant hydroxyl groups, and an increase in cross-link density. For higher loadings of dicyandiamide, the concentration of pendant hydroxyl groups increases and the cross-link density decreases (since dicyandiamide acts as a difunctional chain extender). The increase in hydroxyl groups, and the consequent increase in interchain hydrogen bonding, results in an increase in the stiffness of the system.

1.3.2.2 Dicy/Epoxy Acceleration by Ureas

Mechanistic studies of epoxy curing have been conducted to determine the role of substituted ureas, such as N-(3,4-dichlorophenyl)-N',N'-dimethylurea, N-(4-chlorophenyl)-N',N'-dimethylurea, and N-phenyl-N',N'-dimethylurea, in accelerating the dicy/epoxy reaction. In all cases, it has been demonstrated that the release of dimethylamine plays an important role. Three processes for the evolution of this material are proposed:[74]

1. Reaction between the substituted urea and an epoxide group occurs to form dimethylamine and a 2-oxazolidone derivative.

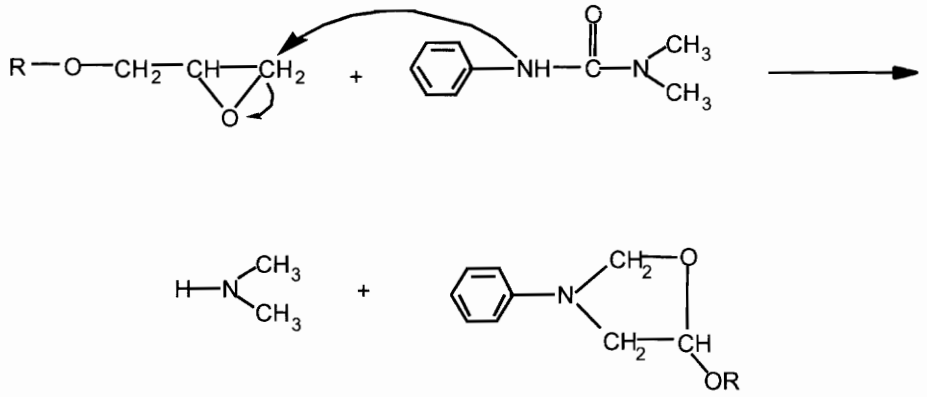

2. Thermal dissociation of the substituted urea occurs to form dimethylamine and an isocyanate.

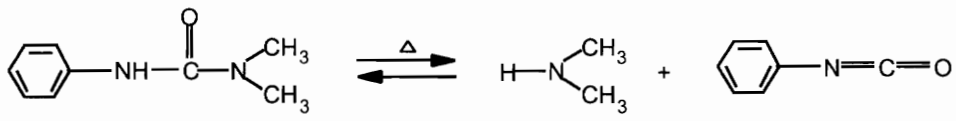

3. Reaction of the substituted urea and dicyandiamide occurs to form dimethylamine and a guanidine derivative.

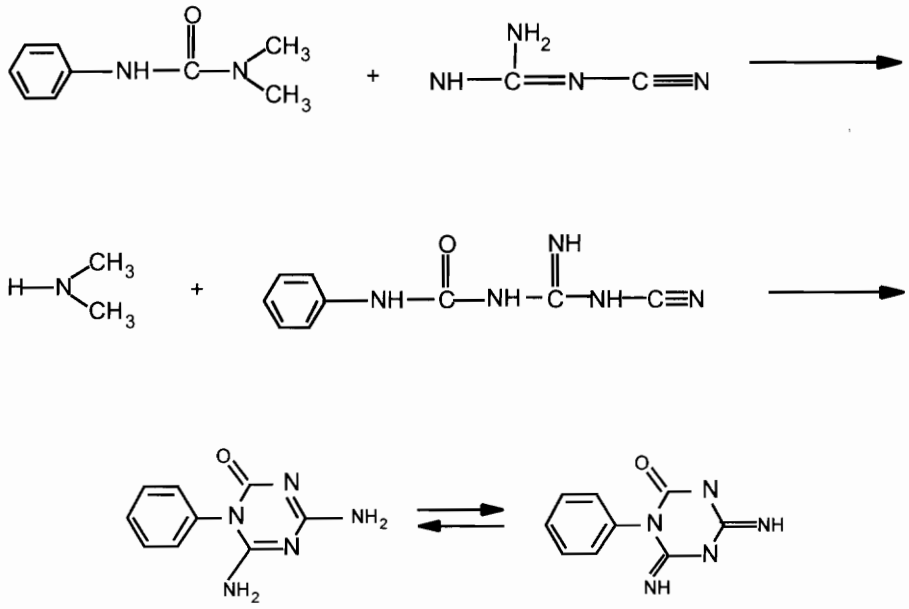

The results of these studies suggest that substituted ureas contribute to the dicy/epoxy reaction through a urea/epoxide reaction, as shown above in number 1. Dimethylamine and a 2-oxazolidone derivative are formed and the dimethylamine attacks the oxirane group of the epoxy resin. Curing occurs through the mechanism described by Saunders and coworkers.[65]

1.4 Adhesive Testing and Analysis

Testing, in general, is the evaluation of the physical, chemical, mechanical, or thermal properties of a material. For bulk materials, mechanical testing focuses on the behavior as a response to some form of applied loading. These types of tests include evaluation of the elastic modulus or stiffness, the yield strength, the fracture stress or ultimate strength, the elongation, and Poisson's ratio.[75] The evaluation of adhesives by mechanical test methods, however, is much more complex. As was explained earlier (see Section 1.1.4), evaluations of adhesive performance actually test the *adhesive system* rather than just the polymeric adhesive. These tests include considerations for the properties of, and contributions made by, the substrates, the interfaces and surfaces, the joint geometry, and the joint assembly process and conditions.

Mechanical testing plays an integral role in the development, qualification, processing, and use of adhesives.[11] Many standardized tests for the evaluation of adhesive performance have been developed, and thorough listings are given in the U.S. Military and Federal Adhesive Specifications and in the American Society for Testing and Materials (ASTM) Standard Test Methods.[76-79] These tests enable equivalent, comparative testing to be conducted in any research facility, and they allow the performance of practical joint designs to be estimated by simulating the geometries and stresses likely to be encountered.[2] More specifically, these tests assist in adhesive development and selection, serve as production quality control measures, and ensure the effectiveness of the bonding process.[80]

Two basic, complementary schools of thought have arisen for the topic of mechanical testing and analysis, specifically in relation to joint design and failure prediction. The first focuses on the nature and magnitude of the stresses found in the test specimens. This information permits quantitative joint design studies and failure predictions. It also permits relation of the measured joint strength to the adhesive properties, joint geometry, test rate, and temperature.[2] It must be emphasized again, however, that the measured joint strengths from most of these standardized tests depend not only upon the degree of intrinsic adhesion, but also upon the properties of the

substrates and upon the specific joint geometry.[2] Because the stress states in a bond region are extremely complex, the information obtained with these types of tests is valid only for that specific geometry. In other words, to determine failure loads for different loading geometries, additional methods are required.[81]

The second school of thought on mechanical testing and analysis of adhesives is fracture mechanics. This approach is generally more useful than the above mentioned ideas for problems concerning crack growth, fracture, and failure prediction. Fracture mechanics is based on the concept that the strength of most real solids is governed by the presence of flaws.[2] These naturally occurring flaws, often termed intrinsic flaws, can be voids, cracks, or inhomogeneities, and they propagate to cause failure. It is therefore the focus of fracture mechanics to mathematically analyze the loads at which the flaws grow, and to describe the manner in which this occurs. Fracture mechanics has been one of the more successful tools used in the evaluation of adhesive system performance. Fracture tests generally display a more controlled failure mode than maximum strength based tests, which usually fail catastrophically (e.g., the single lap shear specimen), and thus allow a more fundamental understanding of the failure mechanisms to be obtained. In fact, fracture mechanics has played an important role in answering some of the fundamental questions concerning the mechanical behavior of rubber-modified epoxy adhesives. A fracture mechanics approach is therefore utilized in this dissertation work as the basis for adhesive system design, testing and analysis.

1.4.1 Introduction to Fracture Mechanics

1.4.1.1 Fracture Characteristics of Bulk Polymers

Thermosetting and thermoplastic polymers, in the glassy state, show an almost linear increase in stress with strain, and fracture occurs at strains of only a few percent. Plastic deformation is not noticeable and macroscopically smooth surfaces are produced. Elastomeric networks, on the other hand, need to be strained by several hundred percent before the strain energy becomes sufficient for unstable rapid crack propagation to occur. Such a rupture is also classified as a brittle fracture since the sample is not subjected to

any noticeable additional deformation between the moment of fracture initiation and termination.[82-83] In accordance with the basic concepts of fracture mechanics, this usually occurs at a flaw or defect in the sample.

For a polymeric material in the rubbery state, when a stress is applied, the first deformation involves shear flow of the polymer molecules past one another. In contrast, bond bending and stretching occur if the material is a glass. Eventually a crack forms, presumably from a preexisting flaw, and then propagates at high speed until catastrophic failure occurs. Although the volume of the sample is increased by the void space, the early formed fibrils hold the material together until the crack grows through the polymer by breaking the chains.[84] For rupture to occur, the energy required to produce the new surface must be balanced by a decrease in stored elastic energy.

Three basic types of crack growth behavior have been described for epoxy materials:[79] brittle stable, brittle unstable, and ductile stable. The load deflection curves for these various responses, collected from compact tension measurements, are shown in Figure 1.3. It should be noted that transition types of crack growth (i.e., slow and controlled growth becomes fast and uncontrolled) have been observed as well.

It is important at this stage of the discussion to distinguish between cracks and crazes. In many cases, glassy polymers stressed below the breaking point develop large numbers of straight zones which are spanned by fibrillar matter. These are termed crazes.[83-86] A craze is not an open fissure but is spanned top to bottom by fibrils composed of highly oriented polymer chains. These crazes are called extrinsic crazes or crazes I. Surface defects are also known to be craze initiation sites. Many polymers, when strained to high levels, tend to deform by opening up small voids throughout the whole body. The deformed regions appear to be white, and thus the phenomenon is termed stress whitening.[87] These intrinsic crazes, or crazes II, are observed for materials strained beyond the yield point.

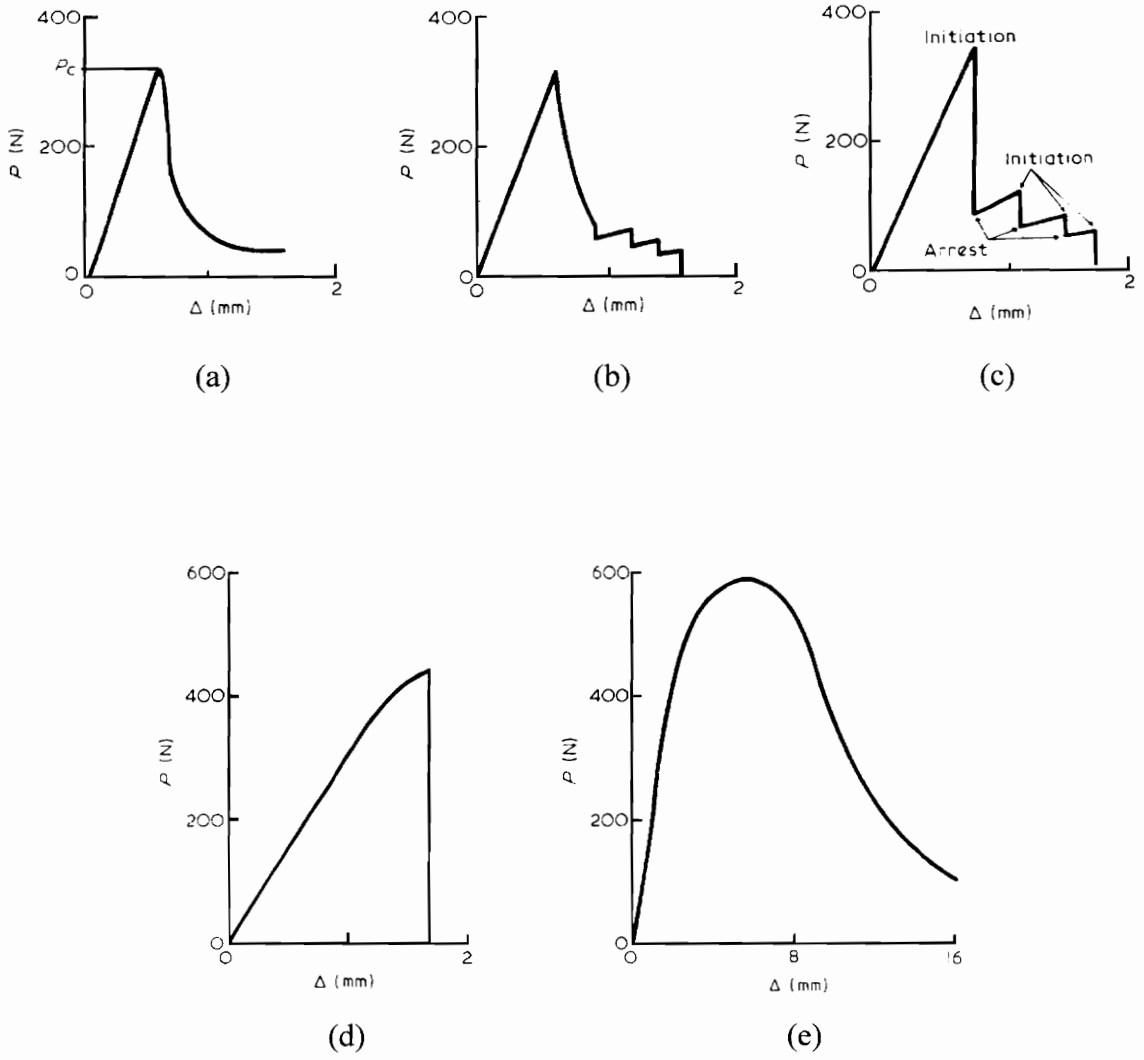

Figure 1.3 Types of crack growth behavior (Ref. 78): (a) brittle stable, (b) brittle stable becomes unstable, (c) brittle unstable, (d) ductile stable becomes unstable, and (e) ductile stable.

1.4.2 Theoretical Approaches to Fracture

There are two main, interrelated, approaches to describing fracture. In the first, based on the work of Griffith, and later Orowan, a global balance of energy is discussed. It states that fracture occurs when sufficient energy is released by growth of the crack to supply the energy requirements of the new surfaces.[2, 88-89] The energy which is released arises from the stored elastic or potential energy of the loading system and can be calculated, theoretically, for any type of test specimen. This approach provides a measure of the energy required to propagate a crack over a unit area and is termed the fracture energy, or critical strain energy release rate (SERR). It is denoted G_c.[2] The second method for describing fracture utilizes the local stress field around the crack tip at the point of fracture.[87] The stress field around a sharp crack, in a linear elastic material, can be defined by a parameter called the stress intensity factor, K. Fracture occurs when the value of K exceeds some critical value, K_c. Therefore, K is a stress field parameter independent of the material, and K_c refers to the fracture toughness, a measure of a material property.[2]

One of the basic goals of fracture mechanics[2] is to identify fracture criteria (such as G_c and K_c) which are, ideally, independent of the test geometry and conditions. Thus, fracture mechanics should help provide a more fundamental understanding of the fracture process. Also, it should be useful in the practical areas of data specification and engineering design, especially in connection with studies of service life prediction.[2]

1.4.2.1 The Energy Balance Approach

Griffith's hypothesis describes quasi-static crack propagation as the conversion of work done, W_d, by the external force and the available elastic energy stored in the bulk of the specimen, U, into surface free energy, γ_m. This is the criterion for fracture and is expressed as:

$$\frac{\partial(W_d - U)}{\partial a} \geq \gamma_m \left(\frac{\partial A}{\partial a}\right) \qquad [1.27]$$

where ∂A is the increase in surface area associated with the change in crack length or crack growth, ∂a. For crack growth occurring in a specimen of fixed thickness, b, the criterion becomes:

$$\frac{1}{b}\cdot\frac{\partial(W_d - U)}{\partial a} \geq 2\gamma_m \qquad [1.28]$$

The initial work of Orowan, Rivlin and Thomas, and Berry, examined this criterion with respect to metallic materials, cross-linked rubbers, and poly(methyl methacrylate), respectively.[88,90-91] Examples of fracture test geometries utilized in these types of evaluations are shown in Figure 1.4.[84, 90] In all of the test cases, the energy required for crack propagation was demonstrated to be much greater than twice the surface free energy. There are two main causes for this. Firstly, $2\gamma_m$, which is equivalent to W_A for crack growth at the interface, represents only the energy required to break secondary bonds. In real materials, and along interfaces, rupture of primary bonds is often required. The energy necessary to break these primary and secondary bonds is termed the intrinsic fracture energy, G_0. For perfectly elastic systems, G_0 is the appropriate energy requirement. Secondly, the process of fracture invariably involves localized viscoelastic and/or plastic energy dissipation where high strains are experienced. It is in this manner that liquid rubber additives function to toughen brittle polymer matrices.

If the assumption is made that energy dissipation around the crack tip occurs independently of the specimen geometry and the manner in which the forces are applied, then $2\gamma_m$ can be replaced with G_c, the critical strain energy release rate. For bonded systems which exhibit bulk linear-elastic behavior, the criterion thus becomes:[2]

$$\frac{1}{b}\cdot\frac{\partial(W_d - U)}{\partial a} \geq G_C \qquad [1.29]$$

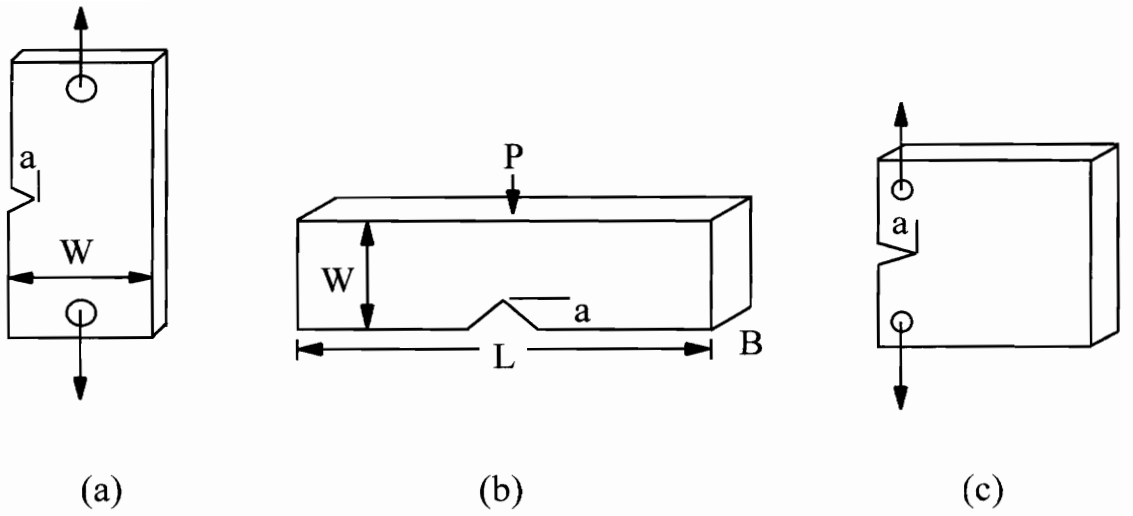

Figure 1.4 Fracture testing geometries: (a) single edge notch tension, (b) single edge notch 3 point bend, and (c) compact tension.

For example, away from the crack tip regions, Hooke's law is obeyed.[2] Equation 1.29 can then be expressed as follows:

$$G_c = \frac{P^2}{2B}\frac{\partial C}{\partial a} \qquad [1.30]$$

where P is the load at the onset of crack propagation and C is the compliance, equivalent to displacement/load. The most important aspect of this result is that for an infinitesimally small amount of crack propagation, this equation is equally valid for fixed-extension or constant-load conditions. It is therefore the basis of many calculations of G_c since if C is determined as a function of a, either experimentally or theoretically, then $\partial C/\partial a$ can be found. Thus, if the load at the onset of crack propagation, P, is measured at a known crack length, the value of G_c can be calculated.[2] This is the basic approach utilized in this dissertation work.

There are two primary advantages to using the energy balance approach. The first is that an unambiguous value of G_c can be calculated from Equations 1.29 and 1.30. This is equally valid for thick or thin adhesive layers and interfacial or cohesive type failures. The fracture toughness, K_c, is not always so easy to determine. The second advantage is that G_c may be related to the intrinsic forces acting in the adhesive or across the adhesive/substrate interface. The mathematical relationships were presented previously in Section 1.2.1.4.2.

1.4.2.2 The Stress Intensity Factor Approach (Bulk Materials)

Figure 1.5 shows a sharp crack tip in a uniformly stressed, infinite, homogeneous plate. Westergaard has developed stress-function solutions which relate the local stress concentration of stresses at the crack tip to the applied stress, σ_0.[92] Assuming Hookean behavior and infinitesimal strains (linear-elastic fracture mechanics, LEFM), for regions close to the crack tip, the solutions can be expressed as:

$$\sigma_{ij} = \sigma_0 \left(\frac{a}{2r} \right)^{1/2} f_{ij}(\theta) \qquad [1.31]$$

where σ_{ij} are the components of the stress tensor at a point, r and θ are the polar coordinates of the point, setting the crack tip as the origin, and 2a is the crack length.[2]

This solution was later modified by Irwin to give:[93]

$$\sigma_{ij} = \frac{K}{(2\pi r)^{1/2}} f_{ij}(\theta) \qquad [1.32]$$

where K is the stress intensity factor. It serves to relate the magnitude of the stress intensity, local to the crack, to the applied load and geometry of the flawed structure.

It is convenient to express the loading of a crack in terms of three orthogonal components which may be superimposed to give any loading state. Mode I is the

cleavage or tensile-opening mode, Mode II is the in-plane shear mode, and Mode III is the antiplane shear mode. These are represented graphically in Figure 1.6. An applied loading may give rise to a mixture of some or all of these and can then be expressed in terms of K_I, K_{II}, and K_{III}. Mode I is usually the most important since it is the most commonly encountered mode. It is also the one that typically causes failure.[2,82,94] However, since crack propagation in joints is often constrained to the adhesive layer, attention must sometimes be given to the other two modes as well.

For each of the loading modes, the crack tip stresses can be derived from the previous equation. For Mode I, the results can be expressed as:

$$\begin{Bmatrix} \sigma_{11} \\ \tau_{12} \\ \sigma_{22} \end{Bmatrix} = \frac{K_I}{(2\pi r)^{1/2}} \cos(\theta/2) \begin{Bmatrix} 1+\sin(\theta/2)\sin(3\theta/2) \\ \sin(\theta/2)\cos(3\theta/2) \\ 1-\sin(\theta/2)\sin(3\theta/2) \end{Bmatrix} \qquad [1.33]$$

for plane stress, $$\sigma_{33} = 0 \qquad [1.34]$$

for plane strain, $$\sigma_{22} = \nu(\sigma_{11} + \sigma_{22}) \qquad [1.35]$$

and, $$\tau_{23} = \tau_{13} = 0. \qquad [1.36]$$

In the plane $\theta = 0°$ the shear stress is zero. Thus, for $\theta = 0°$ the stresses σ_{11}, σ_{22}, and σ_{33} are the principal stresses σ_1, σ_2, and σ_3.

From Equation 1.33 it is evident that as r goes to zero, the stress σ_{ij} goes to infinity. Thus, stress alone does not constitute a reasonable fracture criterion.[2] Irwin has postulated that since the stress field around the crack is defined by K_I, then:[93]

$$K_I \geq K_{Ic} \qquad [1.37]$$

represents a fracture criterion, where K_{Ic} is a critical value for crack growth in a material and, as such, is a material property. It is often termed the fracture toughness. It should be emphasized that K_{Ic} characterizes the intensity of the stress field ahead of a crack, and is not a stress concentration, η_c, which can be defined by σ_{ij}/σ_0.

The major strength of the stress intensity factor approach is that for any Mode I problem, K_I can be expressed as:

$$K_I = Q\sigma_0 a^{1/2} \qquad [1.38]$$

and therefore, K_{Ic} can always be expressed as:

$$K_{Ic} = Q\sigma_c a^{1/2} \qquad [1.39]$$

where σ_c is the applied stress at the onset of crack propagation and Q is a geometry factor.

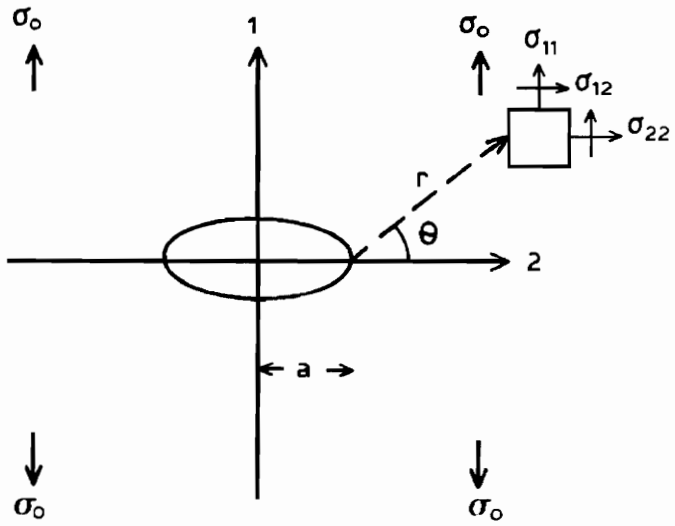

Figure 1.5 Sharp crack in a uniformly stressed infinite lamina (Ref. 2).

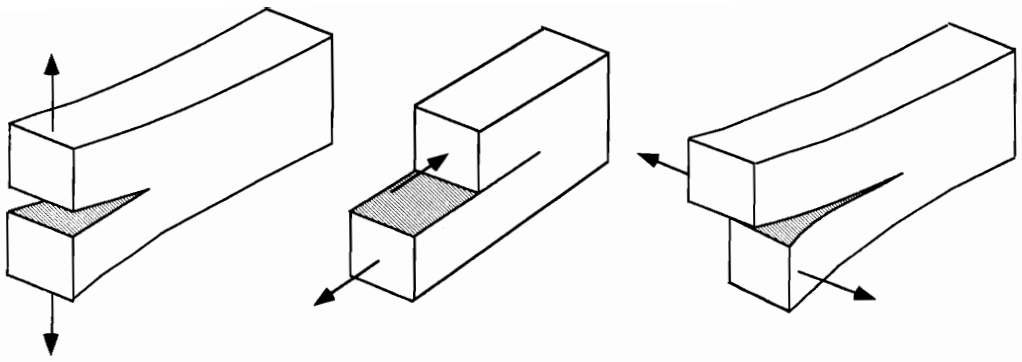

Figure 1.6 Modes of loading (Ref. 2): (a) Mode I, tensile-opening mode, (b) Mode II, in-plane shear mode, and (c) Mode III, antiplane shear mode.

1.4.2.3 The Stress Intensity Factor Approach (At, or Near, Interfaces)

In the development given in Section 1.4.2.2, the case of a crack in a bulk material was considered. However, a second highly important scenario exists and that is the case of a crack at, or very close to, a bimaterial interface. This situation is much more complex than the previous and problems immediately arise. The first problem is that when the joint is subjected to purely tensile or purely shear loads applied normal to the crack, then both tensile and shear stresses are induced about the crack tip. Thus, both K_{Ii} and K_{IIi} terms, the i referring to interface, are necessary to describe the stress field. However, these terms do not have a clearly defined significance as in the bulk case. From mathematical modeling it has been demonstrated that, for linear elastic materials, the local stresses ahead of the crack tip at an interface are proportional to:[2]

$$\frac{f\left(K_{Ii},K_{IIi}\right)}{(2\pi r)^{1/2}}\begin{Bmatrix}\sin\\ \cos\end{Bmatrix}(\zeta \ln r) \qquad [1.40]$$

where ζ is a bimaterial constant and is a function of the moduli and Poisson's ratios of the two materials forming the interface. It is represented by:

$$\zeta = \frac{1}{2\pi} \ln\left[\left(\frac{\beta_a}{G_a} + \frac{1}{G_s}\right) \Big/ \left(\frac{\beta_s}{G_s} + \frac{1}{G_a}\right)\right] \qquad [1.41]$$

where G_a and G_s are the shear moduli of the adhesive and substrate, respectively, β_a and β_s are functions of the Poisson's ratios of the adhesive and substrate, ν_a and ν_s, respectively, such that:

for plane stress, $$\beta_j = (3 - \nu_j) / (1 + \nu_j) \qquad [1.42]$$

for plane strain, $$\beta_j = 3 - 4\nu_j \qquad [1.43]$$

and j is equal to a or s, as required.

From Equation 1.40 it is apparent that the singular behavior of the stresses is proportional to the inverse square root of the distance, r.[2] However, unlike in the case of a bulk material, a serious consequence arises. Very close to the crack tip the stresses are oscillatory and as r goes to zero, possess the highly improbable property of changing signs with increasing frequency. Even less likely, the crack face displacements oscillate and interfere in the vicinity of the crack tip, resulting in an impossible solution.[2] It has been argued that since the oscillatory characteristics are an artifact of the analysis and are confined to the vicinity very close to the crack tip, the solutions do model the near- and far-field stresses reasonably well.[95] However, yet another complication arises in the form of a logarithmic term of a dimensional parameter, r. Thus, the crack tip stresses, and the values of K, become a function of the measuring units of r.[2] Modifications to this analysis, which remove the arbitrary length parameter, have been proposed.[96] These

modifications, nonetheless, utilize scaling and therefore typically assume unrealistic conditions or violate one of the boundary conditions.

For an interfacial crack of length 2a in an infinite sheet under only tensile applied stresses, σ_0, the values of K_{Ii} and K_{IIi} can be represented as follows:[97]

$$K_{Ii} = \sigma_0 \frac{\left\{(2\pi)^{1/2}\left[\cos(\zeta \ln 2a) + 2\zeta \sin(\zeta \ln 2a)\right]\right\}}{\cosh(\pi\zeta)}(a)^{1/2} \qquad [1.44]$$

or,

$$K_{Ii} = \sigma_0 Q_{Ii} a^{1/2} \qquad [1.45]$$

and

$$K_{IIi} = \sigma_0 \frac{\left\{-(2\pi)^{1/2}\left[\sin(\zeta \ln 2a) + 2\zeta \cos(\zeta \ln 2a)\right]\right\}}{\cosh(\pi\zeta)}(a)^{1/2} \qquad [1.46]$$

or,

$$K_{IIi} = \sigma_0 Q_{IIi} a^{1/2} \qquad [1.47]$$

These relationships can simply be recast into an equation of the form $K=Q\sigma_0 a^{1/2}$, as in the case of a crack in a bulk material. However, now there are K_{Ii} and K_{IIi} terms. Also, there are now two geometry factors, Q_{Ii} and Q_{IIi}, which may be a function of the bimaterial constant.[2] More importantly, there is still a logarithmic term of a dimensional parameter, a, in Equations 1.45 and 1.47. Thus, Q and K are dependent upon the units of a, and this makes it extremely difficult to evaluate the Mode I and II contributions independently.

Several researchers have suggested that for cracks at or near the interface, a combined interfacial stress intensity factor, K_{ic}, can be defined for crack growth:[98]

$$K_{ic} = \left(K_{Iic}^2 + K_{IIic}^2\right)^{1/2} \qquad [1.48]$$

This approach not only combines Mode I and Mode II, but it also eliminates the length term. Thus, the values of K_{ic} may be obtained without the ambiguity of the previously mentioned complications. For the situation of applied tensile stresses only:

$$K_{ic} = Q_i \sigma_c a^{1/2} \qquad [1.49]$$

where Q_i is now the relevant geometry factor.

It is important to understand that the above proposals are supported by only a limited amount of experimental evidence.[99] Also, it should be apparent from the development of these proposals that applying the stress intensity approach to bonded systems results in many difficulties. For this reason, many scientists have utilized the energy balance approach when studying crack growth in adhesive systems. However, if the difficulties in the stress intensity factor approach can be solved, it has the potential to be more valuable than the energy balance approach for engineering design and lifetime prediction.[2]

1.4.2.4 Relationships Between G and K

In LEFM, the fracture energy, G_c, and the stress intensity factor, K_c, can be related. Consider the case of a crack in a homogeneous body, where a simple relationship exists between G and K, under plane strain conditions. This equation is given by:[93,100]

$$G_c = \frac{(1-\nu^2)}{E} K_{Ic}^2 + \frac{(1-\nu^2)}{E} K_{IIc}^2 + \frac{(1-\nu^2)}{E} K_{IIIc}^2 \qquad [1.50]$$

or equivalently:

$$G_c = G_{Ic} + G_{IIc} + G_{IIIc} \qquad [1.51]$$

where, for Mode I:

$$G_{Ic} = \frac{K_{Ic}^2}{E} \qquad \text{(plane stress)} \qquad [1.52]$$

and,

$$G_{Ic} = \frac{K_{Ic}^2}{E}(1-\nu^2) \qquad \text{(plane strain)} \qquad [1.53]$$

For a crack in the center of an adhesive layer, and not in the vicinity of the interface, the above equations are still valid.[100] By utilizing the appropriate value of the tensile modulus of the adhesive, E_a, G(joint) and K(joint) can be correlated. For plane strain conditions:

$$G_{Ic}(joint) = \frac{K_{Ic}^2(joint)}{E_a}(1-\nu_a{}^2) \qquad [1.54]$$

For a crack at an interface, no clear relationship has been established. However, multiple researchers have suggested that the appropriate value of the modulus is some weighted average of the moduli of the materials which form the interface.[47, 98, 101] G_{ic} and K_{ic} may then be related by:

$$G_{ic} = K_{ic}^2 \cdot \frac{1}{2}\left(\frac{1}{E_a}+\frac{1}{E_s}\right)\left(\frac{2\alpha_m - 1}{\alpha_m^2}\right) \qquad [1.55]$$

where

$$\alpha_m = \frac{\xi+1}{\chi+1} \qquad [1.56]$$

and,

$$\xi = \frac{E_s}{E_a} \qquad [1.57]$$

$$\chi = 1+\frac{E_s}{2}\left(\frac{1+\nu_a}{E_a}-\frac{1+\nu_s}{E_s}\right) \qquad [1.58]$$

It should be noted that the exact form of these relationships is very important. Although it may not appear in the final form of the equation, the relationships are often derived using a modulus term. Obviously the correct modulus term must be used.[2] In relation to this, another important point should be mentioned. There are no relationships readily available for the case of a crack not actually at, but very close to, the interface. The correct modulus term would most likely be an average based on the moduli of the bulk and interface.[2]

1.4.3 The Double Cantilever Beam Fracture Specimen

When properly analyzed, the conventional double cantilever beam fracture specimen, illustrated in Figure 1.7, can be used to ascertain much useful information about the failure characteristics of adhesively bonded systems. While it has been extensively and successfully used in the testing and analysis of composites, it has, until recently, received relatively limited use in the evaluation of structural adhesive materials.[102-103] Rather, the tapered double cantilever beam specimen (TDCB) has been utilized, mainly because it offers a constant strain energy release rate testing configuration. During the introduction of fracture mechanics into the testing and analysis of adhesive bonds, the TDCB joint was used extensively by Mostovoy and Ripling.[104]

From the widespread use of the conventional DCB specimen in the composites industry, many corrections for ideal beam theory, or alternate methods of analysis, have been derived. These allow calculation of the strain energy release rate from experimental data.[102-103,105-111] The need for a new analysis method arises, however, because of the notable discrepancies that exist between ideal beam theory and the actual (experimental) performance of adhesively bonded DCB specimens.[71,112] For example, crack tip rotations and deflections are rarely zero, large deflections of the cantilever arms are often observed, and end blocks or tabs are often used to aid in loading the specimen. Although some of these corrections could possibly be used to properly evaluate adhesively bonded DCB joints, another method of analysis exists that is often easier to implement and

usually generates more accurate results. This analysis technique is known as the compliance method. It will be presented in more detail (Section 1.4.3.2.1).

1.4.3.1 Fracture Characteristics of The Double Cantilever Beam Specimen

The DCB joint can be tested under a wide variety of loading conditions, each offering an entirely different set of behavior characteristics. These unique behavior characteristics can be used to conduct different types of tests with the same joint geometry. For example, the research reported in this dissertation uses the same DCB joint geometry, with two different loading conditions, to conduct static and fatigue evaluations. The static DCB tests are carried out in displacement control to take advantage of the stability of the joint under this loading condition. The fatigue DCB tests utilize either displacement or load control. Displacement control is used to more accurately establish the existence and location of threshold values. Load control tests are used to determine the failure characteristics of adhesive joints, away from threshold values, while minimizing the effects of plastic zones at the crack tip. Lastly, while not utilized in this work but worth mentioning here, a unique loading arrangement for the conventional DCB joint has been developed by D. Dillard and coworkers.[71] It produces a nearly constant strain energy release rate without the extensive sample preparation needed with the TDCB test. These loading conditions and their respective DCB fracture characteristics as a function of crack length are given in Figure 1.8.

It may be considered a disadvantage in some instances that the conventional DCB joint is not a constant SERR test. For example, constant SERR evaluations are particularly amenable to long term durability investigations. However, it can also be advantageous to have the G_{Iapp} vary naturally with crack length. In short term static and fatigue studies, the number of test alterations performed by the researcher can therefore be minimized.

1.4.3.2 Analysis of Double Cantilever Beam Data

As previously mentioned, there are many possible methods available for analysis of data collected with the double cantilever beam test. The raw quantities obtained consist of the applied load (P), the crack length (a), and the opening deflection at the point of load application (Δ). For the purposes of this work, the applied strain energy release rates are determined from which the critical strain energy release rates are calculated. For the fatigue DCB tests, crack growth rates are determined, as well as a function of the applied cyclic strain energy release rates.

An analysis method which will accurately and easily compute these results, for both the quasi-static and fatigue tests, has been determined and extensively studied by Rakestraw and coworkers.[112] The derivation of this method is presented in the following three sections, however in somewhat less detail than in the original publications. In the derivation, comparisons are made with other analysis techniques to demonstrate the utility of the present technique.

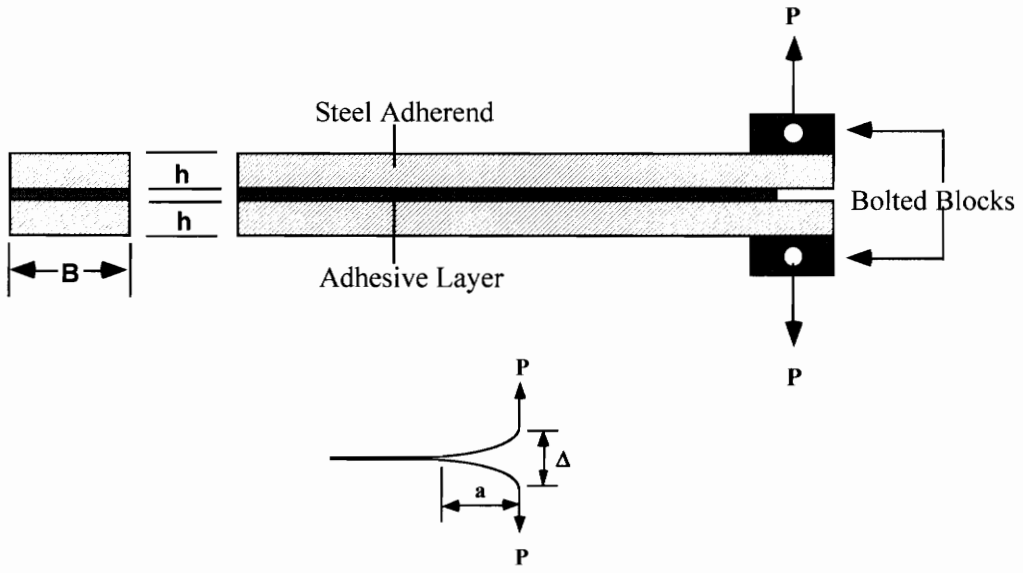

Figure 1.7 Schematic of the DCB specimen (deformed geometry inset).

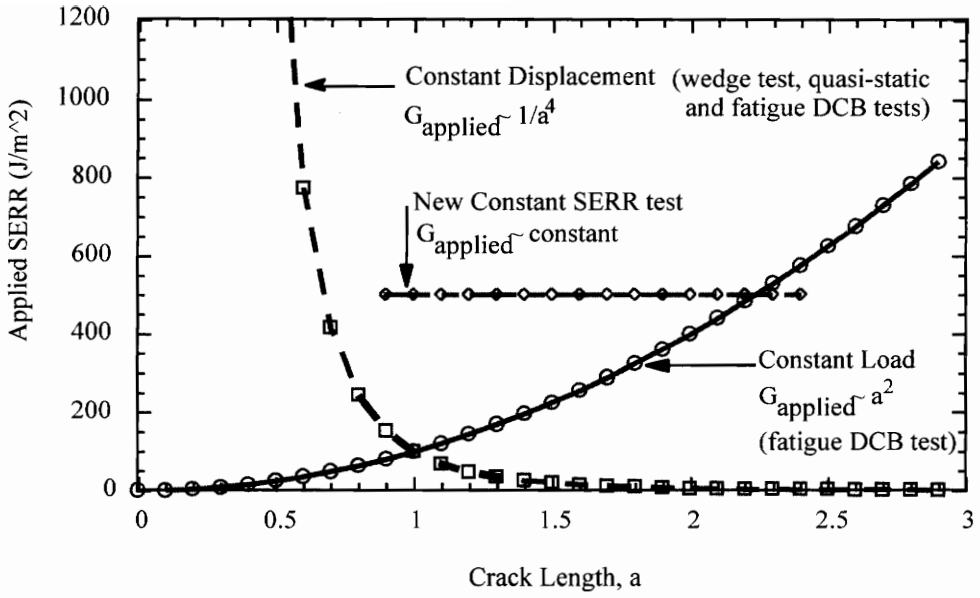

Figure 1.8 Response of the DCB joint under various loading conditions.

1.4.3.2.1 The Compliance Method

Of the many data analysis methods available for the conventional DCB specimen, the compliance method is the most basic since it computes the strain energy release rate from the most fundamental definition for linear systems.[102-103,105-111] The equation for G, based on compliance, is given below:

$$G = \frac{P^2}{2}\frac{\partial C}{\partial A} \qquad [1.59]$$

where P is the load applied to the specimen, C is the compliance of the specimen, and A is the area created during crack growth. Assuming that the width of specimen is constant, Equation 1.59 can be expressed as:

$$G = \frac{P^2}{2B}\frac{\partial C}{\partial A} \qquad [1.60]$$

where a is the crack length (defined as the distance from the point of load application to the debond tip) and B is the specimen width.

Since the load values are experimental numbers, all that is needed is a relationship that accurately defines the compliance of the specimen as a function of its crack length, then simply differentiate that relationship with respect to the crack length. Ignoring the compliance of the thin adhesive layer and any beam-on-elastic-foundation (BEF) effects, ideal beam theory predicts that the P-Δ-a relationship for the DCB joint is:

$$C = \frac{\Delta}{P} = \frac{2a^3}{3EI} \qquad [1.61]$$

where Δ is the specimen opening at the point of load application, E is the modulus of elasticity of the adherends, and I is the moment of inertia of the adherends ($I = bh^3/12$ for rectangular cross-sections). Thus, the Mode I strain energy release rate for the DCB specimen becomes:

$$G_I = \frac{P^2 a^2}{BEI} \qquad [1.62]$$

Rearrangement of Equation 1.61 yields:

$$C^{1/3} = \left(\frac{\Delta}{P}\right)^{1/3} = \left(\frac{2}{3EI}\right)^{1/3} a \qquad [1.63]$$

Equation 1.63 suggests that the cube root of the compliance of the DCB specimen is a linear function of crack length passing through the origin and having a slope determined by the size, shape, and type of material used as the adherend.

When a typical data set from this dissertation research is evaluated (i.e., formulation C2, cure temp = 170 °C, collected as described in Chapter 2), the experimental results do not conform well to Equation 1.63. However, as shown in Figure 1.9, the data does appear to form a fairly straight line, even if it does not pass through the origin. Therefore, the experimental data must be fit according to:

$$C^{1/3} = \left(\frac{\Delta}{P}\right)^{1/3} = m \cdot a + b \qquad [1.64]$$

where m is the slope of the experimental data and b is the y-intercept. When modeled by Equation 1.64, it is found that the data produces an exceptional linear fit (r^2 is typically 0.999), with b not equal to zero. The actual slope does not agree with the slope predicted by beam theory either. Beam theory predictions are shown in Figure 1.9, along with the experimental data to illustrate the observed differences. It should be noted at this point that the raw experimental data, such as those used to prepare Figure 1.9, is not presented in this dissertation. Rather, only the final calculated SERR values are given. The raw data shown serve only to aid in the description of the data analysis process.

The ideal beam theory $(\Delta/P)^{1/3}$ predictions, shown in Figure 1.9, are consistently low compared to the experimental data, even though they do approach the experimental data near the end of the specimen. These differences serve to further demonstrate the need for a better method of analysis.

A more detailed examination of the data shows that differences in ideal beam theory and experimental $(\Delta/P)^{1/3}$ values have an average discrepancy of about 6%. Individual discrepancies range from 1 to 18% depending on the associated crack length. It is important to remember that this is only the first step in the data analysis process, and all subsequent calculations will significantly magnify this error (based on Equations 1.69

and 1.70). Using ideal beam theory to analyze the DCB specimen can be ineffective since comparison between SERR predictions is likely to be meaningless.

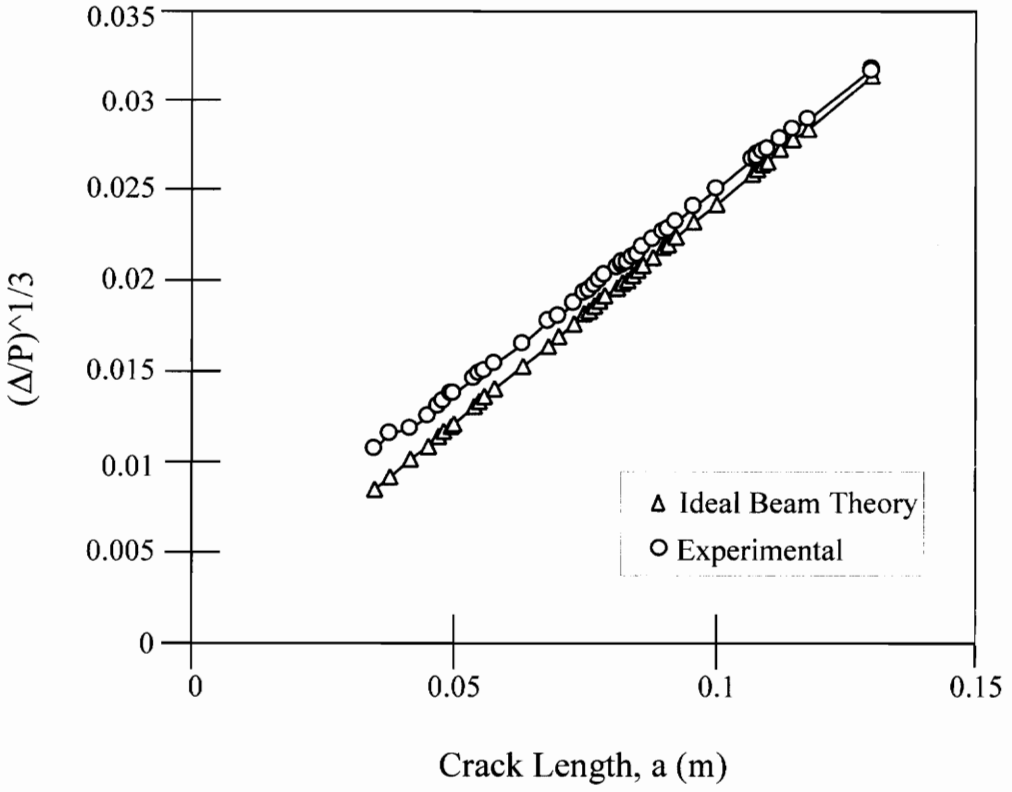

Figure 1.9 Typical DCB $(\Delta/P)^{1/3}$-a results and beam theory predictions.

1.4.3.2.2 Beam-on-Elastic-Foundation Analysis

As mentioned earlier, the differences between ideal beam theory predictions and the actual data are due to incorrect assumptions made in ideal beam theory. The most significant is the basic assumption that the arms of the DCB specimen act as built in cantilever beams. That is, the deflection and rotation of the arms is zero at the crack tip (i.e., at a = 0). Instead, the arms have *both* deflections and rotations at the crack tip and

thus act more like beams on an elastic foundation. Researchers have derived elaborate closed form beam-on-elastic-foundation analysis techniques for the DCB specimen.[108-111] However, as Figure 1.10 shows, these do not model the mechanical behavior of the specimens as well as the compliance method. Figure 1.10 depicts the $(\Delta/P)^{1/3}$ predictions from References 58 and 60 where the actual measured crack length values were used to make all predictions. It must be stated again that the SERR predictions may have an even greater error than those shown in Figure 1.10 since this is only the first step in the calculation of G. Also, Figure 1.10 shows how accounting for shear deformations has no influence on the classical beam theory predictions.

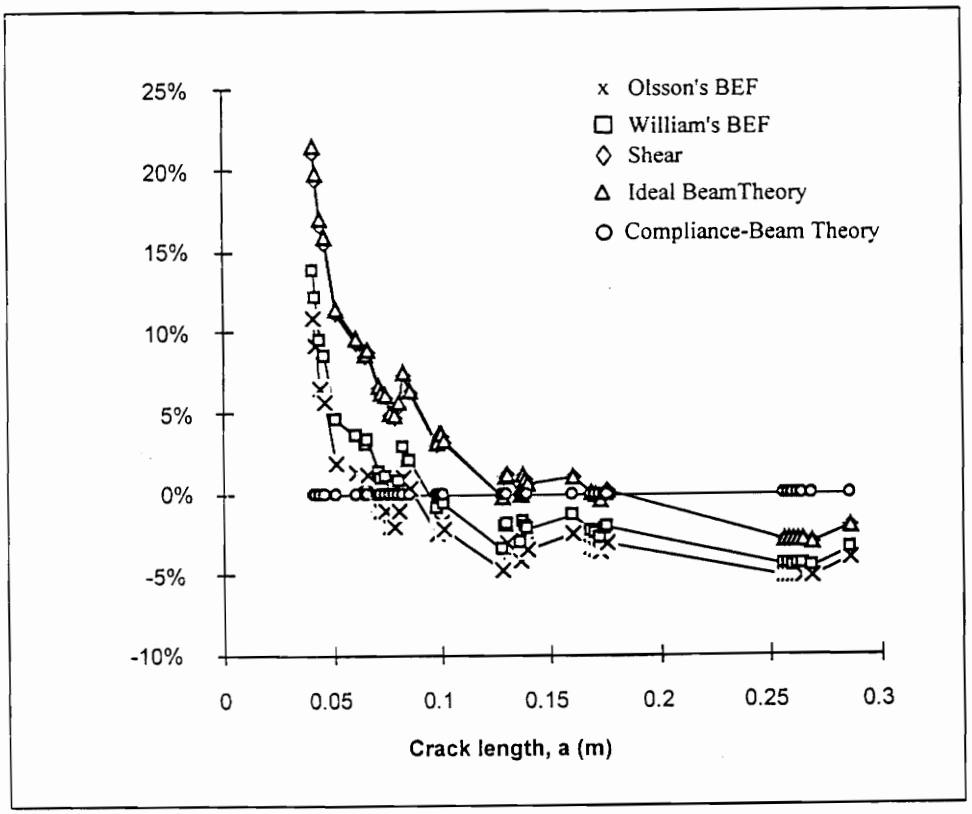

Figure 1.10 Comparison of $(\Delta/P)^{1/3}$ predictions from various theories.

1.4.3.2.3 A Compliance-Beam Theory Model

Although the compliance method of analysis for a DCB joint has been proven to be very accurate, using it in a forceful manner can sometimes hide what is actually happening within the DCB specimen. Therefore, the analysis technique should be reformulated such that the response of the specimen is described in more detail. The best choice of mathematical models for accomplishing this is ideal beam theory, since the concepts are rather simple compared to other analyses and the behavior is easier to visualize (the contribution/influence of each term).

In this section of the dissertation, the compliance analysis technique is formulated so that it closely resembles the ideal beam theory analysis. This facilitates further identification of discrepancies between ideal beam theory and the experimental data as described by the compliance method. The goal is to obtain equations for the compliance method that have forms similar to Equations 1.61 and 1.62.

The first step in the development of a compliance-beam theory model is the comparison of similar equations from each theory. By equating the quantities associated with the crack length, a, in Equations 1.63 and 1.64, and rearranging, a new term is defined:

$$(EI)_{eff} = \frac{2}{3m^3} \qquad [1.65]$$

$(EI)_{eff}$ is the *effective* flexural rigidity of the DCB specimen as defined by the experimental data. Note that $(EI)_{eff}$ is defined for the *entire* specimen, not just for the arms.

Next, examination of Figure 1.9 shows that if the experimental data is extrapolated to intersect the crack length axis, the intersection does not occur at the origin. Instead, the crack length appears to be slightly longer than measured. This makes sense intuitively since the crack tip rotations and deflections that are present would be expected to inflate the deflection at a given load and measured crack length. In

order to make beam theory fit, a crack length adjustment is needed to get the predicted deflections to approach the values obtained experimentally. Therefore, an *apparent* crack length offset is introduced. Equation 1.64 is used to evaluate the necessary crack length offset for each specimen by determining where the line of the experimental data intersects the a-axis. Mathematically this produces the following:

$$x = \frac{b}{m} \qquad [1.66]$$

where x is the *apparent* crack length offset as defined by the experimental data.

The parameters defined in Equations 1.65 and 1.66 depend on many factors, including bond thickness, adhesive and adherend material properties, and possibly even the bond strength. Typical values of x and $(EI)_{eff}$ encountered in this research (i.e., formulation C2, cure temp = 170 °C) were x = 0.010 m and $(EI)_{eff}$ = 148 N·m^2. Ideal beam theory assumes values of 0 m and 110 N·m^2, respectively. It should be noted that the values for $(EI)_{eff}$ are somewhat higher than might be expected. This is, however, of little concern when computing the strain energy release rate values since the basic definition of G is still being used. Only the *form* of the expressions used to obtain the values of G is changing, not the values.

Now, by substituting Equations 1.65 and 1.66 into 1.64, an equation is obtained for the compliance of the DCB specimen. It is based on the compliance method, but resembles the beam theory equation for compliance (Equation 1.61):

$$C = \frac{\Delta}{P} = \frac{2(a+x)^3}{3(EI)_{eff}} \qquad [1.67]$$

The only differences between the two equations are that the cubed quantity in 1.61, namely the crack length, is now the measured crack length plus the apparent crack offset

quantity, x. The product (EI) is replaced by the effective flexural rigidity of the entire specimen, $(EI)_{eff}$.

By differentiating Equation 1.64 with respect to the crack length, a, and substituting the result into Equation 1.60, the compliance method working equation for the DCB strain energy release rate is obtained:

$$G_I = \frac{3mP^2}{2B}(m \cdot a + b)^2 \qquad [1.68]$$

By further substituting Equations 1.65 and 1.66 into 1.68, an equation for the DCB strain energy release rate, that closely resembles the SERR equation obtained from ideal beam theory (Equation 1.62), is produced:

$$G_I = \frac{P^2(a+x)^2}{B(EI)_{eff}} \qquad [1.69]$$

This equation is useful when load control is being used. However, an equation based on displacement control is also needed. This is obtained by solving for P, in Equation 1.67, and substituting the result into 1.69. The result is given below:

$$G_I = \frac{9\Delta^2(EI)_{eff}}{4B(a+x)^4} \qquad [1.70]$$

This result is analogous to the ideal beam theory SERR equation for displacement control.

From these relationships it is apparent why the DCB joint behaves as it does when certain loading conditions are applied to it. Equation 1.69 shows that under constant load conditions the applied SERR increases with any crack growth, while

Equation 1.70 shows that constant displacement conditions result in a lowering of the applied SERR when the crack grows.

A major advantage of the compliance-beam theory method of analysis for the DCB specimen is that *the number of crack length readings required to acquire accurate SERR predictions is greatly reduced.* Usually it is necessary to obtain a crack length reading at every point during the test for which an SERR prediction is desired. This can be almost impossible if the crack is growing rapidly. Also, it may be difficult to visually determine exactly when the crack starts to grow. With this method the computer is allowed to acquire a large set of load and deflection data points, and then a few manually acquired crack length readings are used to determine the experimental parameters in Equation 1.64, namely b and m. These parameters are used with either Equation 1.64 or 1.67 to predict crack length values associated with the load-deflection readings at which no crack length values were acquired. Thus, an accurate SERR prediction for any load-deflection data set can be made.

In summary, the following steps are required to complete the compliance-beam theory data analysis technique for the quasi-static or fatigue DCB tests:

1) Perform a linear regression on the experimental data containing crack length readings. Determine the coefficients m and b in Equation 1.64.

2) Use Equations 1.65 and 1.66 to compute x and $(EI)_{eff}$.

3) Use Equation 1.64 or 1.67 to predict crack lengths for all data sets acquired.

4) Use Equation 1.69 or 1.70 to compute the SERR associated with each data set.

5) Sort the data to determine the critical SERR values.

When the DCB joint is analyzed in the manner just described, the compliance-beam theory method of analysis will automatically account for geometric and material

behavior that deviates from ideal beam theory and other more complicated analysis techniques. It is an accurate mathematical model of the specimen behavior and provides more exact predictions of the applied SERR. Very important to this study is the fact that the analysis technique is equally applicable to the analysis of static or fatigue testing of DCB joints, as indicated in Figure 1.11. This figure, which is analogous to Figure 1.9 for static DCB testing, depicts the results of applying this analysis technique to fatigue data. Although the maximum cyclic loading values (Δ_{max} and P_{max}) are now used, the data can still be modeled to a high degree of accuracy with a straight line.

1.4.3.3 Supplemental Fatigue Data Analysis

For the quasi-static DCB data analysis, all that is necessary is to compute the relevant SERR values and determine which are important (e.g., crack initiation or arrest values). For the DCB fatigue tests the data analysis must be taken one step further. This section summarizes the additional data analysis required for the fatigue data and introduces, briefly, the mathematical model used to characterize the fatigue crack growth. For a more detailed description, see References 71 and 112.

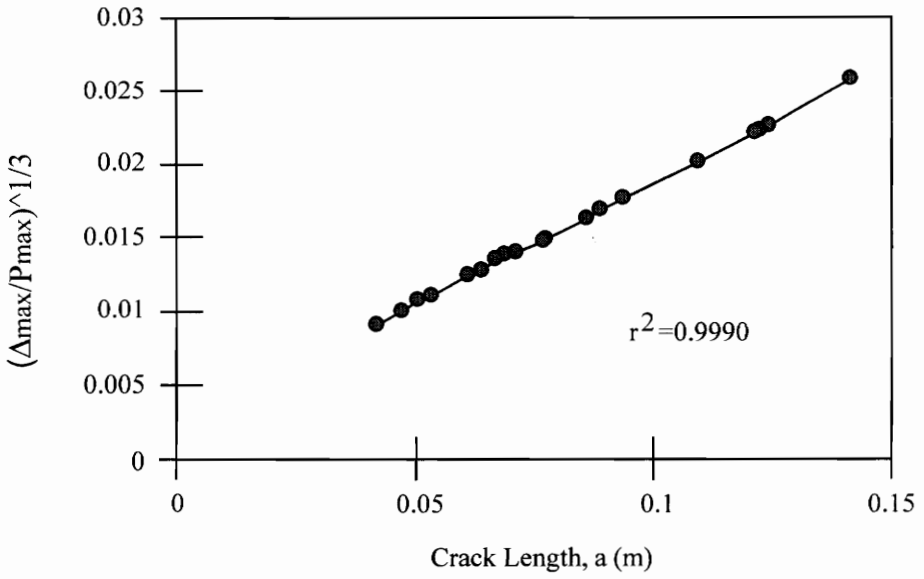

Figure 1.11 A typical $(\Delta_{max}/P_{max})^{1/3}$ -a plot from fatigue test data.

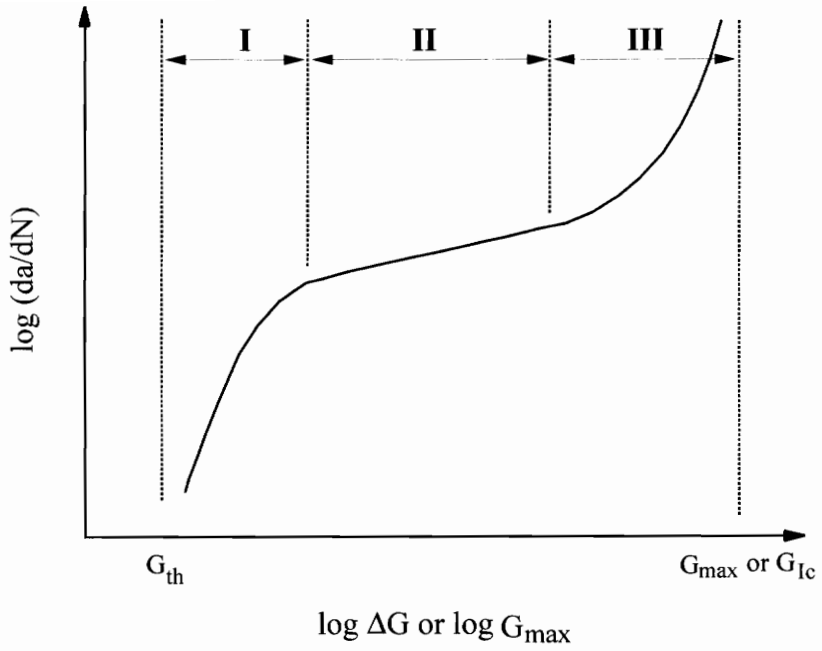

Figure 1.12 A typical fatigue crack growth curve.

A graph showing the typical trends in the fatigue crack growth data is depicted in Figure 1.12. Many fatigue crack growth models have been offered to describe such information. Some are based on empirical observations while others are based on more rigorous theoretical foundations. The model chosen for this research is the widely used empirical equation of Paris and Erdogan. It is expressed as follows:[113]

$$\frac{da}{dN} = C\left(G_{\text{Imax}}\right)^{n} \qquad [1.71]$$

where a is the crack length, N is the number of cycles, and G_{Imax} is the maximum applied cyclic strain energy release rate. C and n are considered system constants and are determined from the experimental data. The constants C and n may be a function of

load, frequency, environment, and R-value. Higher values of C or n indicate that an adhesive system is more susceptible to fatigue crack growth. A high value of n is especially notable because it means a slight change in loading can cause a significant increase in the fatigue crack growth rate thus making the system highly unstable if cracking ever begins. It should be noted that ΔG is often used in the place of G_{Imax} in Equation 1.71. However, recent research suggests that G_{Imax} is a better parameter for use in characterizing the fatigue behavior of adhesively bonded systems.[114-115] The choice of this convention, however, does not significantly alter the results.

The fatigue crack growth model of Equation 1.71 is intended to model the linear portion of Figure 1.12 in Region II. Thus, when trying to determine the constants C and n, care must be taken to ensure that the experimental data from Regions I and III are not present in the data being analyzed. This requires judgment on behalf of the researcher as to where one region ends and another begins, or even if the data can be represented by this model at all. For a more detailed survey of fatigue crack growth models, see References 116 and 117.

A threshold value such as the one depicted in Figure 1.12 may, or may not, be exhibited by a particular material system. Furthermore, attempting to accurately determine if, and where, a threshold value exists on the fatigue crack growth curve may be inhibited by the time and resources required to do so. Some researchers therefore choose to assign the title threshold to very small crack growth rates (usually $< 10^{-8}$ mm/cycle).[118-120] It must be remembered, however, that crack growth may still be occurring and a true threshold value may not have been reached.

After the data analysis procedure has been carried out, the central difference method is used to calculate the terms da, dN, and G_{Imax} for the i^{th} time interval of the fatigue test according to:

$$(da)_i = (a)_{i+1} - (a)_{i-1}$$
$$(dN)_i = (N)_{i+1} - (N)_{i-1}$$
$$(G_{\text{Imax}})_i = \frac{(G_{\text{Imax}})_{i+1} + (G_{\text{Imax}})_{i-1}}{2} \qquad [1.72]$$

Calculating $(da/dN)_i$ is then trivial. The forward and backward difference methods were also investigated, and each produced results almost identical to those of the central difference method. However, since the central difference method is a higher order numerical technique it is chosen as the preferred method.

Next, (da/dN) is plotted versus G_{Imax} on a log-log graph to see if the data follows the expected trend of the fatigue crack growth curve, as shown in Figure 1.12. If it does, the data values from Region II are used to calculate C and n. This is accomplished by performing a linear regression:

$$\log\left(\frac{da}{dN}\right) = n \cdot \log(G_{\text{Imax}}) + C^* \qquad [1.73]$$

C is then calculated by:

$$C = 10^{C^*} \qquad [1.74]$$

Finally, if a G_{th} exists it may be estimated from the da/dN-G_{Imax} graph, a graph which provides a great amount of information about the adhesive system. Although the preceding fatigue data analysis procedure may seem cumbersome, it is actually rather easy to execute and is very amenable to spreadsheet analysis. Once familiar with the data analysis technique, and valid fatigue data have been obtained, it usually takes only a few minutes to obtain the da/dN-G_{Imax} curve along with the system constants C, n, and G_{th}.

1.4.4 The Notched Coating Adhesion Test

As discussed earlier in Section 1.4, the utilization of fracture mechanics concepts can be quite beneficial in the evaluation of adhesive system performance. Fracture mechanics concepts have been applied successfully to the assessment of adhesive toughness, in the determination of bond failure mechanisms, and in the estimation of the service life of flawed structures.[2] Of particular interest to this dissertation work, fracture mechanics based tests have been proven to be highly sensitive to performance variations caused by even minute system variations. Thus, they are well suited for the evaluation of performance changes that result from the alteration of cure conditions, adhesive composition, or substrate surface pretreatments.

Dillard and coworkers have long realized the value of fracture tests in the study of adhesive system performance. They have contributed significantly to our knowledge in the field through extensive analysis of the DCB specimen, the blister and peel test geometries, and the CLS test specimen.[121-123] Also, this research team recently developed another fracture based test for thin adhesive coatings.[123] It is termed the notched coating adhesion (NCA) test and is utilized in this dissertation as a comparative method to the DCB analyses. The NCA geometry is also extremely useful in accelerated durability studies, although it is not used here for that purposed.

The NCA test specimen is quite simple. It consists simply of a uniform, thin layer of adhesive bonded to a single, stiff substrate. A schematic of the specimen is given in Figure 1.13. For testing, a notch is introduced into the adhesive, at the center point, using a small saw and a razor blade. Due to the local stresses, the adhesive layer debonds and sharp cracks are produced at the interphase. The specimen is then loaded, under axial tension (perpendicular to the crack), and the stress causes the adhesive debonds to propagate. Since the specimen is constant in SERR, the debonding does not alleviate the applied strain energy and debonding thus continues at a rapid rate. Using an extensometer, the critical strain at which the debonds propagate is recorded. The critical SERR is then calculated from the critical strain.

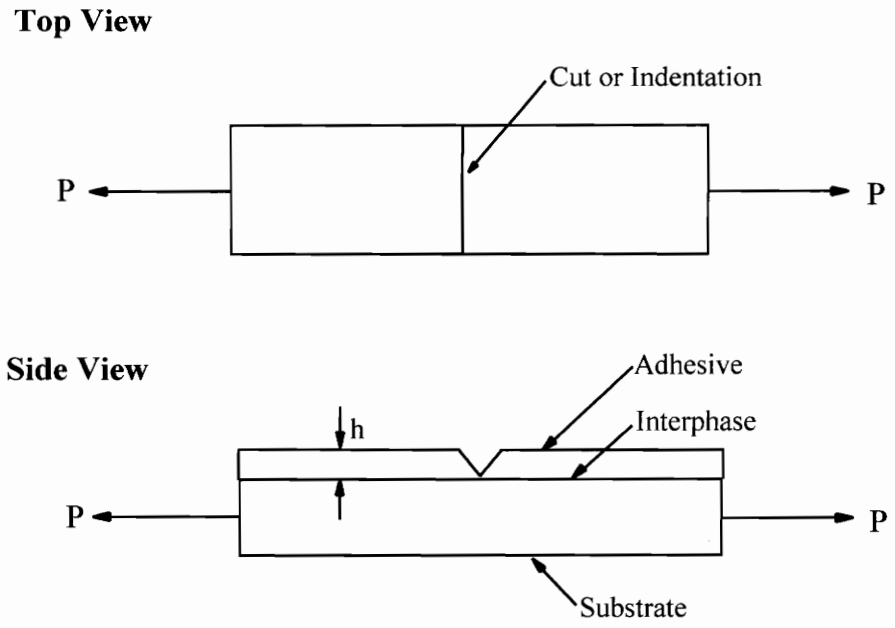

Figure 1.13 Schematic of the NCA test specimen.

If the modulus and stresses are assumed to be uniform across the thickness of the adhesive, and if the specimen is assumed to be semi-infinitely long, the SERR can be derived. This is accomplished by accounting for the residual stress components and the stress caused by the load. The equation for the SERR is thus given as follows:

$$G_c = \frac{Zh}{E}\left[\left(\sigma_t + \sigma_m + \varepsilon E\right)^2 + \left(\sigma_t + \sigma_m - \nu\varepsilon E\right)^2\right]\left[1 + \frac{hE}{HE_s}\right] \qquad [1.75]$$

where Z is the dimensionless driving force, σ_t is the residual biaxial stress due to curing, σ_m is the residual biaxial stress due to moisture swelling, ε is the applied uniaxial tensile

strain, E is the effective modulus of the adhesive, E_s is the modulus of the substrate, H is the substrate thickness, h is the adhesive thickness, and ν is Poisson's ratio.

The SERR obtained through calculation with Equation 1.75 is the total SERR of the system (the combination of Modes I and II). However, if the specimen is modeled as a layered bi-material, where the adhesive is a very thin layer on a very thick substrate, the individual contributions can be elucidated. This is accomplished by applying Hutchinson and Suo's layered bi-material analysis.[123] It expresses the mode mixity as follows:

$$\text{Mode II / Mode I} = (\text{Tan } 52°) = 1.6 \qquad [1.76]$$

Although Chang and coworkers are still involved in a detailed development and analysis of this specimen, it appears at present that it works extremely well for evaluation of interfacial adhesive performance.[123] The NCA results obtained in this dissertation research, presented later in Chapters 3-5, are in good agreement with the DCB results. The NCA analyses, however, offer several advantages over use of the DCB specimen. A typical NCA evaluation takes only 5 min for data collection and analysis, whereas the DCB testing process takes about 2-3 hours. Also, the DCB specimen is more difficult and labor intensive to accurately fabricate.

1.5 Statement of The Research Problem

Dicyandiamide is a widely used latent curing agent in heat cured epoxy adhesives. It has been utilized since the 1940s when epoxy resins were first commercially introduced.[52-53] Since that time a great deal of effort has been focused on deciphering the dicy/epoxy reaction mechanisms. These complex schemes, however, still remain to be fully established. Much time and effort has been exerted, as well, in evaluating the influence of formulation variables and reaction conditions on the bulk mechanical properties of dicy/epoxy systems. It has been demonstrated that small changes in these parameters can result in drastic changes in the mechanical properties of the cured materials.[59, 63-66]

In addition to the perplexity involving the dicy/epoxy reaction mechanisms and structure-property relationships, questions have arisen as a result of the use of reactive rubber toughenners. This has been due, mainly, to a lack of information concerning the mechanics and mechanisms by which toughenners actually improve the bulk fracture performance of adhesives. For example, the influence of energy-dissipating deformations occurring near the crack tip are not well understood. Furthermore, the addition of rubber, which has a relatively low glass transition temperature, results in an adhesive that is more sensitive to temperature and loading rate fluctuations. Consequently, considerable research has been, and still is, directed toward addressing these questions.

Because of the difficulties associated with the bulk material studies, only limited research has progressed to the point of evaluating bonded system performance in relation to formulation and cure condition variations. The studies that have been conducted, unfortunately, have focused on bonded systems that fail cohesively through the adhesive layer. Thus, they have not provided much additional information beyond typical bulk mechanical performance evaluations. The changes that have taken place at the adhesive/substrate interphase (as opposed to in the bulk of the material), and their influences on the bonded system performance, have been completely neglected. Since the failure of structurally bonded systems often occurs at the interphase, especially when

the system has been subjected to harsh environments, it is obvious that much useful and valuable information has been overlooked.

This dissertation examines the adhesive performance of dicy cured epoxy/steel adhesive systems. With a specific focus on interfacial fracture, and through the combination of concepts from chemistry, fracture mechanics, spectroscopy, and microscopy, it provides a unique contribution to the science of adhesion. From a mechanics perspective, a new methodology is developed for testing and analysis of the conventional DCB specimen. The results are verified for interfacial fractures, and a comparative evaluation is given with respect to other fracture and static strength based tests. This methodology serves, throughout the dissertation, as the basis for mechanical testing and analysis. From a chemistry perspective, the influences of several variables, already known to affect the bulk mechanical performance and suspected to affect the epoxy/steel interphase region, are investigated. These variables are, specifically, changes in the toughener level, variation of the dicyandiamide content, and alteration of the cure temperature. Bulk mechanical measurements are conducted to provide background information for comparison with the bonded system fracture data, thus allowing subtraction of bulk mechanical property changes from changes in the adhesive system performance. Spectroscopy and microscopy analyses are also conducted on the neat adhesives and failed fracture specimens to decipher the chemical changes that have occurred. These function, as well, to provide some insight into the locus of, and reasons for, adhesive system failure.

Chapter 2

Experimental

2.1 Adhesive Components and Preparation

The model epoxy systems are composed of a liquid bisphenol A-type resin, a curing agent, a cure accelerator, a filler, and an epoxy terminated elastomeric copolymer. The following is a brief description of these components.

D.E.R. 331 This is a "standard" low molecular weight liquid bisphenol A-type resin available from The Dow Chemical Company. It is used mainly for potting, adhesives, electrical laminates, and civil engineering. Some of the properties are shown below:

Epoxide Eq Wt	182-192 g/eq
Viscosity	11,000-14,000 mPa s
Volatility	100% Non-Volatile

DICYANDIAMIDE Dicy is a solid curing agent, which, when milled into liquid epoxy resins, provides one-package stability for up to six months at ambient temperatures. Cures occur with heating. A tertiary amine accelerator is necessary if rapid cures are desired. Dicy is latent, thus allowing the advantage of curing to the desired result (e.g., "B-Staged" state used in pre-preg applications).

PDMU 3-phenyl-1,1-dimethyl urea is a tertiary amine accelerator for dicy-cured epoxies. The use of 2-3 parts per hundred reduces the curing temperatures of such systems from 177 °C to about 121 °C. Simultaneously, the curing time is reduced. Some properties of this material are given below:

Melting Point	129-135 °C
Solubility	3850 ppm @ 25 °C in Water
	3-7 g in 10 mL acetone @ 25 °C
Stability	Stable to oxidation and moisture.

M-5 SILICA M-5 is a slightly acidic, hydrophillic fumed silica produced by the Cabot Corporation. It has a surface area of 200 (±25) m^2/g. It has a density of 0.0812 g/cm^3, and the particle diameter is 0.014 microns.

KELPOXY Kelpoxy G272-100 is a concentrate of an epoxy terminated elastomeric copolymer designed by Reichhold Chemicals as an additive or modifier to toughen epoxies, epoxy novalacs, and PVC plastisols. Epoxy resin blends containing Kelpoxy exhibit elastomer particles of .01-10 micron diameter which impede the propagation of cracks. The epoxide equivalent weight is approximately 340 g/eq.

The epoxy resins were prepared as follows: D.E.R. 331, dicyandiamide, and PDMU were carefully weighed into a 1 gallon Ross mixing pot. The pot was secured and mixing was initiated at a speed of approximately 18 rpm's. Once the dicyandiamide and PDMU were thoroughly mixed into the resin, the speed was increased to about 72 rpm's. A vacuum was employed at about 28 in. Hg, and mixing was continued for 15 min. Next, the fumed silica was added. The mixer was started at a low speed and increased to a setting of 100 rpm's only after the silica was well blended (wetted). The vacuum was again employed and mixing was continued for another 15 min. Lastly, the Kelpoxy was added. It was mixed with the resin for 5 min under vacuum, or until all air bubbles were pulled from the resin.

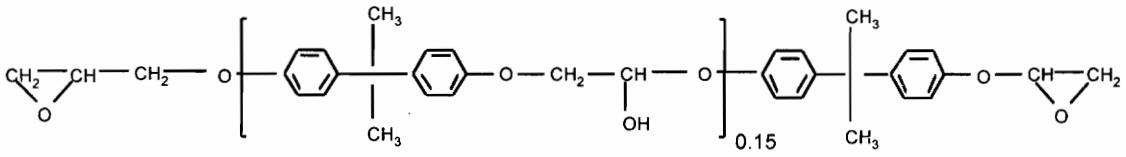

D.E.R. 331

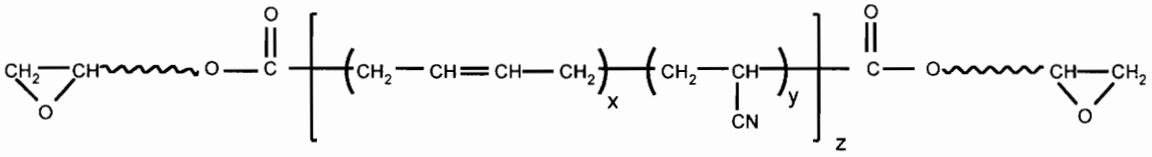

KELPOXY G272-100

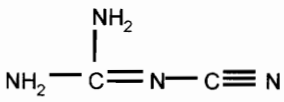

DICY

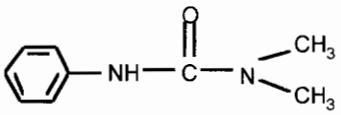

PDMU

Figure 2.1 Schematic representation of the chemical structures of the adhesive system components.

2.2 Neat Adhesive Studies

2.2.1 Tensile Testing

For the bulk adhesives, tensile specimens were utilized to determine the Young's moduli, and where necessary, the yield stresses (σ_y). ASTM type IV test specimens were cast in silicone rubber molds, sandwiched between steel plates to mimic the bonded system cure scenario, and cured at the appropriate temperature for 90 min. To remove small defects and produce more uniform specimens, the tensile bars were hand polished with various grades of sandpaper. All specimens were then stored in a desiccator until the time of analysis.

The analyses were conducted in accordance with ASTM D638 on a screw-driven Instron 4505 test frame.[124] The test temperature was 22 °C, and the relative humidity was approximately 20%. Unless otherwise stated, a constant crosshead displacement rate of 1 mm/min was used. The modulus of elasticity was determined from the slope of the initial linear portion of the stress-strain curve. The offset yield stress, σ_y, was defined as the stress at which a line having the same slope as the region used to obtain the modulus but offset on the strain axis by 0.2%, crossed the experimental stress-strain curve.

All tensile values reported in this dissertation represent averages of a minimum of five equivalent analyses.

2.2.2 Bulk Fracture Testing

Single-edge-notch bend (SENB) specimens were utilized to determine both the plane-strain fracture toughness values (K_{Ic}) and the strain energy release rate values (G_{Ic}) of the bulk adhesives. Specimens with the dimensions of 6.2 mm x 7.4 mm x 51 mm, depicted previously in Figure 1.4, were cut from a cured plate of the polymer using a diamond saw. This plate had been prepared by pouring liquid resin into a heated aluminum mold, followed by curing in a convection oven for 90 min at the appropriate temperature. To facilitate removal of the cured plate, the mold was sprayed with a release agent prior to use. All specimens were stored in a desiccator until the time of

analysis. Each was then precracked immediately prior to testing with a razor blade that had been dipped in liquid nitrogen.

Testing was conducted in accordance with ASTM D5045 on a screw-driven Instron 4505 test frame.[125] A constant crosshead displacement rate of 1 mm/min was used for these tests, and all calculations were based on the equations shown in Table 2.1.

Table 2.1 Single-edge notched bend equations from ASTM D5045.

Method 1	Method 2	Plane-Strain Validity Checks
$G_{Ic} = \frac{(1-\nu^2)K_{Ic}^2}{E_a}$	$G_{Ic} = \frac{U}{BW\phi}$	$B, a, (W-a) \geq 2.5\left(\frac{K_{Ic}}{\sigma_y^{max}}\right)^2$ $\frac{P_{max}}{P_Q} \leq 1.1$

The previously undefined terms in Table 2.1 are as follows: U is the energy associated with the area under the SENB load-deflection curves, B is the width of the specimens, W is the height of the specimens, a is the initial crack length, P_{max} is the maximum load sustained by the samples, P_Q is the load used to calculate K_{Ic} (defined in ASTM 5045), E_a is the modulus of elasticity of the adhesives, ν is Poisson's ratio, f is an energy calibration factor (a function of specimen geometry, and defined in ASTM 5045), and σ_y^{max} is the yield stress of the adhesives as defined by the maximum stress achieved in tensile tests.

Although the plane-strain SERRs for the bulk adhesives were calculated using both methods suggested in ASTM D5045, and shown in Table 2.1, only the values obtained using the energy method (Method 2) are reported in this dissertation. The values obtained from the two methods were usually within 15% of each other. Also, a displacement correction was used to account for the indentation of the specimens upon loading, and the plane-strain validity checks were confirmed. Finally, the SENB values presented in this work represent the averages of at least ten equivalent analyses.

2.3 Adhesive (Bonded) System Evaluations

2.3.1 Single Lap Shear Joint Strength Studies

In order to be able to make comparisons between fracture mechanics results and test geometries which are typically used in industry, single lap shear (SLS) specimens were also prepared and axially tested in accordance with ASTM D1002-72. These were prepared using 2.54 mm x 25.4 mm x 101.6 mm cold rolled steel coupons, with an acetone wipe surface pretreatment, and 0.254 mm glass beads as spacers to control the bond thickness. Glass beads (0.1 wt.%) were blended with the epoxy resin in a plastic bag, and the resin was applied over a 322.58 mm^2 area at one end of each coupon. The coupons were then pushed together and lightly clamped, and the excess adhesive was wiped from the sample. Curing was carried out in a convection oven for 90 min at the desired temperature. Testing was conducted on an MTS model 810 servo hydraulic testing system at a constant displacement rate of 12.7 mm/min. The test temperature was approximately 22 °C, and the relative humidity was approximately 20%. Tensile strengths were computed in accordance with ASTM D1002, and all values presented in this dissertation represent averages of at least ten equivalent evaluations.

2.3.2 Notched coating adhesion Studies

Notched coating adhesion specimens were prepared as follows: 1.5 mm x 12.7 mm x 100 mm cold rolled steel coupons were washed with acetone and stored in a

desiccator, for no longer than one hour, prior to coating. The adhesive was spread over the clean, dry surface with a spatula and was smoothed to the approximate desired thickness using a draw down bar. The coupons were then placed adhesive side up on a Teflon coated steel panel (6 mm x 254 mm x 254 mm) along with spacers of the desired film thickness. Finally, a second Teflon coated steel panel was placed on top forming a sandwich which was then tightly clamped. The whole arrangement was placed in a convection oven, at the desired temperature, and cured for 1.5 hours. After disassembly, the coated steel coupons were easily removed from the plates. The edges were polished with a belt sander, and the specimens were stored in a desiccator, or environmental chamber, until the time of analysis.

The analyses were conducted on a screw-driven Instron 4505 test frame and a 1/2" extensometer was used to monitor the strain. A loading rate of 1 mm/min was employed, and the temperature and humidity were held constant at 22 °C and 20%, respectively. Just prior to testing, the specimens were pre-cracked. This was accomplished by first notching the adhesive layer with a saw and then carefully prying it free of the metal substrate. Care was taken to minimize the amount of debonding which occurred during this procedure (5 mm in each direction was usually adequate). Refer to Figure 1.13 for a schematic of the NCA specimen.

A minimum of three equivalent analyses were used to compute each of the NCA values presented in this dissertation.

2.3.3 DCB Specimen Fabrication Procedure

Double cantilever beam specimens were prepared by adhesively bonding 6.4 mm x 25.4 mm x 184 mm coupons of cold rolled steel. After the adherends were cleansed with acetone, Teflon tabs and wire spacers were taped onto the ends (onto only one of the two pieces used in each specimen). The Teflon tabs, besides helping to control the bond thickness of the panels, aided in the formation of a "void" or pre-crack after being removed (once the cure process was complete). Heat resistant tape was used to hold the Teflon in place and also helped produce the sharp starter cracks. After the wire and

Teflon were in place, the adhesive was poured onto the surface of the steel and smoothed to the desired thickness (0.80 mm) with a clean spatula. Finally, the second adherend was placed on top of the steel plate containing the Teflon, wire, and adhesive. The resulting specimen was then placed in a preheated, programmable hot press and maintained at the desired cure temperature and a pressure of 33 mPa (4.8 psi) for a period of 90 min. After curing, the samples were removed from the press while still hot and allowed to cool slowly to room temperature. The resulting bonded specimens were then drilled, tapped, and polished as necessary for utilization in a specific test procedure (refer to Figure 1.7 for a schematic of the DCB specimen).

Between the surface cleansing process (an acetone wipe) and the panel bonding procedure, no special storage of the prepared panels was used. This was typically less than one hour in time, and there was no apparent surface corrosion on the steel panels prior to the cleaning or bonding processes.

As with all fracture tests, it was essential that the specimens contained sharp starter cracks (to ensure valid and repeatable results). Therefore, sharp pre-cracks were produced by driving a wedge, or razor blade, into the bonded specimens. A clamp was placed approximately 50 mm from the end of the specimen to prevent the crack from propagating too far through the bondline when the wedge was introduced.

In all of the tests, with the exception of those in Chapter 6, care was taken to initiate the crack at the bottom interphase. That is, the crack was started at the steel/epoxy interphase which was on the bottom during the cure cycle in the hot press. Likewise, the NCA tests were all bottom interphase evaluations. For comparative purposes, the Chapter 6 evaluations focused on adhesive system performance when the cracks were initiated at the top interphase. A schematic of the top and bottom interphases is given in Figure 2.2.

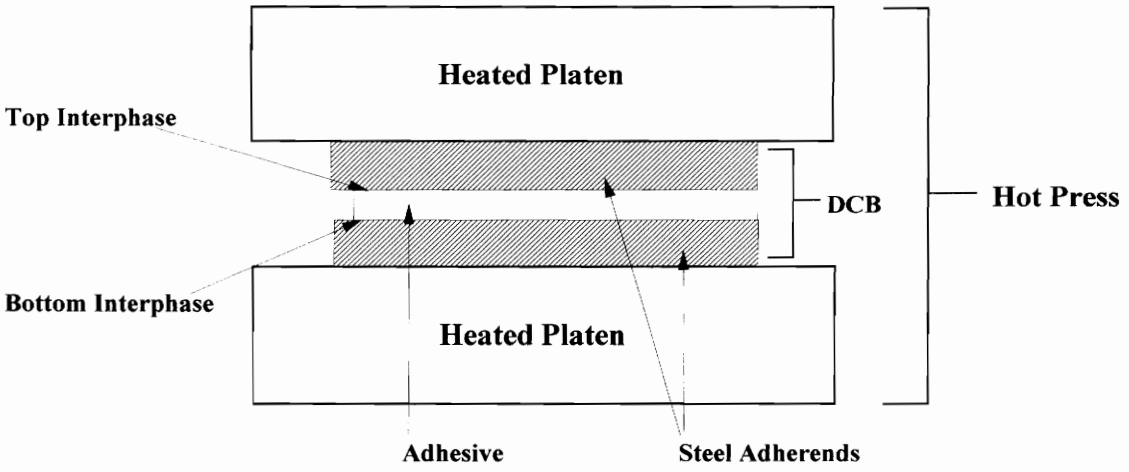

Figure 2.2 Schematic representation of the top and bottom interphases in the DCB specimen (specified by their orientation during the bonding procedure).

2.3.4 (Quasi-)Static DCB Testing Procedure

Static DCB tests were utilized for determination of the initiation (G_c) and arrest (G_a) strain energy release rates of the bonded joints as a function of toughener level, dicy content, and cure conditions. The initiation (or critical) strain energy release rate was defined as the loading level at which crack growth began, while the arrest strain energy release rate was defined as the loading level at which crack growth arrested. These adhesive systems also displayed a rate dependent interfacial failure process which allowed for a maximum strain energy release rate loading (G_{max}) to be achieved. This was sometimes much higher than either the initiation or arrest loading levels. The following testing procedure was used to conduct the static DCB tests.

All static DCB tests were carried out at a constant crosshead displacement rate on a screw-driven Instron 4505 testing frame. After bolting end-blocks to the DCB specimens, they were attached to the load frame using self-aligning pin connections. The crosshead was then set in motion at a constant, user specified rate (1 mm/min unless

otherwise noted). The third loading cycle of Figure 2.3 will now be described to illustrate the typical testing procedure used.

As the specimen was loaded using displacement control, a microscope and either the load-deflection or the load-time curve (these appear as real-time plots on the computer) were used to detect critical events taking place in the specimen. Typical load-deflection and load-time curves are shown in Figure 2.4. When either curve deviated from linearity upon loading, the crack had begun to grow and the critical fracture energy, G_c, had been reached. This observation was confirmed visually using the movable microscope. However, due to the rate dependent interfacial failure of these adhesive systems, the loading value continued to increase. When the load reached a maximum and began to rapidly decrease, the specimen had achieved a maximum loading level for this loading cycle, G_{max}. It should be stated that the existence of a maximum in G is not guaranteed and does not necessarily correspond to a maximum in P. However, it has been confirmed that the two occur almost simultaneously for these particular adhesive systems with G_{max} slightly lagging P_{max} (< 3 sec).

Shortly after P_{max} had been detected (about 5 sec), the crosshead motion was stopped to allow the crack growth to continue naturally until it reached near-equilibrium conditions. The term near-equilibrium is used because the crack was not always allowed to completely stop. The criterion used to establish a reasonable arrest loading level was that the load decreased by less than 1 N/min and no crack growth was observable. This component of the testing procedure was necessary to speed up the static DCB tests. If a test was allowed to continue until the loading level reached complete equilibrium, it may have taken an hour or more for each loading cycle, and this was not feasible. Therefore, this procedure was used to approximate the arrest fracture energy, G_a, and the error induced by this testing strategy was found to be negligible. The vertical lines on Fig. 2.3 resulted from crack growth that occurred while the crosshead was being held constant. Some cracks grew more than 30 mm during these hold cycles. Once G_a was determined, the specimen was unloaded to make sure plastic deformation of the adherends had not occurred. If plastic deformation had occurred, the P-Δ curves would not have returned to

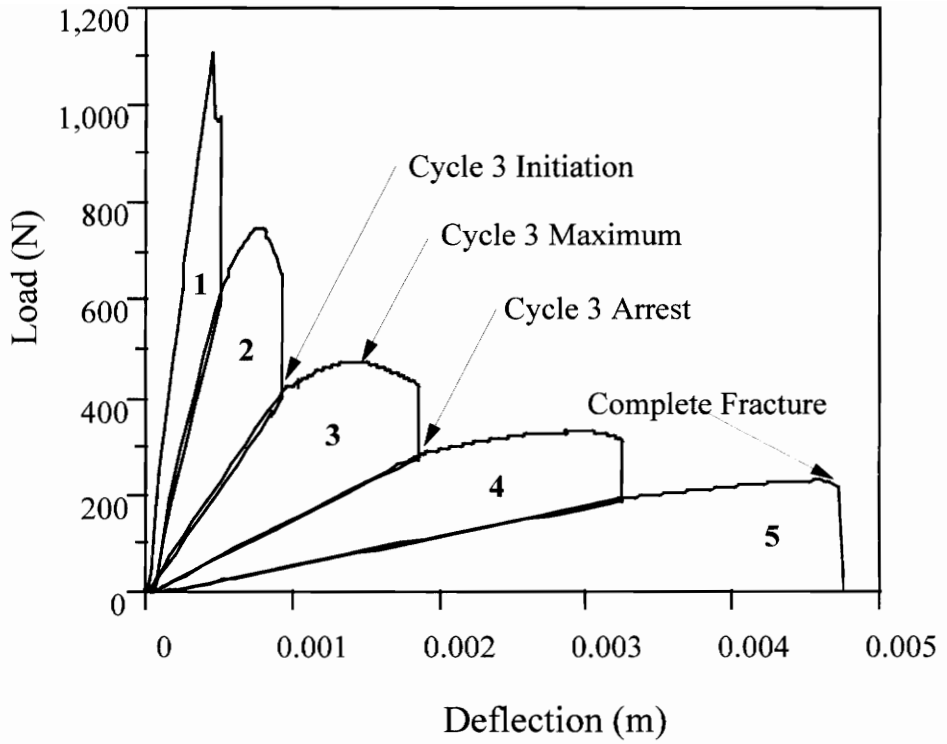

Figure 2.3 A typical load-deflection curve from a quasi-static DCB test.

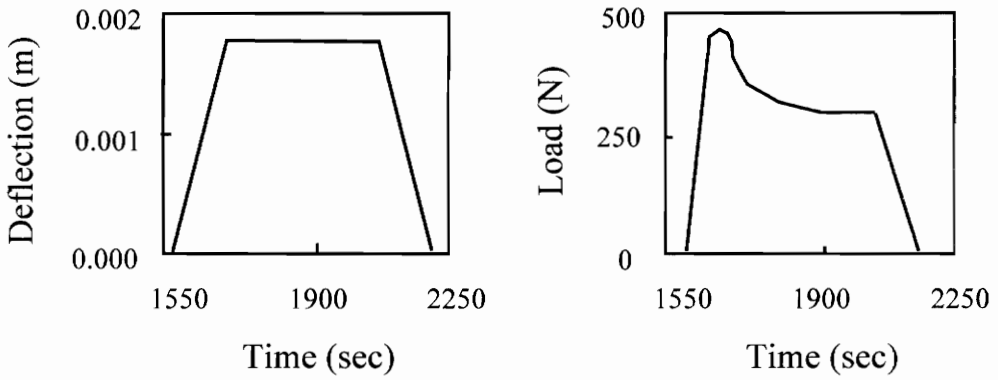

Figure 2.4 Typical deflection-time and load-time curves from quasi-static DCB testing (loading cycle 3 from Figure 2.3).

the origin, but instead would have intersected the deflection-axis to the right of the origin. Finally, this load-hold-unload procedure was repeated until the specimen was fully fractured.

During the testing process just described, the load and deflection readings were acquired at a user specified interval by the computer. This acquisition interval was altered, as necessary, in order to limit the size of the data files. Also, crack length readings were periodically attached to the load and deflection data sets when there was sufficient confidence in the crack length readings (when the crack was growing rapidly it was almost impossible to monitor). The data collected was later used to compute the relevant strain energy release rate values. The SERR values from DCB testing typically represent averages from two or more individual specimens that have undergone three to five loading cycles each.

2.3.5 Fatigue DCB Testing Procedure

Fatigue DCB testing was utilized for determination of the cyclic debond rates of the specimens, as a function of the applied strain energy release rates, over wide rate windows. This approach has been used to describe the fatigue fracture characteristics of metals, and more recently has been used to model the fatigue failure[114,119-120,127-128] of polymers.

Due to the unique failure characteristics of the DCB specimen, the fatigue tests were easier to conduct than were the quasi-static tests. This arises from the fact that the SERR of the DCB specimen is a function of crack length. Thus, it naturally *scans* the applied SERR window as crack growth occurs at a constant cyclic displacement level. For example, if a test is set up in constant displacement control, any crack growth naturally decreases the SERR applied to the specimen (see Equation 1.70). On the other hand, any crack growth that occurs while using load control naturally increases the applied SERR (see Equation 1.69).

All fatigue DCB tests were carried out on a servo-hydraulic MTS 810 testing frame. Data collection was again accomplished using computer controls. The program

allowed the user to visually observe how the test was progressing and helped to ensure that the tests were being performed properly. Automated data collection was especially important for the fatigue tests due to the length of time that was necessary to obtain threshold values (up to two days). The fatigue DCB testing procedure is outlined in the next two paragraphs.

Once the specimen was attached to the load frame using self-aligning pin connections, the MTS was programmed to apply a constant sinusoidal loading to the DCB specimen and either load or displacement control was used. In either case, an R-value of 0.1 was maintained. The R-value is the load ratio and is defined as P_{min}/P_{max}, where P_{min} and P_{max} are the minimum and maximum loads applied during a loading cycle. Unless otherwise stated, it should be assumed that all fatigue tests were carried out at a frequency of 5 Hz using displacement control.

After the loading parameters were set up, the computer was programmed to periodically scan the load and deflection data at high frequency (> 500 Hz) for a user specified interval (usually 5 sec) in order to accurately capture the load and deflection curves being applied to the specimens. The average maximum and minimum values of the cyclic load and deflection data were then computed for the given time interval. These average peak values were saved to a data file along with the number of loading cycles that had elapsed since the beginning of the fatigue test. Visually observed crack length readings were also periodically entered into the data set as with the quasi-static tests. As was shown previously in Figure 1.11, 10-20 crack length readings were usually sufficient over the duration of a test.

2.4 Failure Surface Characterization

2.4.1 X-ray Photoelectron Spectroscopy

X-ray photoelectron spectroscopy (XPS) studies were conducted to quantify the failure surfaces of the SENB, static DCB, fatigue DCB, and NCA specimens. The analyses were performed using a PHI Perkin-Elmer 5400 XPS spectrometer employing a Mg Kα (1253.6 eV) achromatic X-ray source operated at 15 keV with a total power of 400 W. Typical operating pressures were $< 1 \times 10^{-7}$ Torr, and the surface area employed was a 1 mm x 3 mm rectangle. The spectrometer was calibrated to the $4f_{7/2}$ photopeak of gold at 83.8 eV, and all binding energies were referenced to the main C-H photopeak at 285 eV.

Initial wide scans were carried out over a range of 0.0 to 1100.0 eV, and narrow scans were conducted in the carbon 1s, oxygen 1s, nitrogen 1s, silicon 2p, and iron 2p energy regions. Atomic percent compositions were calculated using peak areas and experimentally determined sensitivity factors. Since the bonded fracture specimens *appeared* to fail in an interfacial manner, the two sides are denoted as the "metal" and "adhesive" sides corresponding to their appearances. A sample of the cold rolled steel was also cut from a pretreated plate, prior to bonding, to provide background information. This is denoted as "steel".

Due to the large number of mechanical specimens that were tested for this dissertation work, it was not feasible to perform XPS analyses on each. Thus, only one specimen was typically evaluated. The region of the failure surface that was used in each of the analyses was carefully chosen to be representative of the majority of the specimens from that particular test group. This choice was based upon both the visual appearance of the specimen and upon mechanical performance data.

2.4.2 Electron Microscopy

Electron microscopy analyses were conducted to evaluate the morphology of the adhesives as a function of the test variables studied in Chapters 3-6. Again, these were toughener level, dicyandiamide content, cure temperature, whether the adhesive was

representative of the bulk or interphase, and whether the adhesive was from the top or bottom interphase. This information was also used to explain some of the bonded system performance variations that were observed in the mechanical studies.

As with the XPS analyses, the microscopy studies also had to be limited to a few representative samples. These were carefully selected based on both visual observations and on mechanical performance data. The microscopy samples were prepared for analysis by cryo-ultramicrotoming at -100 °C on a Reichert-Jung FC4 cryo-ultramicrotome. The thin sections were then stained in a RuO_4 vapor for 1 h (the rubber regions appear white and the epoxy matrix appears gray), and the TEMs were collected using a Philips 420T STEM at 100 kV. Magnification levels of 5900x and 18,750x were found to be the most useful in this work.

Chapter 3

An Evaluation of Toughener Content Variations

3.1 Introduction

When used as adhesives, epoxy resins offer automotive and aerospace designers many useful properties such as high modulus, low creep, and stable performance in a wide variety of applications. Unmodified epoxy adhesives are, however, generally quite brittle and offer only minimal resistance to crack growth and impact damage. As a result, adhesive systems that are based on unmodified epoxies can be highly susceptible to catastrophic failure if damages are incurred (cracks, voids, residual stresses, etc.). Researchers have thus proposed many methods to improve the toughness of epoxy based adhesives. One such method consists of adding an elastomeric material to the adhesive system.[129-131] Upon curing, phase separation is induced and the result is a 2-phase thermoset consisting of a glassy matrix (from the epoxy resin) and dispersed, spherical domains of elastomer. This type of modified system is typically quite resistant to crack growth. In addition, only minor concessions must be made with respect to the other desirable physical and thermal properties of the system to achieve the improvements.

A great deal of effort has been exerted to evaluate the exact influence of the dispersed elastomeric phase on the mechanical performance and morphology of epoxy based adhesives.[129-131] Initial studies in this area focused on model systems using catalytic cures, such as piperidine cures, and significant increases in the bulk and adhesive fracture energies were correlated with increases in toughener content (5-15x greater fracture energies than the control were obtained with an addition of approximately 15 phr toughener). Morphological variations were observed and correlated with performance, as well. However, since commercially available structural adhesive materials are generally not based on piperidine, the focus of this research has recently shifted. A common application for elastomer modified epoxies is in 1-part structural adhesives based on dicyandiamide (latent cure systems), and studies utilizing

this type of system have been documented in the open and patent literature. Most of these, however, have focused only on the general performance differences observed between dicyandiamide and piperidine cures.[130]

Since relatively few studies have been published on elastomer toughened, latent cure systems, the research of Chapter 3 was directed toward providing a comprehensive evaluation of such. The performance properties of the bulk materials and bonded systems were carefully determined using a combination of fracture and static strength based tests. Spectroscopy and microscopy analyses were used as well to elucidate any chemical or morphological changes that had occurred. A thorough assessment of all the data was made, and the bulk material parameters were related to the bonded system performance. The adhesive systems utilized in this research consisted of model dicyandiamide cured epoxies that were modified with variable amounts of toughener. cold rolled steel was used as the substrate material in all bonded system studies.

An additional point of support for the relevance of this research is the fact that a majority of the studies reported in the literature have utilized commercially available adhesive formulations.[132-138] As discussed in Section 1.3.1, these are rather complex due to the number of (and interactions amongst) constituents from which they are prepared. In most cases the adhesives were designed to fail cohesively, and thus the studies were essentially evaluations of bulk mechanical parameters. In this work, the adhesives were designed to fail at the metal/adhesive interphase rather than through the adhesive layer. A true study of interfacial fracture was thus achieved. This is the only known piece of research dealing specifically with the interfacial fracture of dicyandiamide cured, rubber toughened, epoxy bonded steel adhesive systems (as a function of toughener content in Chapter 3, as a function of dicyandiamide content in Chapter 4, as a function of cure temperature in Chapter 5, and as a function of top vs. bottom interphase in Chapter 6).

3.2 Experimental

3.2.1 The Adhesive System

Beginning with a basic latent cure, structural type epoxy formulation, three adhesives were developed for use in evaluating the influence of toughener content on the interfacial fracture performance of epoxy/steel adhesive joints. A summary of the formulations is given in Table 3.1:

Table 3.1 Model formulations with variable toughener levels (wt.%).

Formulation	A2	C2	E2
D.E.R. 331	88.5	69.1	52.6
Dicy	4.4	4.1	3.8
PDMU	1.8	1.6	1.5
M-5 Silica	5.3	4.9	4.5
Kelpoxy G272	0.0	20.3	37.6

These adhesive systems are quite typical of materials currently used in the automotive and aerospace industries. As mentioned previously (Section 3.1), however, they are simpler in design (the number of components has been limited). Since the goal of this section of the dissertation was to evaluate the influence of toughener content on the bulk mechanical and adhesive properties of latent cure adhesive systems, the toughener levels were varied from 0 to 37.6% by weight. Utilizing the epoxide equivalent weights of the D.E.R. and Kelpoxy, and assigning dicyandiamide a functionality of four, the amine hydrogen to epoxide end group ratio was calculated to be 0.47. This was maintained at a constant level in all three systems.

3.3 Results and Discussion

3.3.1 Bulk Mechanical Tests

From the tensile and fracture toughness tests it was determined that the bulk mechanical properties of the adhesives are highly dependent upon the toughener content. As the toughener content was increased from 0 to 37.6% by weight, the modulus decreased from 3.39 ± 0.11 to 2.22 ± 0.10 GPa. The results are shown in Figure 3.1. The plane-strain fracture toughness values (K_{Ic}) increased from 0.820 ± 0.048 to 1.875 ± 0.158 $MPam^{1/2}$, and the critical bulk strain energy release rate values (G_{Ic}) increased from 293 ± 33 to 1840 ± 240 J/m^2. These values, calculated from the SENB evaluations, are illustrated in Figures 3.2 and 3.3, respectively.

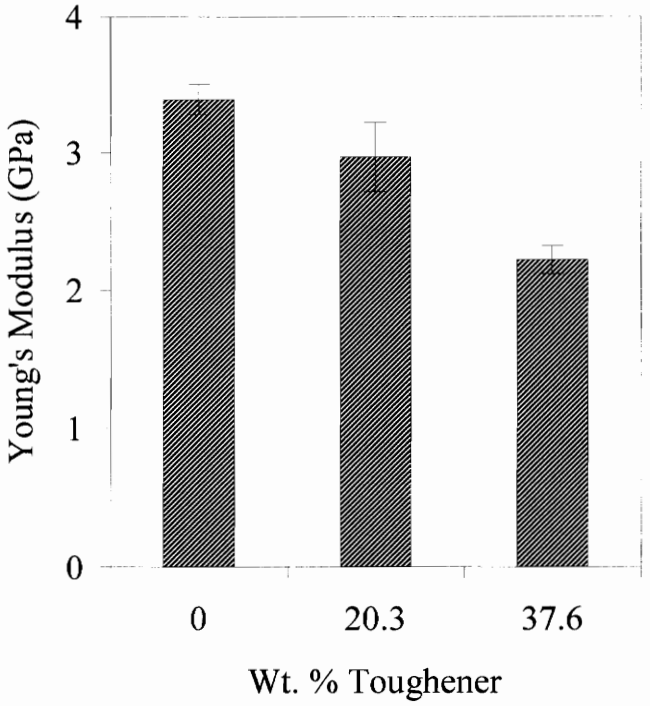

Figure 3.1 The influence of toughener content on the bulk modulus.

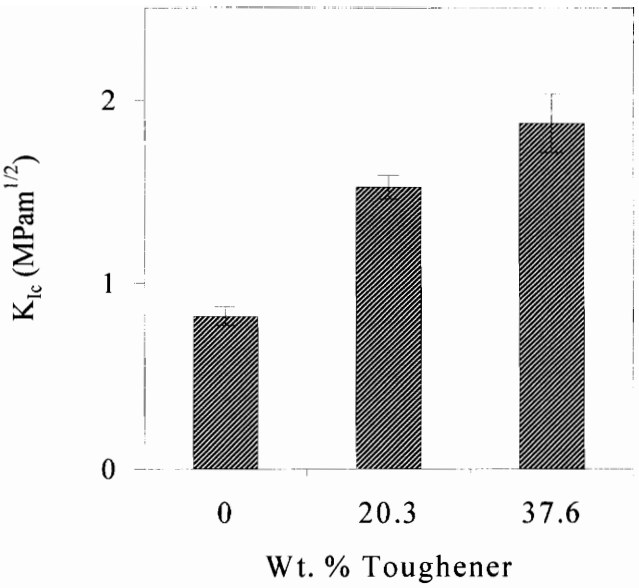

Figure 3.2 The influence of toughener content on the bulk adhesive K_{Ic}.

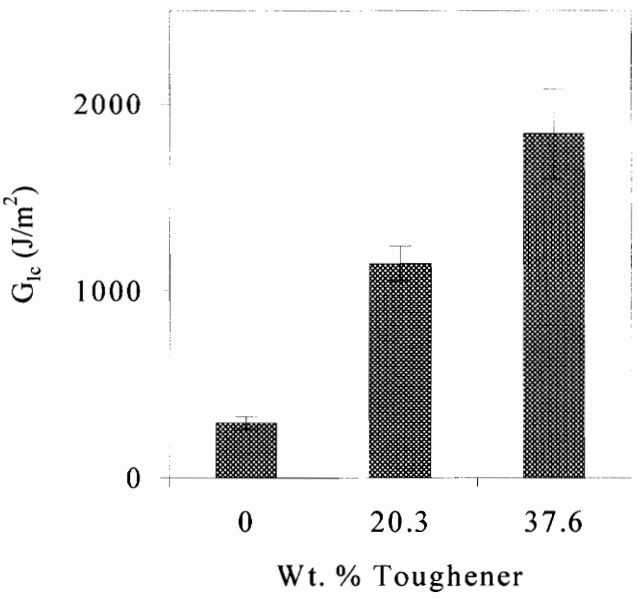

Figure 3.3 The influence of toughener content on the bulk adhesive G_{Ic}.

In addition to the measured changes in bulk material performance, some visual observations were documented. In both the tensile and SENB tests, stress whitening of the bulk adhesives was detected during sample deformation. For the three formulations evaluated, it was noted that as the elastomer content increased, the amount of stress whitening in the neck region of the tensile bars increased. In a similar fashion, the stress whitened bands on the fracture surfaces of the SENB specimens increased in size. These observations are quite important, as they can be correlated with the micromechanisms of toughening, and thus the increases in the bulk mechanical and fracture properties of the systems.

More precisely, the stress whitening observed in these materials is a result of the initiation and growth of voids in the elastomeric particles. These voids greatly enhance the occurrence of plastic shear-yielding, and it has been demonstrated by Kinloch and others that plastic shear-yielding in the adhesive system matrix is the main source of energy dissipation and increased toughness in 2-phase materials.[139] Such deformations occur due to the interactions between the stress field ahead of the crack tip and the elastomer particles. Therefore, to better understand the exact role of the elastomer domains in toughening the adhesive, it is necessary to first consider the stress fields surrounding them. The toughening micromechanisms initiated by these stresses can then be evaluated and discussed.

Equations have been derived by Goodier for the stresses around an isolated elastomeric particle embedded in an isotropic, elastic matrix that has been subjected to an applied uniaxial stress away from the particle.[140] For the elastomer, which generally has a much lower shear modulus than the matrix, the maximum stress concentration occurs at the particle equator. Provided the particle and matrix are well bonded, the stress is triaxial tension and occurs due to the volume constraint represented by the bulk modulus of the elastomer (similar to that of the matrix). This also means that, unlike a hole which would produce a stress concentration similar in magnitude, the elastomer can bear some of the stress at the crack front. Along with the high shear deformations which

elastomers can withstand, this explains why the dispersed particles are effective in producing significant increases in the toughness of brittle materials.

The stress field associated with the elastomer particles results in the initiation of two processes (micromechanisms) that can strongly interact and significantly toughen a brittle material. These are matrix shear-yielding and particle cavitation. Matrix shear-yielding is the first process that occurs, and it is due to the elastomer particles acting as initiation sites for plastic shear deformations. Since there are many particles in a toughened system, each contributing to the dissipation of plastic energy, it becomes obvious why toughness is higher in modified versus unmodified systems. Also, since these shear deformations typically initiate at one particle and end at another, they tend to remain localized. This minimizes the growth and breakdown of voids and crazes, thus preventing premature crack formation.[140]

The second process initiated by the stress field around the elastomer particles is particle cavitation. Two possible explanations have been proposed to explain the cavitation phenomenon.[141] In the first, as the adhesive matrix undergoes deformation due to the applied stress, the cavity occupied by the elastomer increases in size. Thus, when the elastomer particle debonds or is cleaved, it collapses back into the cavity. In the second theory, since the coefficient of thermal expansion of the rubber is greater than that of the matrix, as the cured adhesive cools the elastomer undergoes triaxial stresses. Then, when split by an advancing crack, the elastomer particles contract and form depressions.

As mentioned above, shear-yielding and particle cavitation may strongly interact to toughen a brittle material. Cavitation lowers the extent of triaxiality of the stress in the adjacent adhesive matrix, and since the yield stress increases with increasing constraint, it effectively reduces the stress required for shear-yield formation. Thus, cavitation promotes extensive plastic shear deformations in the matrix of the material. Again, it is the presence of localized shear-yielding at many sites in the system that gives rise to improved fracture properties.

3.3.2 Adhesive Evaluations (Static)

Along with the bulk mechanical tests, the bonded system evaluations showed an appreciable dependence on the toughener content. As the Kelpoxy was increased from 0.0 to 20.3% by weight, the SLS strength increased from 3579 ± 289 psi to 5720 ± 237 psi, then decreased to a value of 5220 ± 123 psi as the Kelpoxy was increased to 37.6% by weight. These results are shown in Figure 3.4. The SERR values from the static DCB and NCA evaluations, given in Figures 3.5 and 3.6, respectively, showed a pronounced dependence on toughener concentration as well. SERR values from the static DCB tests increased from 79 ± 12 to 377 ± 40 J/m^2, and the NCA SERR values increased from 108 ± 17 to 576 ± 15 J/m^2.

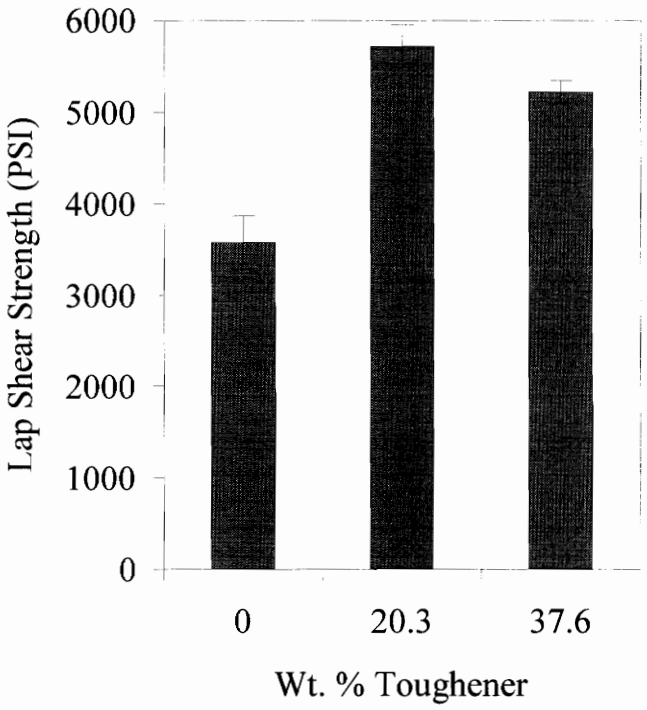

Figure 3.4 Single lap shear strength as a function of toughener content.

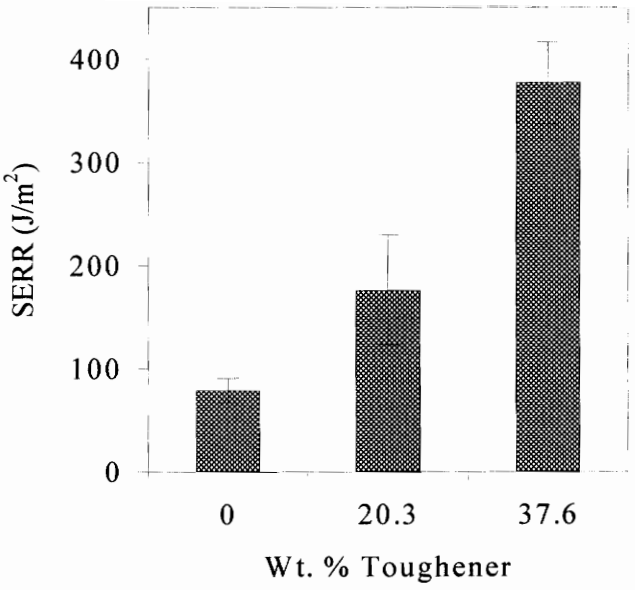

Figure 3.5 Static DCB response as a function of toughener content.

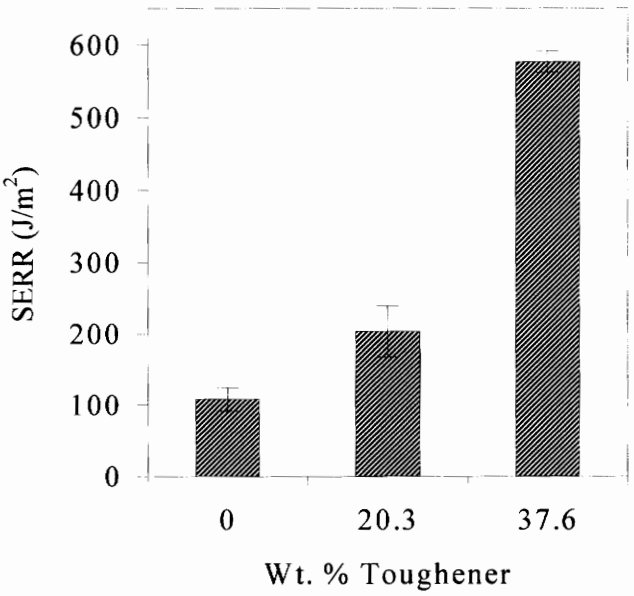

Figure 3.6 NCA performance as a function of toughener content (mode I).

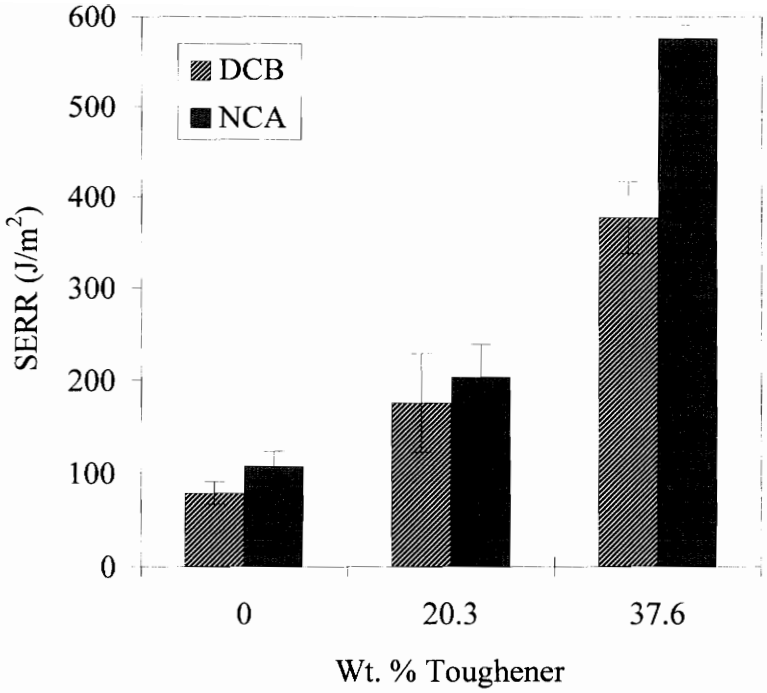

Figure 3.7 Comparison of DCB and NCA (mode I component) SERR values as a function of toughener content.

As stated previously, the NCA fracture analyses were conducted to provide a second fracture mechanics based testing method for comparison with the DCB evaluations. The SERR values from both the NCA (mode I component, only) and DCB analyses are depicted in Figure 3.7, and these demonstrate the same basic trends. As the toughener content was increased, the SERR values increased. In addition, these values are in relatively decent agreement, but with the NCA values surpassing the DCB values for the most highly toughened materials.

Several general explanations for the differences in the NCA and DCB test results may be hypothesized. It should be noted, however, that only limited analytical studies have been conducted. Firstly, the NCA test produces a mixed mode I and mode II

loading, and the values reported in this dissertation are the extracted mode I SERR values (see Section 1.4.4). The DCB specimen, on the other hand, produces a purely mode I loading. Secondly, the crack growth rates utilized in the two tests are significantly different. In the DCB evaluations the rates are carefully controlled (1 mm/min), whereas in the NCA evaluations the rates are much higher and not well controlled. Thirdly, the results of the NCA tests are valid only if the adhesive layers are not plastically deformed. While no massive plastic deformation of the adhesive layers was visually obvious (e.g., necking), stress whitening and microcracking (in the highly toughened systems) did occur. Lastly, from the XPS analyses it was apparent that the NCA specimens failed in a more uniform, cleanly interfacial manner. While failure of the static DCB specimens definitely occurred in the region of the epoxy/steel interphase, the crack growth path often seemed "rough" and inconsistent. In addition, the NCA failures always occurred closer to the steel/epoxy interface (closer to the metal surface).

The single lap shear specimens were tested in accordance with ASTM standards to provide a static strength based test for comparison with the fracture mechanics based results. As depicted in Figure 3.4, the SLS strength reached a maximum at the addition of 20.3% by weight toughener (Formulation C2), and then decreased as the toughener level was increased to 37.6% by weight (Formulation E2). This observation is important because the fracture mechanics based DCB and NCA tests showed a continued increase in toughness with *each* increase in toughener content (see Figure 3.7). This discrepancy in the adhesive testing results is not thought to be in error as the reproducibility of both the SLS and fracture evaluations was excellent.

Why then do the SLS results obtained in this research exhibit a decrease in strength for the adhesive containing the highest level of toughener, while the DCB and NCA fracture tests predict a continual increase in toughness? It is believed that the discrepancy arises from the different mechanistic features of adhesion evaluated in each type of test. To understand this phenomenon, it is necessary to look at a few features of the SLS specimen. Firstly, it is well documented that even though the SLS test is considered a shear test, SLS joints loaded in tension actually fail due to the transverse

tensile (peel) stresses.[117] Secondly, the effects of adherend and adhesive yielding in SLS specimens have been analyzed, and the results suggest that if gross adherend yielding is present, "*the adhesive will appear to be weaker*" if the simple ASTM analysis procedure is used.[117] It is therefore possible that the addition of toughener causes an increase in adhesion strength, which in turn results in an increase in adhesive and adherend yielding. Each of these leads to increases in the out-of-plane deformations, and thus the peel stresses, at the ends of the laps. In the SLS tests conducted for this dissertation, the steel adherends were routinely plastically deformed (permanently bent) when testing the stronger adhesive formulations. This was not compensated for in the data analysis, and a decrease in SLS performance was thus observed for Formulation E2 even though it actually formed the toughest adhesive joint as determined by fracture testing.

A good adhesion test, regardless of whether it is a fracture or static strength based test, should be able to detect changes in bonded system performance due to adhesive or surface chemistry variations, variations in the fabrication procedure (e.g., cure conditions), or variations in the test parameters (test temperature, rate, etc.). Although only one example is discussed in this dissertation, during the course of this research project there were many discrepancies observed between the results of the fracture based tests (DCB and NCA) and the SLS tests. As already stated, however, the results of both types of testing were quite reproducible. After careful evaluation of the experimental observations mentioned in the previous paragraphs, especially those concerning the SLS test and the relatively simple SLS data analysis technique, it is believed that the fracture tests provide a more fundamental indication of adhesive performance. It is true that the SLS test is a more commonly used test geometry and it may be more representative of actual adhesive joints, but one must be able to accurately measure and detect changes in the adhesion performance of a test joint as a function of the system variables. From this perspective, the fracture based testing and analysis methods are clearly more effective.

3.3.3 Adhesive Evaluations (Fatigue)

Just as with the static type of fracture evaluations, the fatigue DCB performance evaluations showed a strong dependence on the toughener content. As the toughener content was increased from 0 to 37.6% by weight, fatigue performance greatly improved. For example, to produce a constant crack growth rate of 1 x 10^{-6} m/cycle, the applied SERR for adhesive A2 was about 30 J/m^2, the applied SERR for adhesive C2 was about 80 J/m^2, and the applied SERR for adhesive E2 was about 180 J/m^2. These results are represented graphically in Figure 3.8.

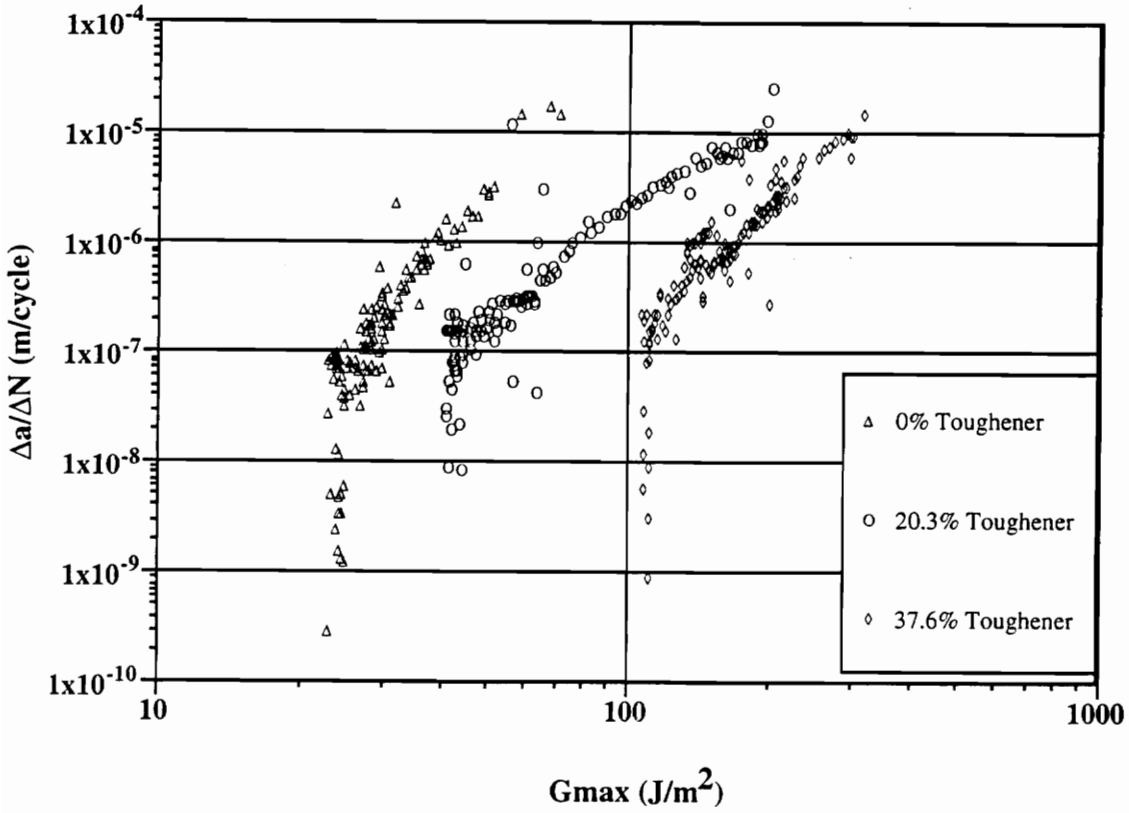

Figure 3.8 Fatigue DCB response as a function of toughener content.

3.3.4 TEM Studies

There are many microstructural features of elastomer toughened thermosetting adhesives which can influence the bulk mechanical and fracture properties of the system. With regard to the matrix phase, consideration must be given to crosslink density, glass transition temperature, and concentration of the non-phase-separated elastomer. With regard to the elastomeric phase, consideration must be given to volume fraction, particle size, particle size distribution, adhesion across the particle/matrix interface, morphology, and glass transition temperature. Unfortunately, few definitive studies have been conducted to elucidate the exact role of these microstructural features in the toughening of multiphase systems. In most of these studies critical features were routinely omitted and/or several features were simultaneously varied. Thus, only generalities are known concerning the interrelationships between the chemistry, microstructure, and resulting mechanical properties.

For example, consider the early work of Sultan and McGarry which dealt with the size of the elastomer particle domains.[142] They proposed that large particles (craze initiators) were more effective at toughening thermosets than were small particles (shear-yield initiators). However, the evidence for crazing was suspect and this idea has since been disproved. In addition, in these studies the volume fraction of elastomer was not considered and several features were simultaneously varied.

The microscopy evaluations presented in this dissertation are not intended to be definitive or quantitative, as that is not the primary focus of this work. Rather, they are utilized only as a means of screening for any significant changes that have occurred in the systems. Specifically, these studies were conducted to evaluate whether or not the system variables (toughener content in Chapter 3) produced any changes in the typical elastomer particle size, particle size distribution, or particle/system morphology. These findings were then related, where possible, to any changes that were observed in the bulk mechanical, fracture, or adhesive properties of the systems.

The transmission electron micrographs of the toughener variable bulk fracture specimens were acquired as described in Section 2.4.2. The results, given in Figure 3.9,

show the 2-phase morphologies of the systems. Apparent are the rubber rich regions (light areas), the matrix (gray areas), and the much smaller fumed silica particles (black). As was expected, both the particle size and system morphology depended greatly on the toughener content. For increases in the toughener content from 0 to 20.3% by weight, the morphology showed roughly spherical rubber particles with an average diameter of approximately 0.5 microns. As the toughener content was increased to 37.6% by weight, the morphology became less regular. The now large rubber phases began to tend toward co-continuity.

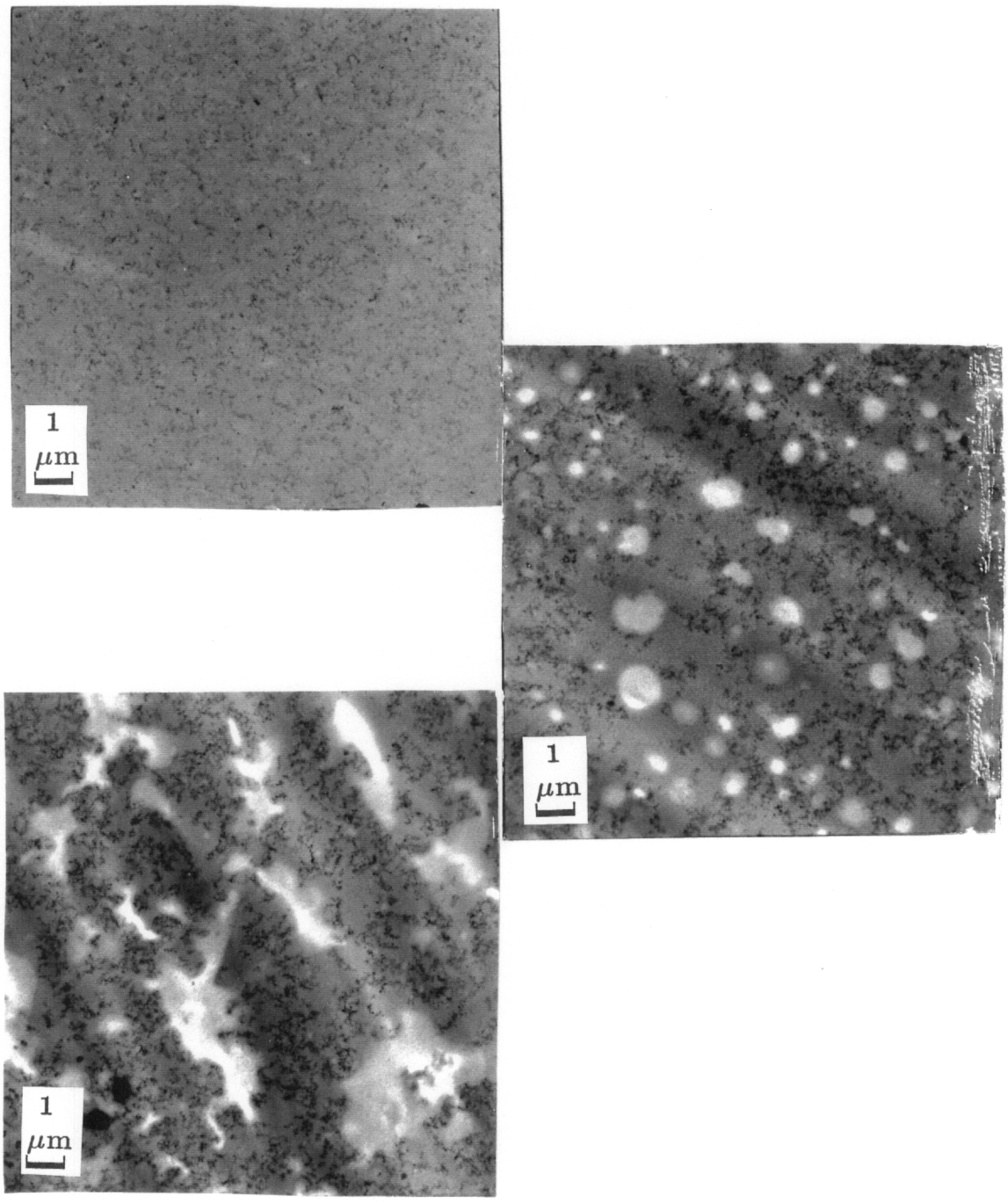

Figure 3.9 Transmission electron micrographs of the bulk adhesives. From top to bottom, 0 wt.% toughener, 20.3 wt.% toughener, and 37.6 wt.% toughener.

3.3.5 XPS Failure Surface Evaluations

X-ray photoelectron spectroscopy (XPS) studies were conducted to quantify the failure surfaces of the SENB, static DCB, fatigue DCB, and NCA specimens. Since the bonded specimens *appeared* to fail in an interfacial manner, the two sides of the DCB and NCA specimens are denoted in the tables as the "metal" and "adhesive" sides corresponding to their appearances. A sample of the cold rolled steel was also cut from a pretreated plate, prior to bonding, and analyzed to provide background information. This is represented in the tables as "steel".

The results of these XPS evaluations are summarized in Tables 3.2-3.8. Table 3.2 gives the failure surface compositions obtained from the SENB specimens, Tables 3.3 and 3.4 give the failure surface compositions for the static DCB specimens, Tables 3.5 and 3.6 give the failure surface compositions for the NCA specimens, and Tables 3.7 and 3.8 summarize the results from the failed fatigue DCB specimens.

Table 3.2 Surface compositions (at.%) for the bulk adhesive (SENB) failures as a function of toughener content.

Formulation (% Toughener)	**A2 (0%)**	**C2 (20.3%)**	**E2 (37.6%)**
Carbon	77.9	79.0	78.4
Oxygen	17.9	15.5	16.7
Nitrogen	3.1	3.5	2.5
Iron	<0.2	<0.2	<0.2
Silicon	1.1	2.1	2.4

Table 3.3 Surface compositions (at.%) for the static DCB failures (adhesive side) as a function of toughener content.

Formulation (% Toughener)	A2 (0%)	C2 (20.3%)	E2 (37.6%)
Carbon	77.3	77.6	77.0
Oxygen	15.8	15.5	19.0
Nitrogen	4.3	3.4	3.6
Iron	<0.2	<0.2	<0.2
Silicon	2.6	2.1	1.2

Table 3.4 Surface compositions (at.%) for the static DCB failures (metal side) as a function of toughener content.

Formulation (% Toughener)	A2 (0%)	C2 (20.3%)	E2 (37.6%)	Steel
Carbon	52.9	71.0	56.2	51.7
Oxygen	30.7	24.4	34.8	37.5
Nitrogen	6.8	1.7	3.3	<0.2
Iron	8.6	2.9	6.7	10.3
Silicon	1.0	<0.2	<0.2	<0.2

Table 3.5 Surface compositions (at.%) for the NCA failures (adhesive side) as a function of toughener content.

Formulation (% Toughener)	A2 (0%)	C2 (20.3%)	E2 (37.6%)
Carbon	77.5	81.8	80.2
Oxygen	12.2	14.6	16.7
Nitrogen	9.6	3.0	3.0
Iron	<0.2	<0.2	<0.2
Silicon	0.7	0.6	<0.2

Table 3.6 Surface compositions (at.%) for the NCA failures (metal side) as a function of toughener content.

Formulation (% Toughener)	A2 (0%)	C2 (20.3%)	E2 (37.6%)	Steel
Carbon	55.6	53.0	56.0	51.7
Oxygen	32.1	35.1	32.9	37.5
Nitrogen	4.9	1.9	2.4	<0.2
Iron	7.3	10.0	8.7	10.3
Silicon	<0.2	<0.2	<0.2	<0.2

Table 3.7 Surface compositions (at.%) for the fatigue DCB failures (adhesive side) as a function of toughener content.

Formulation (% Toughener)	A2 (0%)	C2 (20.3%)	E2 (37.6%)
Carbon	81.5	81.1	79.3
Oxygen	16.5	15.5	17.1
Nitrogen	2.1	2.0	3.6
Iron	<0.2	<0.2	<0.2
Silicon	<0.2	1.5	<0.2

Table 3.8 Surface compositions (at.%) for the fatigue DCB failures (metal side) as a function of toughener content.

Formulation (% Toughener)	A2 (0%)	C2 (20.3%)	E2 (37.6%)	Steel
Carbon	48.8	52.6	47.9	51.7
Oxygen	39.1	36.4	39.1	37.5
Nitrogen	1.7	1.9	2.0	<0.2
Iron	10.4	9.8	11.0	10.3
Silicon	<0.2	<0.2	<0.2	<0.2

In all cases the surface analysis results are generally consistent with the visual observation that failure occurred in the region of the epoxy/steel interphase. This conclusion is based on a comparison of the metal side surface iron values from the failed specimens (fatigue DCB, static DCB, and NCA) with the nonbonded steel surface iron values. Overall, the former ranged from 2.9 to 11.0 at.%, and the latter was 10.3 at.%. In addition, the adhesive side iron values were all determined to be < 0.02 at.%, which leads to the conclusion that none of the metal substrate material was removed with the adhesive during bond failure.

While it is evident that all of the systems failed in the region of the epoxy/steel interphase, it is also evident that for the different test specimens, these failures occurred at different locations within the interphase. For the static DCB tests, the surface iron values for the metal side of the failures varied from about 3 to 9 at.%, with an average value of 6.1 at.%. Since the surface iron value for the nonbonded steel was determined to be 10.3 at.%, the failures were thus concluded to occur well into the interphase region and not at the adhesive/steel interface. In the static DCB tests, a small amount of the adhesive, either in the form of islands or a thin film, was most likely left on the metal substrates after failure. With the fatigue DCB and NCA tests, on the other hand, the failures occurred much closer to the surface of the metal (nearly interfacial in nature). The metal side surface iron values were determined to be, on the average, 10.4 and 8.6 at.%, respectively. In these cases, the adhesives most likely peeled cleanly from the metal substrates (with, perhaps, minuscule amounts of the adhesives left behind).

This combination of fracture tests, with each producing crack growth and failure at a different location in the interphase, provides a unique means to gauge fracture performance across the entire interphase region. For instance, it is demonstrated that failure of the NCA specimens occurs more closely to the surface of the steel than does failure of the static DCB specimens. Thus, by comparison of the fracture values, as shown in Figure 3.7, the locale of failure can be correlated with fracture performance. However, because of the differences in the specimens, as discussed in Section 3.3.2 (test rate, mode mixity, etc.), caution must be exercised in making a direct comparison of the

findings. Regardless, from the testing results it is apparent that the toughener content, while significantly impacting the fracture performance, does not influence the location of failure in the bonded joints. That is, within a given set of tests (DCB or NCA), the failures consistently occur at the same location regardless of the particular adhesive formulation being tested.

By comparison of the bulk fracture surfaces (SENB) with the adhesive sides of the bonded system failures, one anomaly consistently showed up in the results. This was the presence of an elevated (average) nitrogen level (see Tables 3.2, 3.3, 3.5, and 3.7). In addition, when the nonbonded metal surface values were compared with the values for the metal sides of the bonded system failures, the same trends were noted (see Tables 3.4, 3.6, and 3.8). Because the nitrogen level was elevated in both of the cases, and especially since nitrogen was not present on the steel prior to bonding, these results suggested migration or concentration of a nitrogen containing adhesive constituent at the interphase. Some of the possibilities include an increased concentration of toughener, dicyandiamide, or PDMU. Since the nitrogen level did not increase with increasing toughener content, the first option can be ruled out. And since the migration or sedimentation of dicyandiamide to the interphase has been previously reported by other researchers, it would thus seem to be the most logical explanation.[143-144] The research of Chapter 4 therefore focuses on this idea.

Some additional and more detailed information concerning the bonded system failures can be obtained from these analyses through careful inspection of the C 1s and O 1s photopeaks. The C 1s photopeaks for adhesives A2 and E2, taken from the failed bulk (SENB) specimens and the failed fatigue DCB (adhesive side) specimens, are given in Figures 3.10 and 3.11. This combination of photopeaks allows for direct comparison of the chemical functionalities present at the interphase (again, very close to the steel in the case of the fatigue DCB specimen) with those present in the bulk of the material.

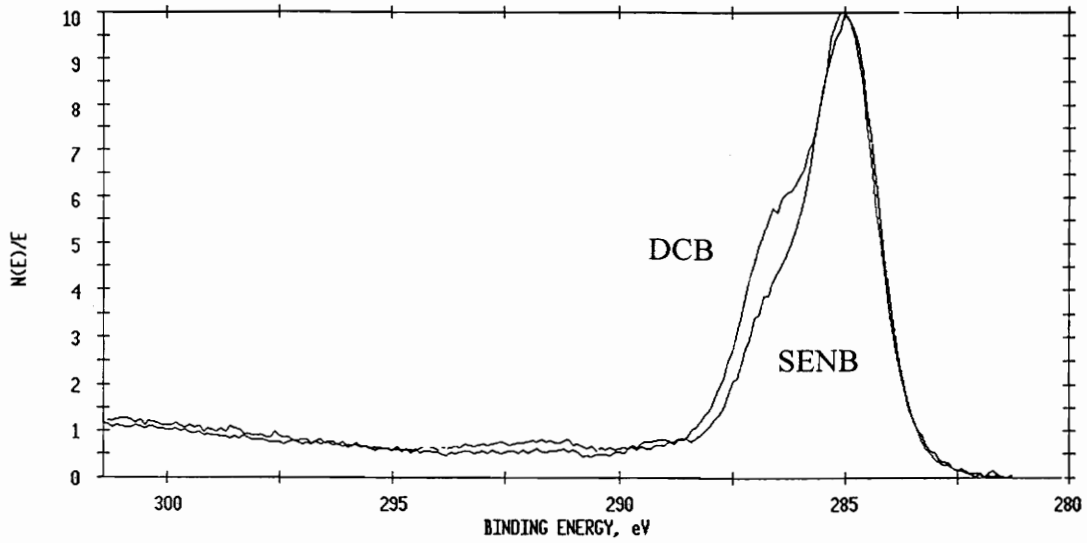

Figure 3.10 Montage of C 1s photopeaks from fatigue DCB (adhesive side) and bulk SENB failure surface analyses (adhesive A2).

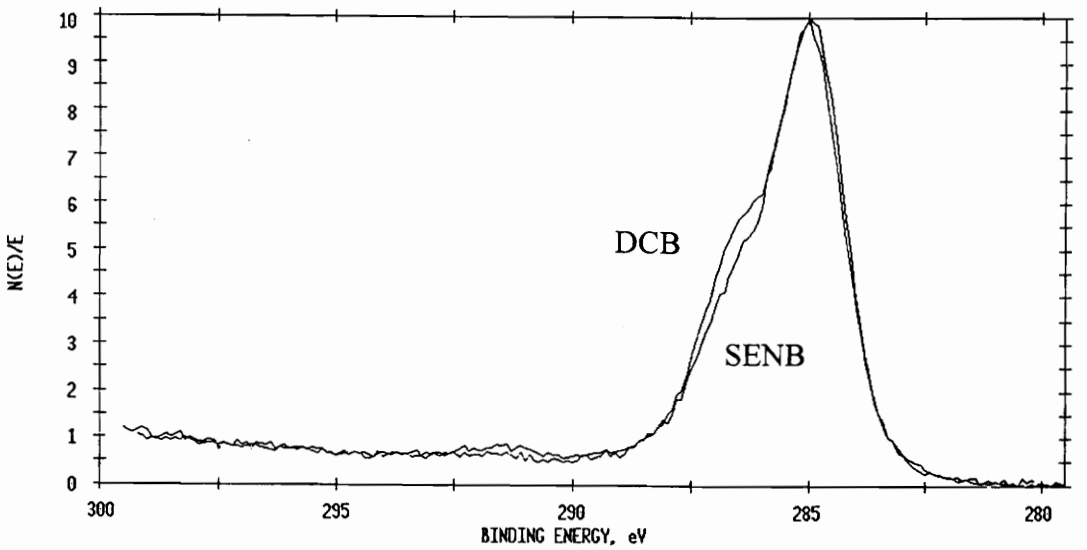

Figure 3.11 Montage of C 1s photopeaks from fatigue DCB (adhesive side) and bulk SENB failure surface analyses (adhesive E2).

From these plots it is obvious that the chemical composition of the bonded system interphase and the bulk adhesive are not equivalent (as was already suggested by the elevated nitrogen levels). In both adhesives A2 and E2, a shoulder appears in the interphase C 1s photopeak at approximately 286.5 eV and may be indicative of a number of things. Some of the options include an increased pendant hydroxyl concentration (C-O-H, indicative of the epoxy/dicy reaction), an increased ether concentration (C-O-C, indicative of the etherification side reaction), or an increased number of carbon-nitrogen linkages (C-N, indicative of reacted or unreacted dicyandiamide). All of these options are correlative, as well, with the increased surface nitrogen values noted in Tables 3.3-3.8.

In an attempt to better explain the elevated nitrogen levels on the metal failure surfaces, analyses were conducted on the C 1s and O 1s photopeaks from the surfaces of the nonbonded steel and the metal side of a fatigue DCB failure (since the fatigue failures were very close to the metal surface). This combination of photopeaks allowed for direct comparison of what was present on the metal both before and after the bonding process. For time and space constraints, only one representative example is presented in this dissertation. The overlay plots, utilizing adhesive E2, are given in Figures 3.12 and 3.13. From the C 1s photopeaks it is obvious that the steel surface is altered through the bonding process. This conclusion is based on the large difference in the carbon peaks that appears in the form of a shoulder at 286.5 eV. Since the chemical shift associated with C-O or C-N is about 1.5 eV (from 285 eV), it is again reasoned that this peak arises from one of the options mentioned above (an increased pendant hydroxyl concentration, an increased ether concentration, or an increased concentration of carbon-nitrogen bonds). From the O 1s peaks shown in Figure 3.13, the presence of C-O is confirmed through the appearance of a shoulder in the peak at 533.5 eV (a 1.5 eV shift from 532 eV). Unfortunately, the resolution of the XPS is not sufficient for determination of whether this shoulder is specifically from organic hydroxyl groups or ether formation. Regardless, these results lead to the conclusion that dicyandiamide concentrates (most likely) at the adhesive/metal interphase during the cure cycle.

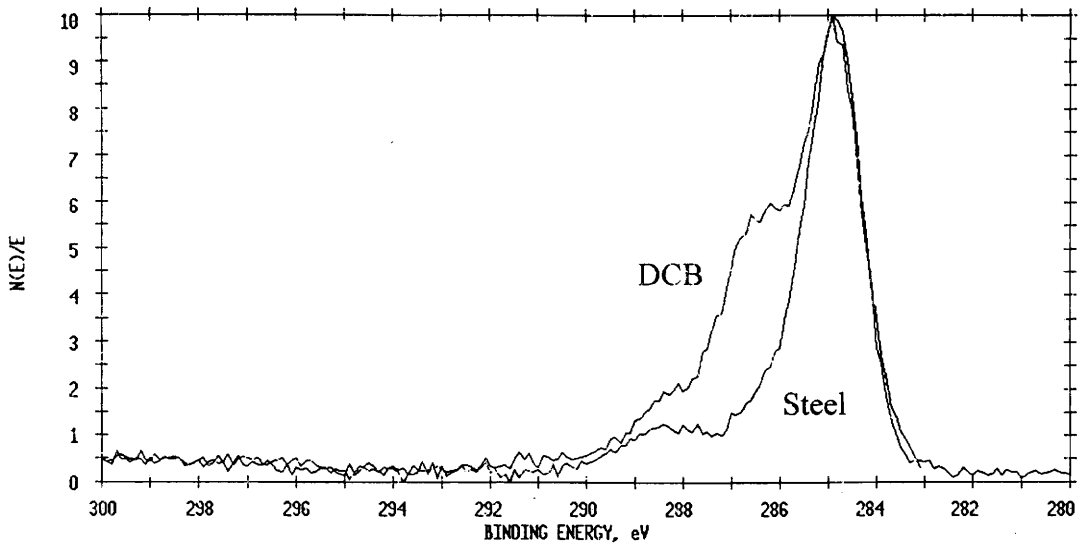

Figure 3.12 Montage of C 1s photopeaks from nonbonded steel and fatigue DCB (metal side) failure surface analyses (adhesive E2).

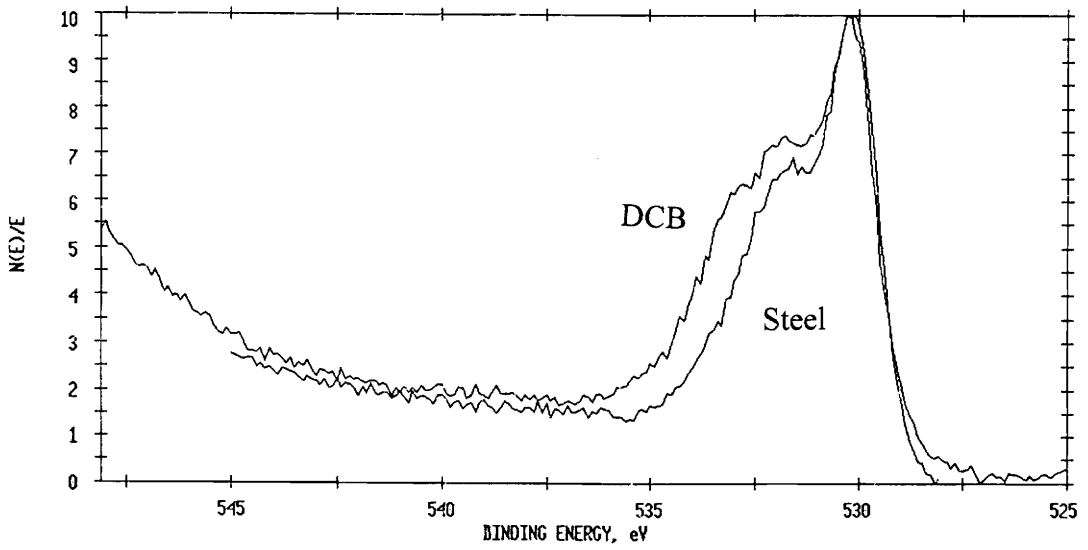

Figure 3.13 Montage of O 1s photopeaks from nonbonded steel and fatigue DCB (metal side) failure surface analyses (adhesive E2).

Chapter 4

An Evaluation of Curing Agent Content Variations

4.1 Introduction

Although focusing on different aspects of the bulk mechanical and adhesive properties of latent cure epoxy systems, the studies presented in each of Chapters 3-6 were conducted for many equivalent reasons. These reasons are presented at various points throughout the entire introduction (Chapter 1) and are summarized fully in Section 1.5. Some of the reasons are also given in Section 3.1, along with additional details on the concepts specific only to Chapter 3. For the purposes of clarity and completeness, the format utilized in Chapter 3 is also applied to Chapters 4-6. That is, at the beginning of each chapter the general concepts are briefly covered, then the specific concepts (relevant only in that chapter) are discussed in more detail.

As mentioned previously in Chapter 1, dicyandiamide is a widely used latent curing agent in heat cured epoxy adhesives (structural materials). Accordingly, much effort has been exerted to evaluate the mechanistic features of the dicy/epoxy reactions. In addition, the bulk mechanical properties of dicy/epoxy systems have been studied as a function of formulation and cure condition variations, and it has been demonstrated that even small fluctuations in these parameters can greatly influence the behavior of the cured materials.[59,63-66] However, because of the complexity involved in conducting comprehensive studies of this type, almost no research has progressed to the level of evaluating these parameters in bonded systems (adhesive systems). Of the studies that have been conducted, most have looked only at materials that failed in a cohesive manner. The influence of formulation and cure condition variations on the adhesive/substrate interphase region were therefore neglected. Since the failure of structural adhesives often occurs at the interphase, especially under adverse environmental conditions, the need for a thorough interfacial assessment is obvious.

Beyond the general ideas presented above, the results of Chapter 3 lead to some specific reasons for pursuing this work. Primarily they suggest that the interphase region

in dicyandiamide cured epoxy/steel adhesive systems possesses a different chemical composition than the bulk of the adhesive. Thus, if fracture testing is conducted and the system failures occur in a cohesive manner, the results may not be applicable if failures later shift to the interphase (e.g., under hot, humid conditions). It has been suggested in the literature that these chemical differences (bulk vs. interphase) are caused by an elevated concentration of dicyandiamide at the steel/epoxy interphase region.[143-144] It is proposed, as well, that this elevated concentration of dicyandiamide can drastically alter the performance of the bonded structure (under any conditions). The specifics of how this occurs, however, are not completely understood. Since dicyandiamide is generally insoluble in epoxy resins, it is thought that it may influence the performance by forming flaws (the undissolved crystals function as stress concentrators). However, it is also known that the reaction mechanisms in latent cure systems depend highly upon the dicyandiamide concentration. Thus, by settling to the interphase and increasing the concentration in that region, it may promote one type of chemical reaction versus another (e.g., chain extension versus etherification). As a result, the bonded system performance may be altered.

Since relatively little is known about the influence of the curing agent content on the bulk mechanical and interfacial fracture properties of dicyandiamide cured epoxy systems (epoxy/steel systems), this section of the dissertation focuses on providing relevant and useful information on the topic. Both general and specific concepts, such as those discussed in the previous text, are investigated. From a general perspective, mechanical performance data is acquired for both bulk and bonded (interfacial fractures) systems, and correlations are made with the dicyandiamide content variations. More specifically, chemical information from microscopy and spectroscopy evaluations of the failure surfaces is utilized in an effort to understand how the interphase region is influenced. It should be noted, however, that the detail of the chemical information is limited by the resolution of the surface analysis instrumentation (C-O-C, C-O-H, and C-N cannot be separated).

4.2 Experimental

4.2.1 The Adhesive System

A series of dicyandiamide cured epoxy adhesives was developed for use in evaluating the influence of curing agent content on the bulk mechanical and adhesive properties of latent cure adhesive systems. Since adhesive C2 (utilized in the studies of Chapter 3) demonstrated the most well controlled crack growth and failure characteristics, it was used as the basis upon which this series of materials was designed. Two additional formulations were prepared by increasing the concentration of dicyandiamide in one case, and decreasing the amount of dicyandiamide in the other. The respective levels of dicyandiamide in adhesives A2, C2, and E2, in wt.%, were 2.5, 4.1, and 6.2. The amine hydrogen to epoxy group ratios were 0.30, 0.47, and 0.70, respectively. This series of materials, therefore, varied only in the curing agent content, and all other components were held constant. The compositions are given in Table 4.1.

Table 4.1 Model epoxy formulations with variable levels of Dicy (components in wt.%).

Formulation	C1	C2	C3
D.E.R. 331	69.1	69.1	69.1
Dicy	2.5	4.1	6.2
PDMU	1.6	1.6	1.6
M-5 Silica	4.9	4.9	4.9
Kelpoxy G272	20.3	20.3	20.3

4.3 Results and Discussion

4.3.1 Mechanical Tests

From the tensile and fracture toughness tests, it was demonstrated that the bulk mechanical and fracture properties of the model adhesive systems was not influenced by variations in the dicyandiamide content. Over the dicyandiamide content range of 2.5 to 6.2% by weight, the bulk modulus values were unaffected. The experimentally determined values for the K_{Ic}, and G_{Ic} as well, were not statistically different from one formulation to another. These findings are depicted graphically in Figures 4.1, 4.2, and 4.3, respectively.

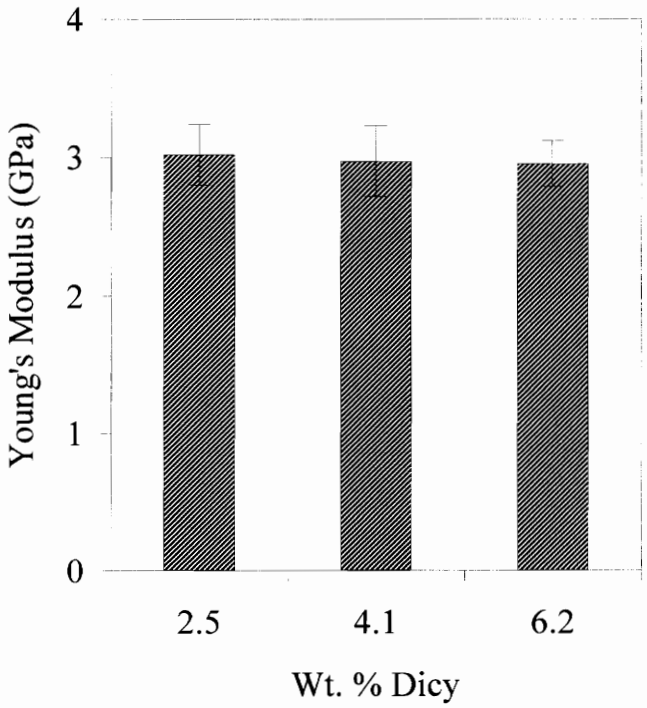

Figure 4.1 The influence of Dicy content on the bulk modulus.

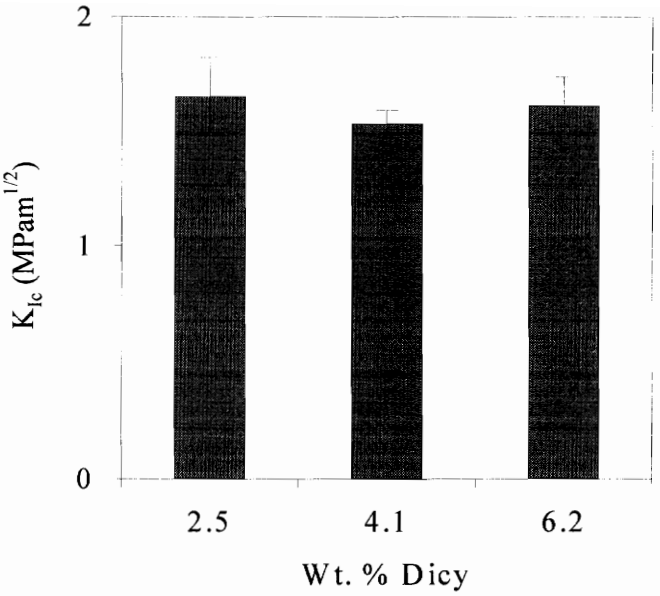

Figure 4.2 The influence of Dicy content on the bulk adhesive K_{Ic}.

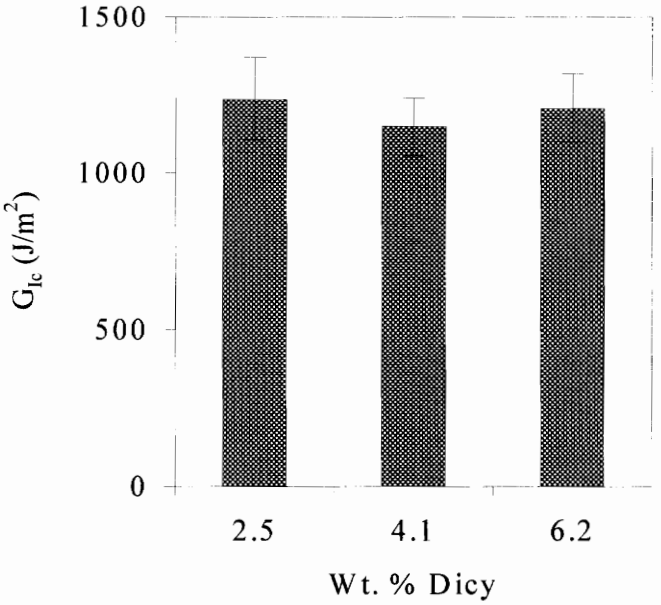

Figure 4.3 The influence of Dicy content on the bulk adhesive G_{Ic}.

The results of the bulk mechanical evaluations indicate that the performance properties of these latent cure epoxy systems are independent of the curing agent content. For increases in dicyandiamide concentration within a given formulation (as outlined in Table 4.1), the modulus values were shown to remain essentially constant. In addition, there were no visually discernible differences in the appearances of the test specimens during loading and subsequent failure. Since the bulk modulus of a polymeric material is determined from stress-strain measurements at low levels of strain, these results are not surprising. The resistance of a polymeric material to these low level deformations arises primarily from intermolecular interactions and is relatively independent of the crosslink density (the main material parameter expected to change as the dicyandiamide content is varied).[146] Thus, even if notable changes in the crosslink density are induced through modification of the curing agent to epoxy ratio, changes in the modulus may not be significant or detectable in these glassy systems.

In agreement with the tensile studies, the fracture evaluations also failed to demonstrate any correlations with the curing agent content of the adhesive. However, unlike the bulk modulus, the fracture toughness is a material property that does depend upon the crosslink density. Accordingly, it should be sensitive enough to detect any chemical variations that have occurred in the bulk of the systems. Based on this, it seems obvious that the changes in curing agent content do not alter the chemistry or mechanics of the bulk materials. Furthermore, from this conclusion it can then be theorized (as discussed earlier) that the dicyandiamide, if not working in the bulk of the adhesive, must be moving to the interphase region through sedimentation. These concepts are further investigated and discussed in the bonded system studies of Sections 4.3.2-4.3.3 and the failure surface analyses of Section 4.3.5.

4.3.2 Adhesive Evaluations (Static)

The performance of the bonded systems, unlike the performance of the bulk materials, showed an appreciable dependence on the concentration of curing agent. As the dicyandiamide level was increased from 2.5 to 6.2% by weight, the SLS strength increased from 4490 ± 404 to 5789 ± 168 psi. These results are shown in Figure 4.4. The SERR values from the DCB and NCA tests, given in Figures 4.5 and 4.6, respectively, showed a pronounced change as well. The SERR values from the static DCB tests decreased from 292 ± 21 to 181 ± 25 J/m^2 and the SERR values from the NCA tests decreased from 340 ± 44 to 191 ± 44 J/m^2.

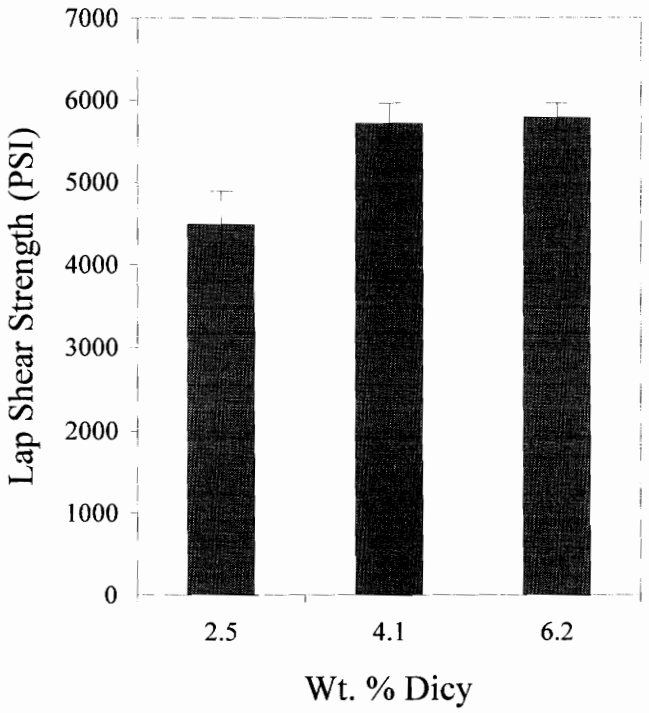

Figure 4.4 The influence of Dicy content on single lap shear strength.

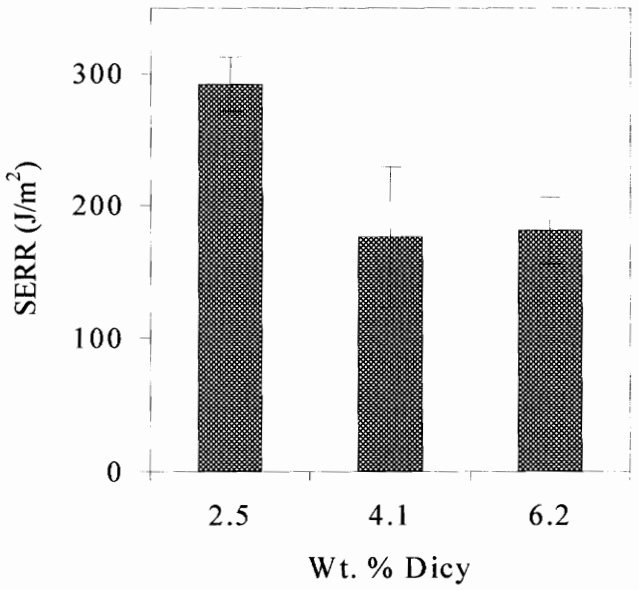

Figure 4.5 Static DCB performance as a function of Dicy content.

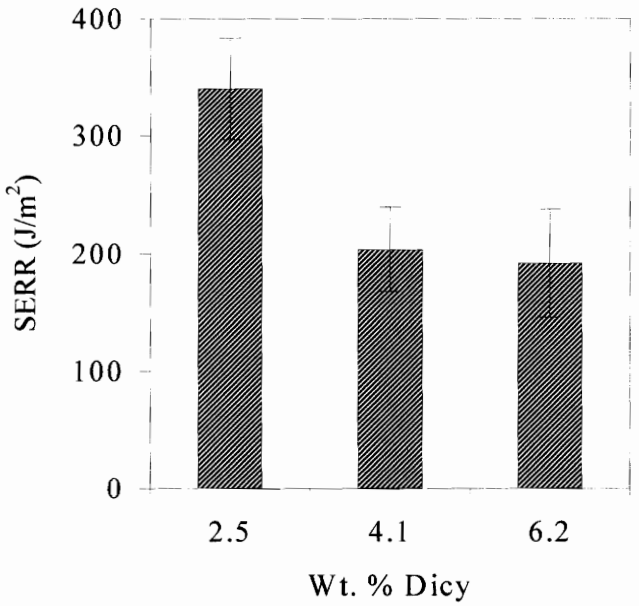

Figure 4.6 NCA performance (mode I) as a function of Dicy content.

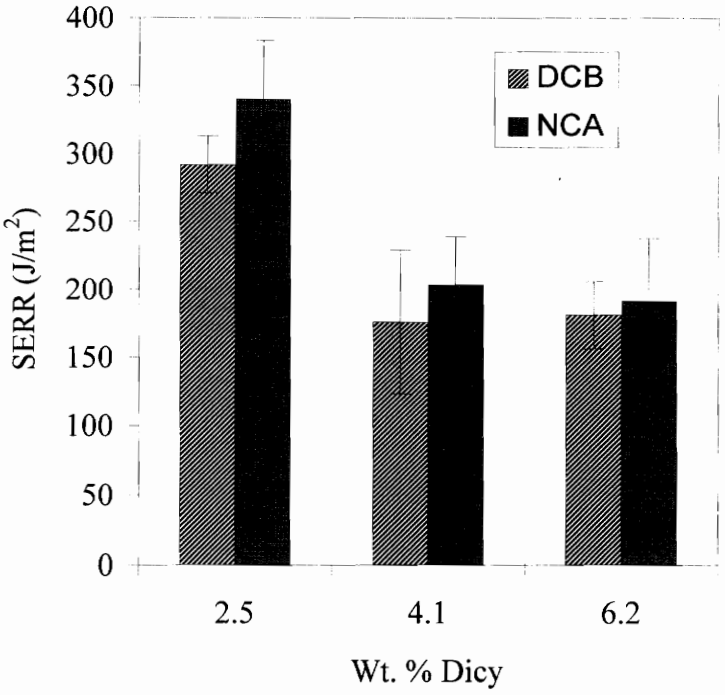

Figure 4.7 Comparison of DCB and NCA (mode I component) SERR values as a function of Dicy content.

Together with the findings of the bulk mechanical studies, the adhesive performance evaluations support the concept of dicyandiamide sedimentation (concentration at the interphase) in latent cure epoxy systems. This conclusion is based on the fact that, although the bulk material properties were shown to be independent of dicyandiamide concentration, the adhesive performance properties were shown to be greatly dependent. Namely, as the curing agent concentration was increased within a given adhesive formulation, the bulk mechanical properties remained essentially unchanged. The bonded system failure values, however, were greatly altered. Since the failures were all interfacial in nature, the influence of the dicyandiamide concentration

on the bulk mechanical and adhesive properties of the systems was considered to be limited to the adhesive/substrate interphase region. A more detailed discussion of these results, including correlations with chemical information from the XPS analyses, is given in Section 4.3.5.

The SERR values from both the NCA (mode I component) and DCB analyses are depicted in Figure 4.7. These results demonstrate the same basic trends and show relatively decent agreement in the numerical values as well. For increases in the concentration of dicyandiamide in the adhesives, from 2.5 to 4.1% by weight, the interfacial SERR values were found to decrease. Then, as the dicyandiamide level was increased to 6.2% by weight, the interfacial SERR values remained unchanged. In comparison, the SLS strength was found to increase as the dicyandiamide level was raised to 4.1% by weight. Then, as the level was increased to 6.2% by weight, the value remained nearly unchanged. The SLS data are shown graphically in Figure 4.4. From a mechanics perspective, all of these findings are in good agreement with the results of Chapter 3. That is, for both of the system variations studied thus far (toughener content variations in Chapter 3, dicyandiamide content variations in Chapter 4), the NCA and DCB specimens produced the same basic fracture trends and values (statistically equivalent in most cases). The SLS analyses, on the other hand, consistently produced opposing results. This last finding can be readily explained in terms of the mechanistic features of adhesion measured in static strength based tests versus fracture mechanics based tests, and the underlying details have already been discussed extensively in Section 3.3.2.

In both the fracture and static strength based tests it is interesting that the bonded system performance changes dramatically, then levels off as the dicyandiamide content is continually increased. This leads to the conclusion that there is a critical loading level for the dicyandiamide beyond which adhesion is influenced less significantly. Since the failures are interfacial in both types of testing, this critical level must depend not upon the chemical and mechanical properties of the bulk adhesive, but on the chemical and mechanical properties of the adhesive/substrate interphase. Utilizing the hypothesis of

dicyandiamide sedimentation, it appears once again that as the curing agent concentration is increased, the amount of sedimentation increases and the adhesion performance is altered. Thus, at some dicyandiamide level between 2.5 and 4.1% by weight, the interphase has already become significantly weakened. Even if the dicyandiamide level is further increased (further increasing the amount of sedimentation), no additional detrimental effects are noted.

4.3.3 Adhesive Evaluations (Fatigue)

Although the static type fracture performance evaluations all showed a strong dependence on the dicyandiamide content, the differences were not as significant in the fatigue DCB tests. For both increases and decreases in dicyandiamide content, from the base formulation C2, the fatigue performance was improved. For example, at a constant SERR of 100 J/m^2, the crack growth rate for C1 was about 8 x 10^{-6} m/cycle, the crack growth rate for C2 was approximately 8 x 10^{-5} m/cycle, and the crack growth rate for C3 was approximately 2 x 10^{-6} m/cycle. These results are shown below in Figure 4.8 and are explained in greater detail in Section 4.3.5.

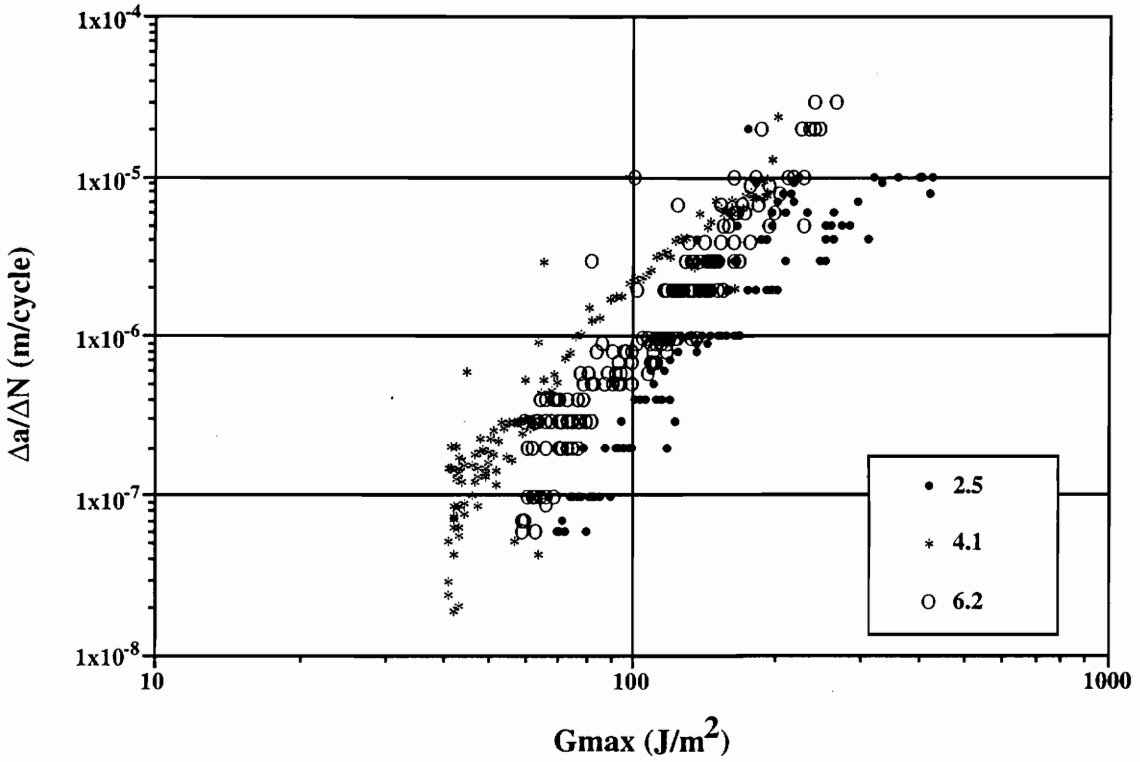

Figure 4.8 Fatigue DCB response as a function of Dicy content. Legend values indicate 2.5, 4.1, and 6.2% by weight dicyandiamide.

4.3.4 TEM Studies

It was already reviewed in Section 3.3.4 that there are many microstructural features of elastomer toughened thermosetting adhesives that can influence the bulk mechanical and fracture properties of the system. With specific regard to the elastomeric phase, consideration must be made for volume fraction, particle size, particle size distribution, adhesion across the particle/matrix interface, morphology, and glass transition temperature. Unfortunately, few definitive studies have been conducted to elucidate the exact role of these microstructural features in the toughening of multiphase systems, and in most cases these studies were critically flawed. Thus, only generalities are known concerning the interrelationships between the chemistry, microstructure, and resulting mechanical properties. The TEM studies presented in this dissertation are utilized only for screening purposes. Specifically, they were conducted to evaluate whether the system variables (dicyandiamide concentration in Chapter 4) produced any changes in the typical elastomer particle size, particle size distribution, or particle/system morphology. These findings were then related, where possible, to any changes that were observed in the bulk mechanical, fracture, or adhesive properties of the systems.

Transmission electron micrographs of the bulk fracture specimens clearly demonstrated the characteristic 2-phase morphology of the toughened systems, and it was found that this bulk morphology was not influenced by the dicyandiamide concentration variations. The rubber phase, in all of the formulations, retained its roughly spherical shape and size of approximately 0.5 microns in diameter. The TEM images are shown in Figure 4.9. From this it was theorized that perhaps morphological changes were occurring only in the region of the interphase, since that is also where the XPS analyses of Chapter 3 detected chemical functionality variations. To test this theory, a sample was taken from the bottom interphase, evaluated, and visually compared to the bulk. No differences were distinguishable. The rubber phase remained nearly spherical and the diameter was unchanged as well (0.5 microns). These images are shown in Figure 4.10.

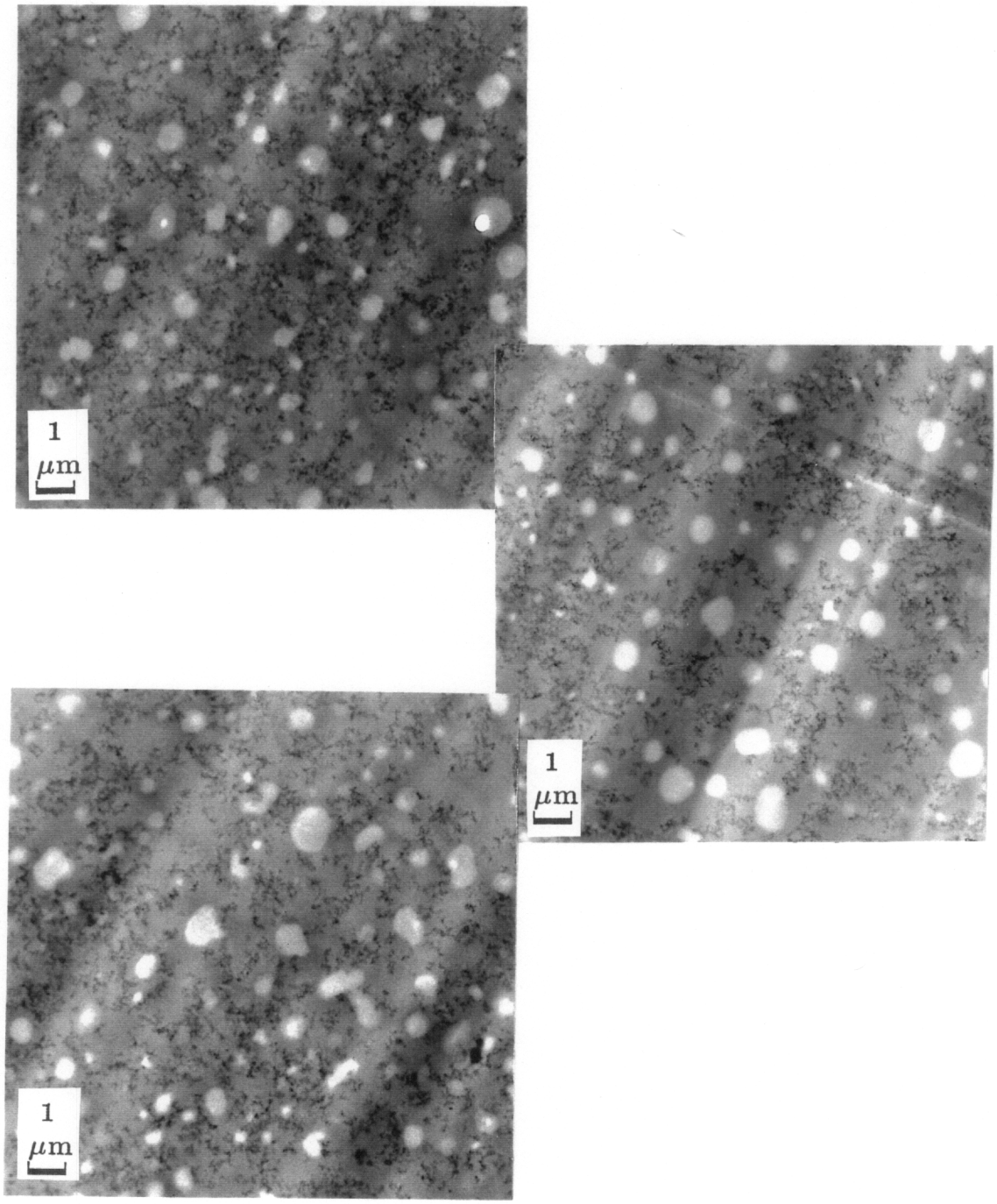

Figure 4.9 Transmission electron micrographs of the bulk adhesives. From top to bottom, 2.5 wt.% Dicy, 4.1 wt.% Dicy, and 6.2 wt.% Dicy.

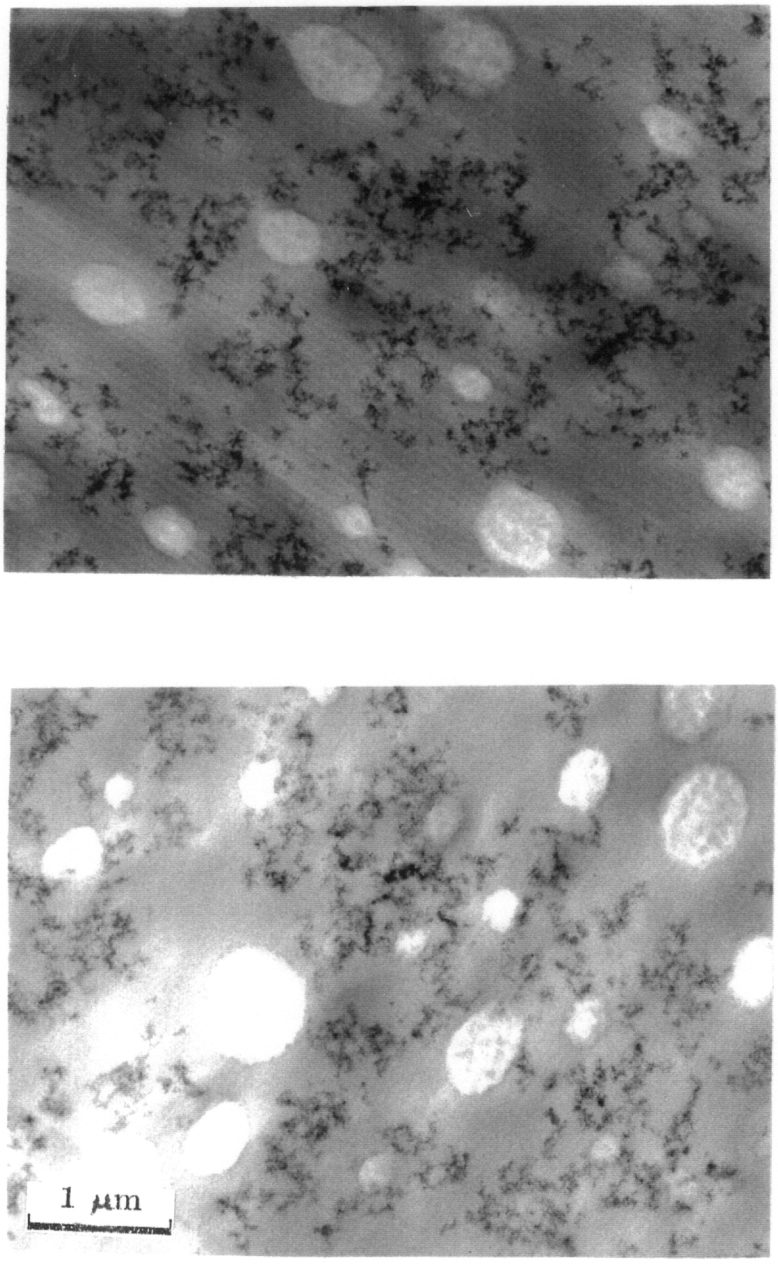

Figure 4.10 Transmission electron micrographs of adhesive C2. From top to bottom, the bulk adhesive (SENB) and the DCB bottom interphase.

4.3.5 XPS Failure Surface Evaluations

X-ray photoelectron spectroscopy (XPS) studies were conducted, in an identical fashion to the studies described in Chapter 3, to quantify the failure surfaces of the SENB, static DCB, fatigue DCB, and NCA specimens. The two sides of the broken bonded specimens are denoted in the tables as the "metal" and "adhesive" sides corresponding to their appearances, and the nonbonded steel is denoted as "steel".

The results of these XPS evaluations are summarized in Tables 4.2-4.8. Table 4.2 gives the failure surface compositions obtained from the SENB specimens, Tables 4.3 and 4.4 give the failure surface compositions for the static DCB specimens, Tables 4.5 and 4.6 give the failure surface compositions for the NCA specimens, and Tables 4.7 and 4.8 summarize the results from the failed fatigue DCB specimens.

Table 4.2 Surface compositions (at.%) for the bulk adhesive (SENB) failures as a function of Dicy content .

Formulation (Wt.% Dicy)	C1 (2.5%)	C2 (4.1%)	C3 (6.2%)
Carbon	76.2	79.0	76.9
Oxygen	18.0	15.5	16.2
Nitrogen	2.6	3.5	4.3
Iron	<0.2	<0.2	<0.2
Silicon	3.3	2.1	2.7

Table 4.3 Surface compositions (at.%) for the static DCB failures (adhesive side) as a function of Dicy content.

Formulation (Wt.% Dicy)	C1 (2.5%)	C2 (4.1%)	C3 (6.2%)
Carbon	83.2	77.6	77.0
Oxygen	13.0	15.5	17.7
Nitrogen	2.7	3.4	3.2
Iron	<0.2	<0.2	<0.2
Silicon	1.1	2.1	2.2

Table 4.4 Surface compositions (at.%) for the static DCB failures (metal side) as a function of Dicy content.

Formulation (Wt.% Dicy)	C1 (2.5%)	C2 (4.1%)	C3 (6.2%)	Steel
Carbon	77.0	71.0	65.5	51.7
Oxygen	17.6	24.4	26.8	37.5
Nitrogen	2.6	1.7	1.5	<0.2
Iron	2.8	2.9	6.3	10.3
Silicon	<0.2	<0.2	<0.2	<0.2

Table 4.5 Surface compositions (at.%) for the NCA failures (adhesive side) as a function of Dicy content.

Formulation (Wt.% Dicy)	C1 (2.5%)	C2 (4.1%)	C3 (6.2%)
Carbon	81.1	81.8	81.0
Oxygen	15.8	14.6	14.8
Nitrogen	2.8	3.0	3.6
Iron	<0.2	<0.2	<0.2
Silicon	0.4	0.6	0.5

Table 4.6 Surface compositions (at.%) for the NCA failures (metal side) as a function of Dicy content.

Formulation (Wt.% Dicy)	C1 (2.5%)	C2 (4.1%)	C3 (6.2%)	Steel
Carbon	51.7	53.0	54.9	51.7
Oxygen	36.7	35.1	34.4	37.5
Nitrogen	1.8	1.9	1.7	<0.2
Iron	9.9	10.0	8.4	10.3
Silicon	<0.2	<0.2	0.7	<0.2

Table 4.7 Surface compositions (at.%) for the fatigue DCB failures (adhesive side) as a function of Dicy content.

Formulation (Wt.% Dicy)	C1 (2.5%)	C2 (4.1%)	C3 (6.2%)
Carbon	81.6	81.1	79.5
Oxygen	14.9	15.5	15.9
Nitrogen	2.0	2.0	2.5
Iron	<0.2	<0.2	<0.2
Silicon	1.0	1.5	1.8

Table 4.8 Surface compositions (at.%) for the fatigue DCB failures (metal side) as a function of Dicy content.

Formulation (Wt.% Dicy)	C1 (2.5%)	C2 (4.1%)	C3 (6.2%)	Steel
Carbon	50.0	54.6	53.1	51.7
Oxygen	38.2	34.4	31.7	37.5
Nitrogen	1.2	1.9	6.7	<0.2
Iron	10.6	9.2	8.6	10.3
Silicon	<0.2	<0.2	<0.2	<0.2

A comparison of the surface compositions from the bulk (SENB) fractures produced some interesting results. As the dicyandiamide concentration was increased across a set of formulations (as in Table 4.1), the nitrogen level increased very slightly (see Table 4.2). It was thus suggested that the bulk adhesive chemistry could be influenced by the curing agent concentration. However, since the bulk mechanical evaluations of Section 4.3.1 did not show any performance variations with these changes, the results quickly became suspect. It was therefore necessary to evaluate the C 1s and O 1s photopeaks (presented in Figures 4.11 and 4.12) to gain further information into this phenomenon. With the photopeaks and mechanical data it was determined that any differences in the chemical compositions were minimal, and overall, variations in the dicyandiamide concentration did not produce any significant changes in the chemistry or mechanics of the bulk materials.

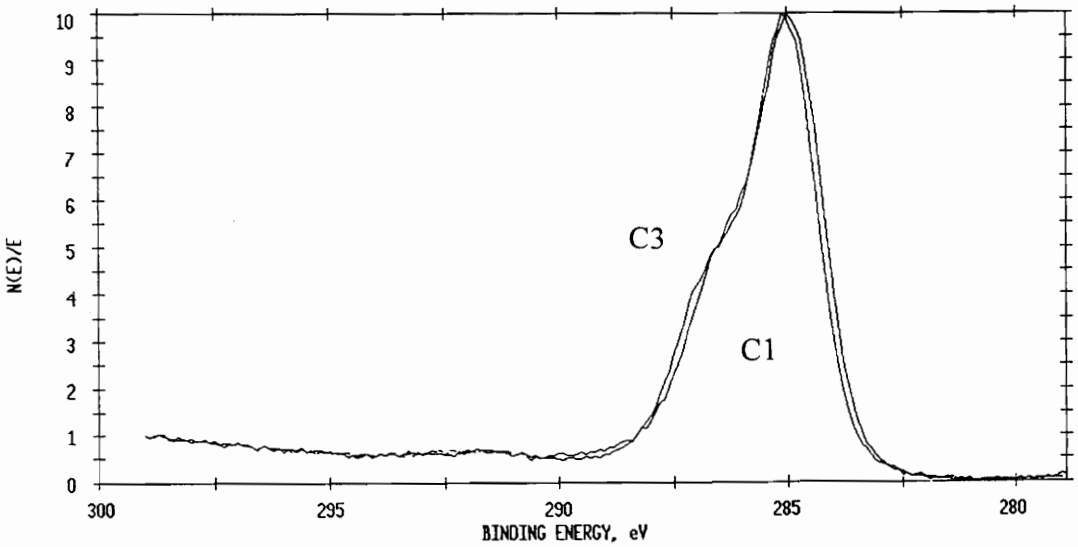

Figure 4.11 Montage of C 1s photopeaks from the bulk fracture (SENB) analyses (adhesives C1 and C3).

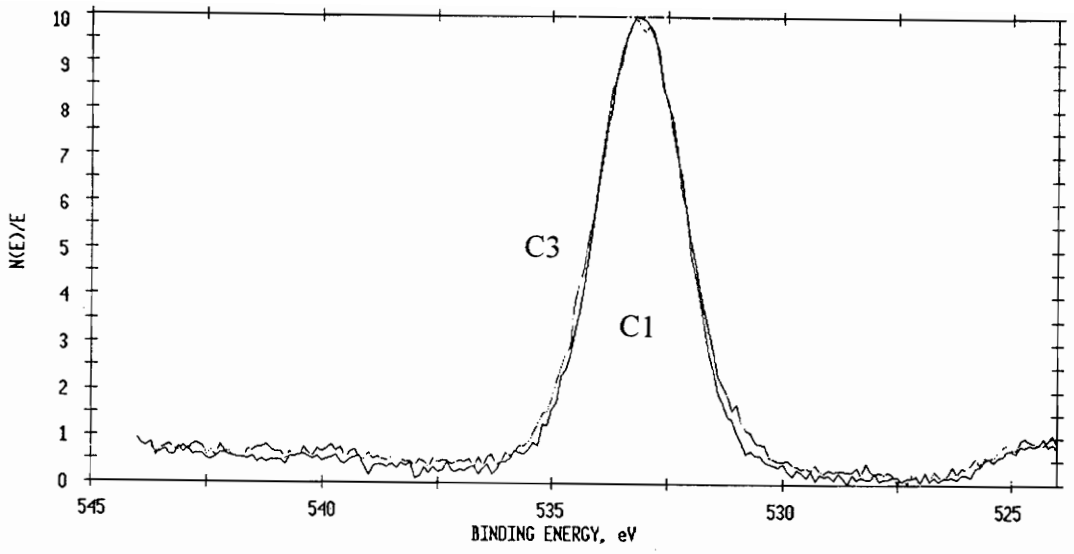

Figure 4.12 Montage of O 1s photopeaks from the bulk fracture (SENB) analyses (adhesives C1 and C3).

The results of the studies from Chapter 4 indicate that the chemistries of the bulk and interphase regions are not equivalent in these systems (latent cure epoxies). This point was stressed in Chapter 3, and therefore another elaborate discussion is not necessary. Rather, the focus is shifted to the region of the interphase which is the main point of interest in the studies of Chapter 4. From the results of the bonded system failure surface analyses it was shown that the fractures occurred in the region of the epoxy/steel interphase. This was based on a comparison of the metal side surface iron values from the failed specimens (fatigue DCB, static DCB, and NCA) with the nonbonded steel surface iron values. The bonded system values ranged from 2.7 to 10.6 at.% , with the nonbonded steel value at 10.3 at.%. In addition, the adhesive side iron values were all determined to be < 0.02 at.%, which lead to the conclusion that none of the failures occurred within the surface layers of the metal.

Although all of the systems failed in the region of the epoxy/steel interphase, for the different types of test specimens the fractures occurred at different locations within the interphase (as in Chapter 3). With the static DCB specimens, the average surface iron value for the metal side of the failure was about 4.0 at.%. With both the fatigue DCB and NCA analyses, the average metal side surface iron values were determined to be about 9.5 at.%. Thus, the static DCB specimens most likely failed well within the interphase region, thus leaving a thin coating of adhesive material on the metal substrate. The fatigue DCB and NCA specimens, on the other hand, probably peeled cleanly from the surface of the metal substrate (leaving only trace amounts of adhesive). From these results it was also noted that the curing agent content, while significantly influencing the interfacial fracture properties of the bonded systems, did not appear to have any impact on the location of the failures within the interphase. That is, within a given set of tests, failures consistently occurred at one location regardless of the adhesive formulation being tested.

In an effort to better understand the exact influence of dicyandiamide concentration on the interphase region (influences on both chemical and mechanical properties), analyses of the C 1s and O 1s photopeaks from the metal side of the NCA failures were conducted. These are presented in Figures 4.13 and 4.14 and demonstrate quite clearly a variation in the interphase chemistry as a function of curing agent content. It is difficult to relate this general information to chemical specifics, but if reasonable thought and consideration are given to the specific reaction mechanisms (as outlined in Section 1.3.2), then explanations such as the following can be justified. As the concentration of dicyandiamide is increased in these formulations, sedimentation to the interphase likewise increases and a dicyandiamide rich phase is formed. This results in an inefficient cross-linking in the vicinity of the metal surface, since at high dicyandiamide levels chain extension is the favored reaction scheme. In addition, a decrease in the interfacial fracture performance is noted. These results are clearly demonstrated by the increase in the shoulder of the O 1s photopeak at 533.5 eV, a 1.5 eV

shift (from 532 eV) in the binding energy due to formation of C-O-H, and the simultaneous increase in the failure surface nitrogen levels (see Tables 4.5-4.6).

Surface analyses from either the NCA or fatigue DCB specimens could have been utilized to provide the previously discussed information, since failures in both occurred at approximately the same location in the epoxy/steel interphase region. However, because the results of the fatigue DCB tests did not follow the trends established by all of the other studies (static DCB and NCA), the NCA failures were chosen. Specifically, the results of the fatigue tests (shown in Figure 4.8) demonstrated that at either the lowest or highest concentrations of dicyandiamide, 2.5 or 6.1% by weight, respectively, improved interfacial fracture performances were noted in comparison to the mean dicyandiamide level of 4.1% by weight. It is important to point out that this particular set of fatigue test results does not correspond well with the other (static) tests, but because it is an isolated finding it does not merit a great deal of explanation. A slight variation in even a seemingly minor control, such as the relative humidity of the testing laboratory, could have easily produced these altered results. Furthermore, the focus of this dissertation work has been mainly on static fracture testing, and the fatigue studies were used only to provide interfacial failures that occurred more in the vicinity of the metal substrate surface.

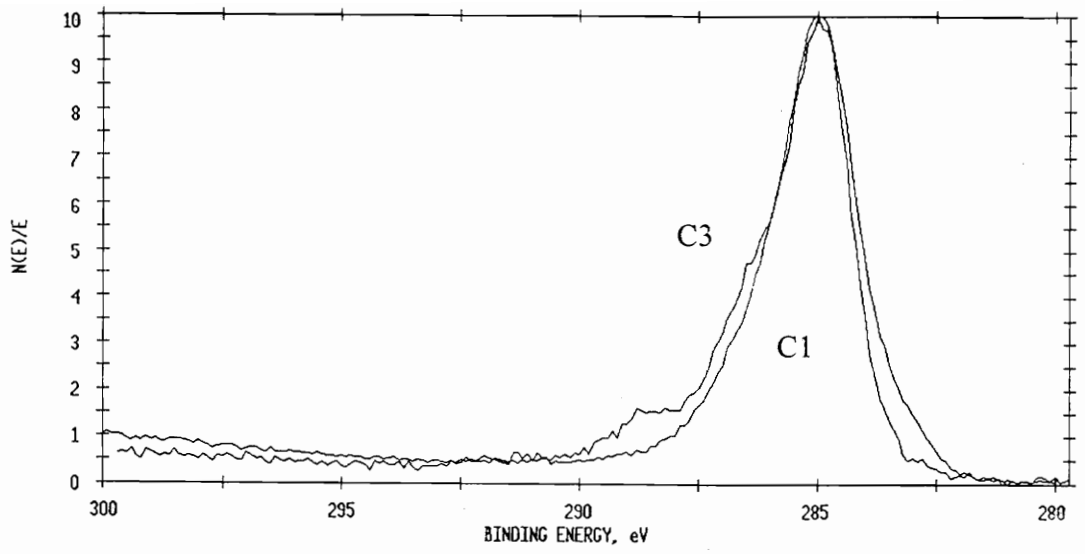

Figure 4.13 Montage of C 1s photopeaks from the NCA (metal side) failure surface analyses (adhesives C1 and C3).

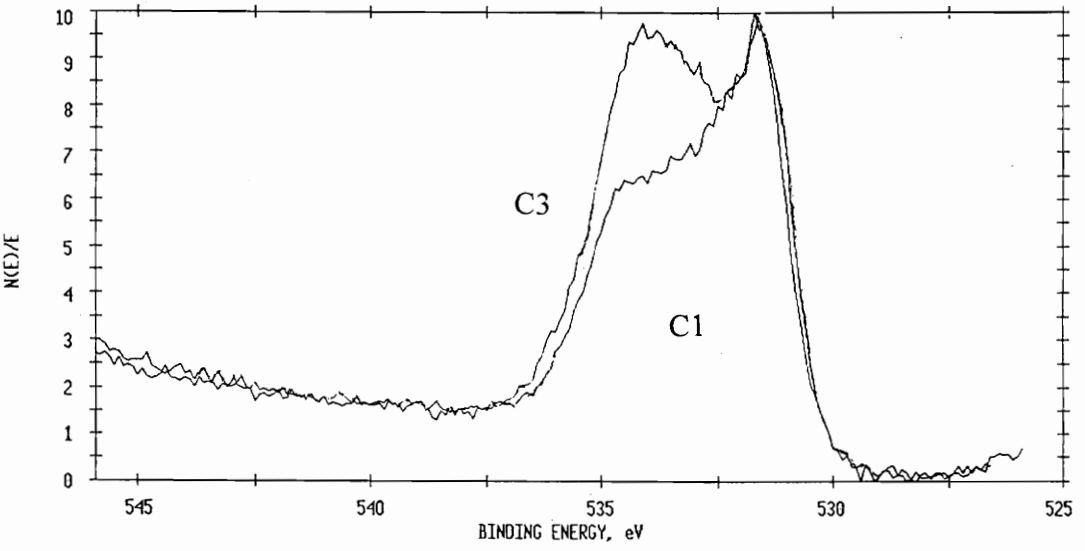

Figure 4.14 Montage of O 1s photopeaks from the NCA (metal side) failure surface analyses (adhesives C1 and C3).

Chapter 5
An Evaluation of Cure Temperature Variations

5.1 Introduction

The results of the research conducted for Chapter 4 lead to the research ideas focused upon in Chapter 5. These studies indicated that the bulk adhesive properties of latent cure epoxy systems were not influenced by variations in the curing agent content, but that the interfacial fracture properties of bonded systems depended greatly upon the concentration of dicyandiamide. Based on these results and the data from the failure surface analyses, and utilizing the available literature on the topic, several reasonable explanations for these findings were proposed. In the first case, it was theorized that during the cure cycle the dicyandiamide settled to the interphase and the undissolved crystals formed points of stress concentration. Thus, as the dicyandiamide content was increased, the number of stress concentration sites increased, and the overall interfacial fracture performance declined. In the second case, it was again theorized that the dicyandiamide settled to the interphase. This time, however, it was assumed that some or all of it dissolved in the epoxy resin. Therefore, in the vicinity of the steel substrate the concentration of dicyandiamide available for reaction was greatly increased. Since chain extension is the favored reaction pathway at high concentrations of dicyandiamide, this condition resulted in an inefficient crosslinking at the interphase. The interfacial fracture performance was accordingly decreased.

To further investigate the findings of Chapter 4, it was proposed that the influence of curing agent content on the bulk mechanical and adhesive properties of latent cure epoxy systems could be assessed by simply altering the cure temperature. This idea was based upon the fact that in nearly all epoxy related applications in which dicyandiamide is utilized, it is not soluble in the resin at room temperature and it is not very reactive at temperatures below 100 °C. At elevated temperatures (120-180 °C), however, it readily dissolves and reacts. In other words, the solubility of dicyandiamide in epoxy resins is highly dependent on the temperature. An equation which relates the temperature to the

amount of dicyandiamide which is soluble in a DGEBA resin has been developed by Hagnauer and coworkers.[54] It is a generalized expression only, dependent upon many factors (outlined in the publication), and given as follows:

$$\frac{\text{Dicyandiamide(g)}}{\text{Resin(100g)}} = 0.0227e^{0.0216T} \qquad [5.1]$$

where T is the cure temperature (°C). It does, however, demonstrate nicely how variations in the concentration of dicyandiamide can be produced through variations in the cure temperature. To better clarify this concept, consider the following. A given amount of dicyandiamide is added to the resin to act as the curing agent. This is the *total* amount of curing agent. However, because of the relative insolubility and low reactivity of dicyandiamide in epoxy resins, it typically exists in two different physical forms as the adhesive is heated and cured. First, there is the solid, undissolved material that has the potential to settle to the interphase and form stress concentrators. It is termed the *solid* portion. Secondly, there is the dicyandiamide which is dissolved in the resin and is thus responsible for crosslinking of the system. It is termed the *reactive* portion.

The analyses of Chapter 4 focused on varying the *total* amount of curing agent while maintaining a constant cure temperature. Thus, only the *solid* portion of the dicyandiamide changed from one formulation to the next, and the *reactive* content remained nearly constant. In the analyses of Chapter 5, curing agent content variations were studied by varying the temperature at a constant *total* dicyandiamide concentration. This resulted mainly in variations in the *reactive* dicyandiamide content, but also in small changes in the *solid* dicyandiamide content. In addition, the temperature was varied along with the *total* dicyandiamide content. This provided more studies of the same nature (i.e., variations mainly in the *reactive* dicyandiamide content) but at different isothermal cure temperatures. All of these together, by design, provided a significant amount of information on the interrelationships among *total, solid,* and *reactive* dicyandiamide contents, cure temperature, and bulk and bonded properties.

5.2 Experimental

The studies of Chapter 5 were conducted using the adhesive formulations summarized in Tables 3.1 and 4.1 (utilized in Chapters 3 and 4). As discussed in Section 5.1, this provided analyses on systems with constant total dicyandiamide concentrations and systems with variable total dicyandiamide concentrations. In addition, both untoughened and toughened formulations were tested. In the first case, the total dicyandiamide concentration was fixed as the cure temperature was varied. This effectively altered the amount of reactive dicyandiamide while maintaining a nearly constant level of solid dicyandiamide. In the second case, both the total dicyandiamide content and the cure temperature were varied. This effectively altered both the total and solid concentrations of dicyandiamide. By design, however, these simultaneous changes basically reproduced the first study described above (constant dicyandiamide, variable cure temperature), but at different total concentrations of dicyandiamide and different isothermal cure temperatures.

All of the sample preparation and testing procedures utilized in the studies of Chapter 5 were conducted in the same manner as those in Chapters 3 and 4. The isothermal cure temperatures utilized were 130 and 150 °C, however, instead of 170 °C.

5.3 Results and Discussion

5.3.1 Mechanical Tests

From the tensile and bulk fracture tests it was demonstrated that, for these model epoxy systems, changes in the cure temperature produced significant changes in the bulk material properties. While the modulus values shown in Figures 5.1 and 5.2 did not illustrate any definite trends, the K_{Ic} and G_{Ic} values shown in Figures 5.3-5.6 generally increased as the cure temperature increased from 130 to 170 °C.

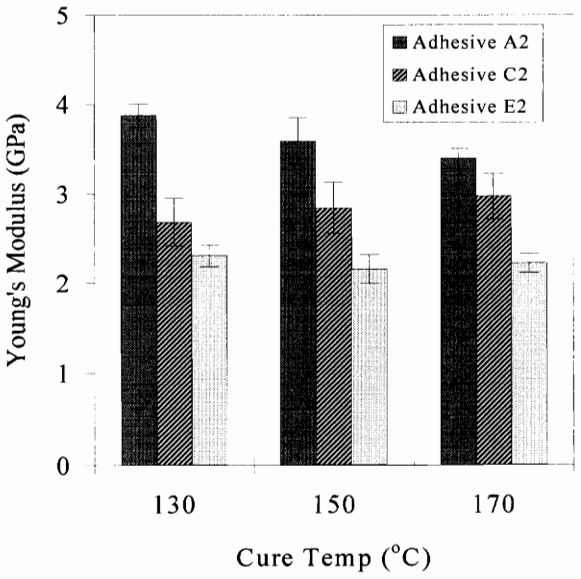

Figure 5.1 The bulk moduli as a function of the cure temperature (adhesives A2, C2, E2).

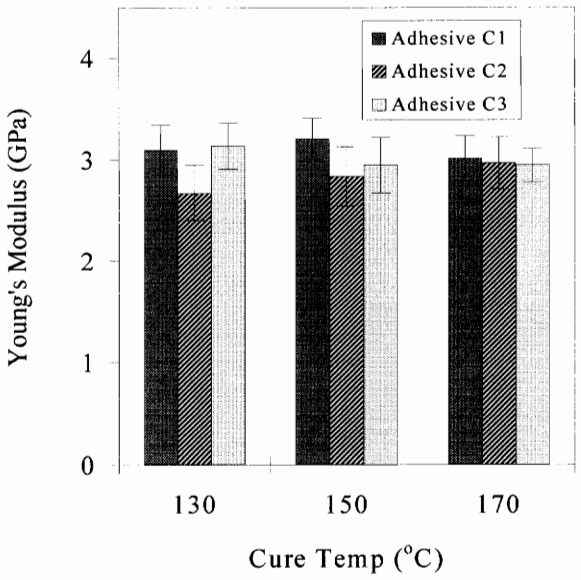

Figure 5.2 The bulk moduli as a function of the cure temperature (adhesives C1, C2, C3).

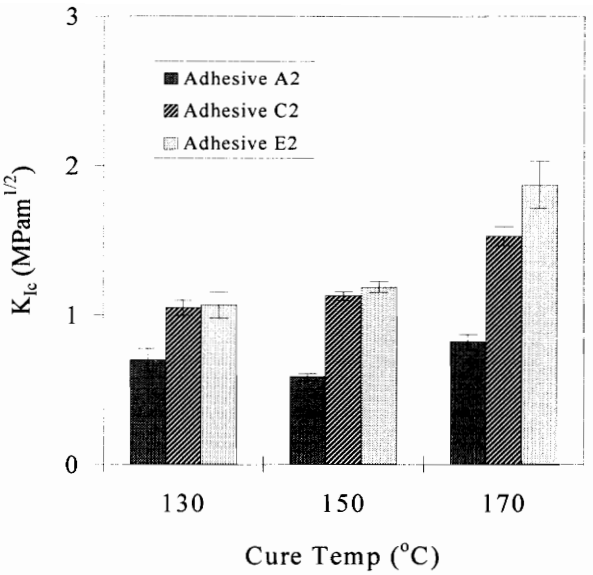

Figure 5.3 The influence of the cure temperature on the bulk adhesive K_{Ic} (adhesives A2, C2, E2).

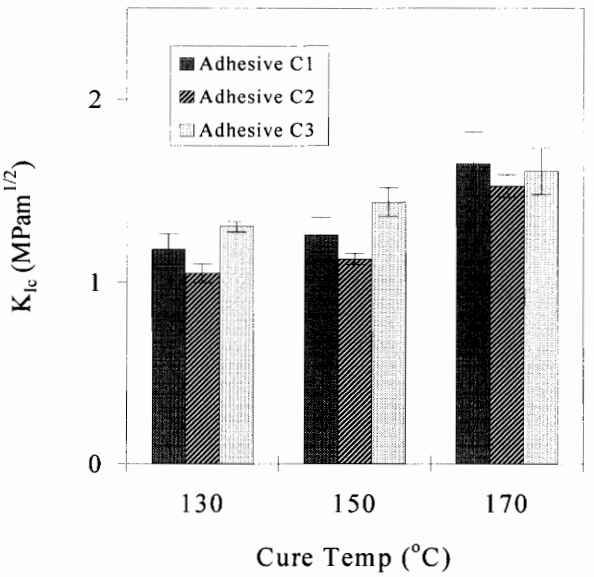

Figure 5.4 The influence of the cure temperature on the bulk adhesive K_{Ic} (adhesives C1, C2, C3).

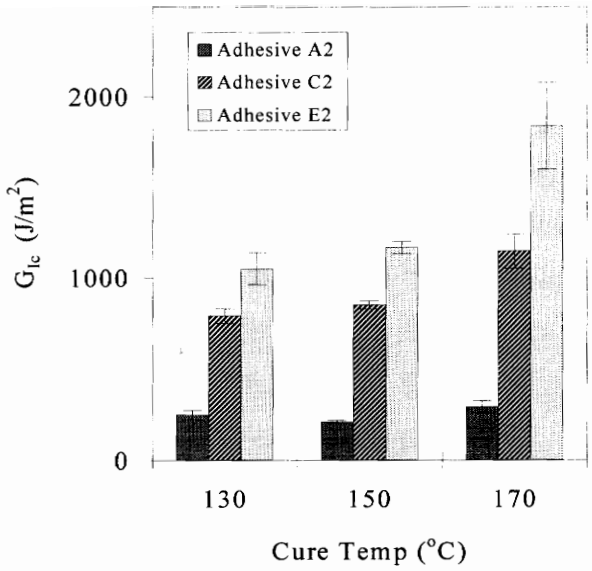

Figure 5.5 The influence of the cure temperature on the bulk adhesive G_{Ic} (adhesives A2, C2, E2).

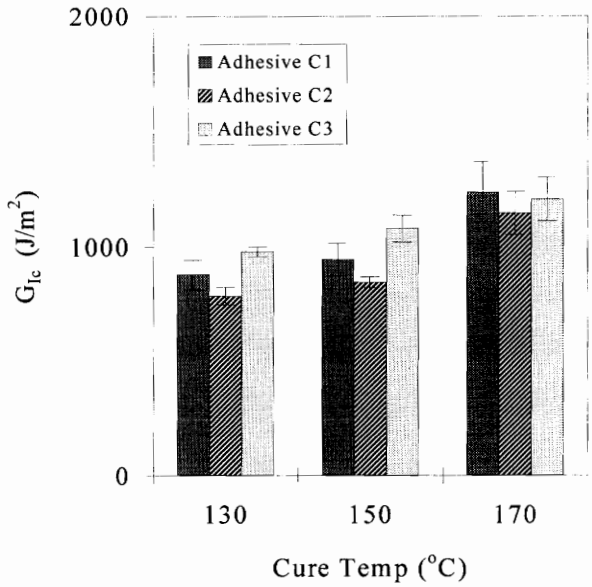

Figure 5.6 The influence of the cure temperature on the bulk adhesive G_{Ic} (adhesives C1, C2, C3).

The results of the bulk modulus evaluations indicate that the properties of these latent cure epoxy systems are independent of the cure temperature. For both the toughener variable (Table 3.1) and the dicyandiamide variable (Table 4.1) systems, as the cure temperature was increased from 130 to 170 °C in 20° increments, the modulus values were shown to remain essentially constant. As already discussed in Section 4.3.1, however, since the bulk modulus of a polymeric material is determined from stress-strain measurements at low levels of strain, notable changes in the modulus would not be expected (unless drastic system alterations had occurred).

The results of the bulk fracture evaluations, on the other hand, clearly demonstrated strong correlations with the cure temperature. For both the toughener variable and dicyandiamide variable systems, increases in the cure temperature generally resulted in increases in the K_{Ic} and G_{Ic} values. With the toughener variable systems it was noted that the temperature dependencies of the K_{Ic} and G_{Ic} values increased with increasing toughener content. That is, as the cure temperature was increased, adhesive E2 increased in fracture performance more significantly than did adhesive A2. With the dicyandiamide variable systems it was noted that the temperature dependencies of the K_{Ic} and G_{Ic} values were constant as the dicyandiamide content was increased. All three formulations showed nearly equivalent behavior with respect to the cure temperature variations, especially at the higher temperatures, regardless of the dicyandiamide concentration.

Evaluations of the dicyandiamide variable systems also suggest the possibility of dicyandiamide sedimentation (once again). This is based on the fact that, for any given isothermal cure temperature (130, 150, or 170 °C), adhesives C1, C2, and C3 all demonstrate nearly equivalent fracture properties. Thus, it is apparent that the bulk fracture properties of these latent cure epoxy systems are independent of the total curing agent concentration. It could be theorized from these results, as well, that since the dicyandiamide concentration at a fixed cure temperature does not affect the bulk material, it must be concentrating elsewhere in the system (interphase) and having an

impact there (see Section 5.3.2). These results are in agreement with the results of the Chapter 4 evaluations (see Section 4.3.1).

Since the bulk fracture properties vary from one isothermal cure temperature to another for adhesives C1, C2, and C3, it is also apparent that the bulk properties are dependent upon the reactive dicyandiamide concentration. Stated another way, the K_{Ic} and G_{Ic} values for the adhesives are equivalent at each isothermal cure temperature. However, as the cure temperature is increased, and thus the amount of reactive dicyandiamide is increased, the fracture values likewise increase (each formulation increases equivalently). Since the change in cure temperature substantially impacts only the reactive dicyandiamide concentration, and only slightly affects the solid dicyandiamide content, these findings seem to indicate that the reaction mechanisms contribute significantly to the performance properties of the bonded systems.

All of the findings discussed in the previous several paragraphs are statistically significant and conceptually important. The idea of dicyandiamide sedimentation is once again suggested, and for the first time in any of this research, the reaction mechanisms are specifically implicated in contributing to bonded system performance. Due to the significance of these findings, a more thorough assessment and discussion of each is given in the sections on bonded systems (Section 5.3.2) and failure surfaces (Section 5.3.5).

5.3.2 Adhesive Evaluations (Static)

The results of the adhesive evaluations exhibit an appreciable dependence on the cure temperature. As shown in Figures 5.7 and 5.8, the SLS strength values increase with increasing isothermal cure temperature (from 130 to 170 °C). The SERR values, determined from the DCB and NCA tests and shown in Figures 5.9 through 5.12, also demonstrate a pronounced dependence on the cure temperature. The specific responses of these specimens to the cure temperature variations, however, are more difficult to generically (generally) describe.

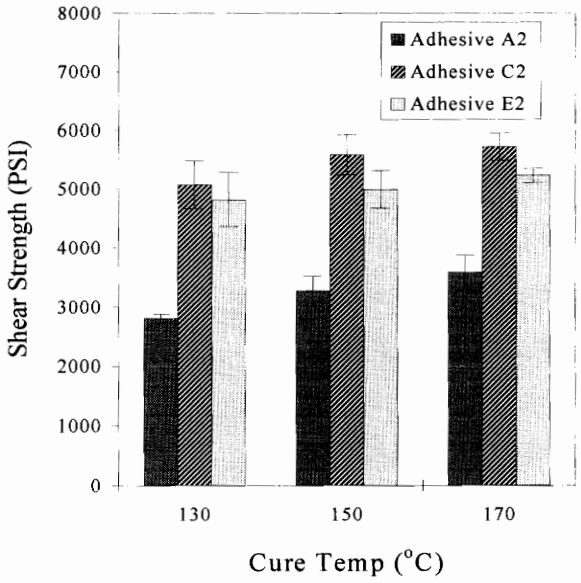

Figure 5.7 SLS strength as a function of cure temperature (adhesives A2, C2, E2).

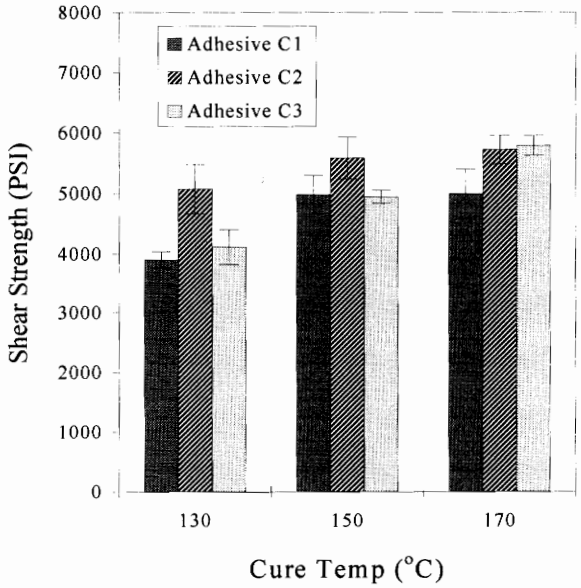

Figure 5.8 SLS strength as a function of cure temperature (adhesives C1, C2, C3).

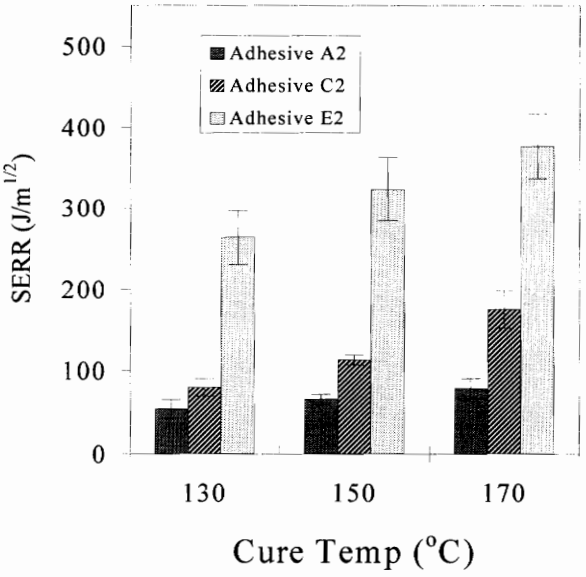

Figure 5.9 Static DCB performance as a function of cure temperature (adhesives A2, C2, E2).

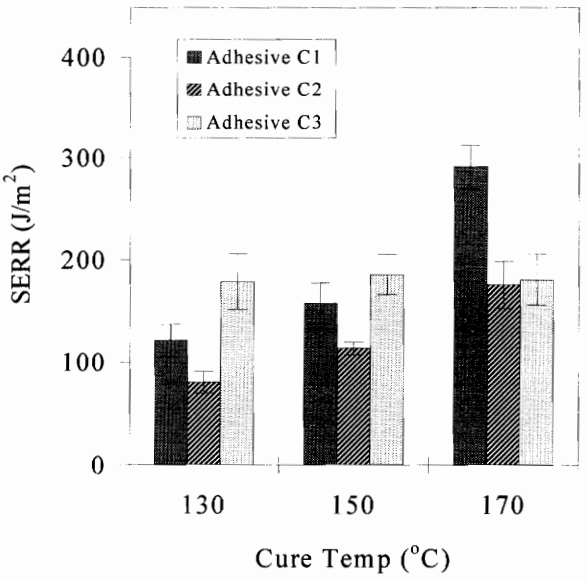

Figure 5.10 Static DCB performance as a function of cure temperature (adhesives C1, C2, C3).

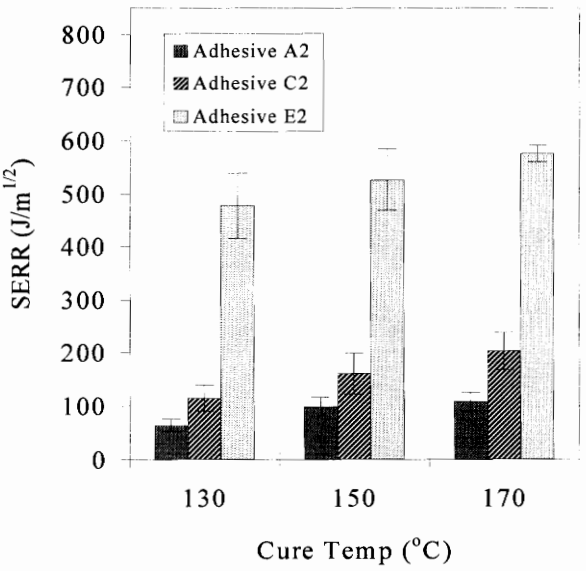

Figure 5.11 NCA performance as a function of cure temperature (adhesives A2, C2, E2).

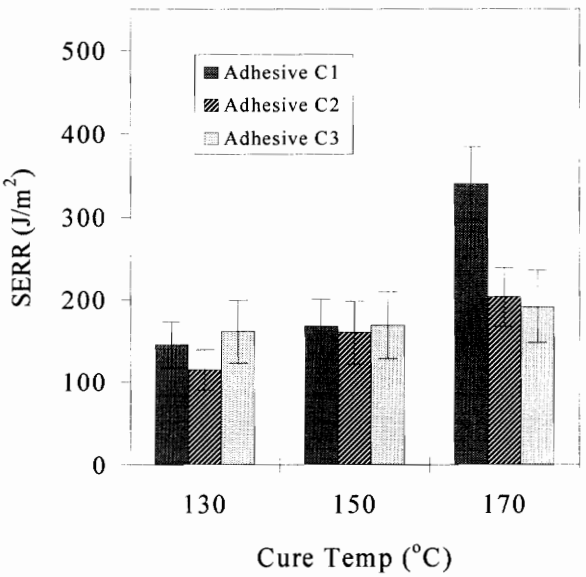

Figure 5.12 NCA performance as a function of cure temperature (adhesives C1, C2, C3).

There are many interesting results which arise from the bonded system evaluations. Due to the vast number of tests utilized in this stage of the research project (all differing in formulation, test specimen geometry, and cure temperature), it is difficult to isolate and discuss any generally occurring trends. In fact, possibly the only result that can be generalized over all of the testing is that, along with the findings of the bulk fracture analyses, the results of the bonded system studies indicate that the adhesion performance of these systems is highly dependent upon the cure temperature. Thus, rather than oversimplifying the results in order to make generalizations, the following discussions work through the results from each type of testing in great detail (e.g., SLS, static DCB, and NCA). Where pertinent, comparative discussions of the different test results are given.

The SLS strength values for the toughener and dicyandiamide variable systems are given in Figures 5.7 and 5.8. These plots demonstrate the same basic responses with respect to the concentrations of toughener and dicyandiamide that were noted in Chapters 3 and 4. Additionally, they show a superficial dependence on the isothermal cure temperature. That is, at a given isothermal cure temperature, increases in the toughener content from 0 to 20.3% by weight produce an increase in the SLS strength values. The values then either plateau or decrease a little as the toughener content is increased to 37.6% by weight. And as the isothermal cure temperature is increased, the individual values increase again, minimally. For the dicyandiamide variable systems at a fixed isothermal cure temperature, increases in dicyandiamide content from 2.5 to 4.1% by weight generally produce an increase in the SLS strength values. The values then either slightly decrease or plateau as the dicyandiamide content is increased to 6.2% by weight. And as the isothermal cure temperature is increased, the SLS values are likewise increased very slightly, overall.

The results of the NCA and DCB analyses also demonstrate trends consistent with those established in Chapters 3 and 4, and this information is presented graphically in Figures 5.9-5.12. The trends in these results are essentially opposite (again) the trends from the SLS studies (see Section 3.3.2 for a detailed explanation). They demonstrate

that as the toughener level is increased, at constant isothermal cure temperature, the interfacial fracture performance increases. Then, as the isothermal cure temperature is increased, the fracture performance again increases very slightly. It is also apparent in these results, not unlike in the results of the bulk fracture studies, that as the toughener content is increased the dependence upon the isothermal cure temperature increases. In other words, the fracture toughness of adhesive E2 is more dramatically improved than the fracture toughness of adhesive A2 as the isothermal cure temperature is increased.

For the dicyandiamide variable systems it is difficult to isolate specific trends in the data. This is a result of the fact that, just as with the fatigue evaluations of Chapter 4, the data for adhesive C2 seems out of place. There are many possibilities for why this has occurred, but these will not be discussed. Rather, it should simply be understood that some of the experimental values measured throughout this dissertation, especially on systems prepared with adhesive C2, are suspect. Therefore, the trends in the data should be taken from formulations C1 and C3. With this in mind, for the dicyandiamide variable systems at a fixed isothermal cure temperature, increases in dicyandiamide content from 2.5 to 4.1% by weight generally produce a decrease in the interfacial fracture values. The values then plateau or slightly increase as the dicyandiamide content is increased to 6.2% by weight. Overall, as the isothermal cure temperature is increased, the interfacial fracture values are likewise increased.

One very distinct trend that is obvious in the interfacial fracture results, however, is the increasing temperature dependence of the adhesive systems with increasing dicyandiamide concentration. Thus, as the cure temperature is increased from 130 to 170 °C, the fracture performance of adhesive C1 changes more drastically than does the fracture performance of adhesive C3. In fact, while the fracture results for adhesive C1 change dramatically, changes in the fracture properties of adhesive C3 are statistically insignificant. These results very clearly support the concept of dicyandiamide sedimentation, since at a given isothermal cure temperature every formulation has essentially the same concentration of reactive dicyandiamide (see Equation 5.1). Thus,

all that varies is the solid dicyandiamide concentration. This most likely influences the interfacial fracture performance by settling to the interphase region.

5.3.3 TEM Studies

The microstructural features of elastomer toughened thermosetting adhesives (latent cure epoxies) associated with the bulk mechanical and fracture properties of such systems were already reviewed in Sections 3.3.4 and 4.3.4. Specifically, the features of elastomer volume fraction, particle size, particle size distribution, adhesion across the particle/matrix interface, morphology, and glass transition temperature were discussed. It must be stated again here, however, that the TEM studies presented in this dissertation are utilized only for screening purposes, and not for definitive evaluations of the previously mentioned concepts. These analyses were conducted to evaluate whether the system variables (cure temperature variations in Chapter 5) produced any significant changes in the typical elastomer particle size, particle size distribution, or particle/system morphology. These findings were then related, where possible, to any changes that were observed in the bulk mechanical, fracture, or adhesive properties of the systems.

Transmission electron micrographs of the bulk fracture specimens clearly demonstrated the characteristic 2-phase morphology of the toughened systems, and it was found that this bulk morphology was not influenced by the cure temperature variations. For time and space considerations, however, only one representative evaluation is presented. The analyses of bulk samples of adhesive C2, cured at 130, 150, and 170 °C, demonstrated that regardless of the cure temperature, the rubber domains were roughly spherical with an average diameter of approximately 0.5 microns. The TEM images of these samples are shown in Figure 5.13.

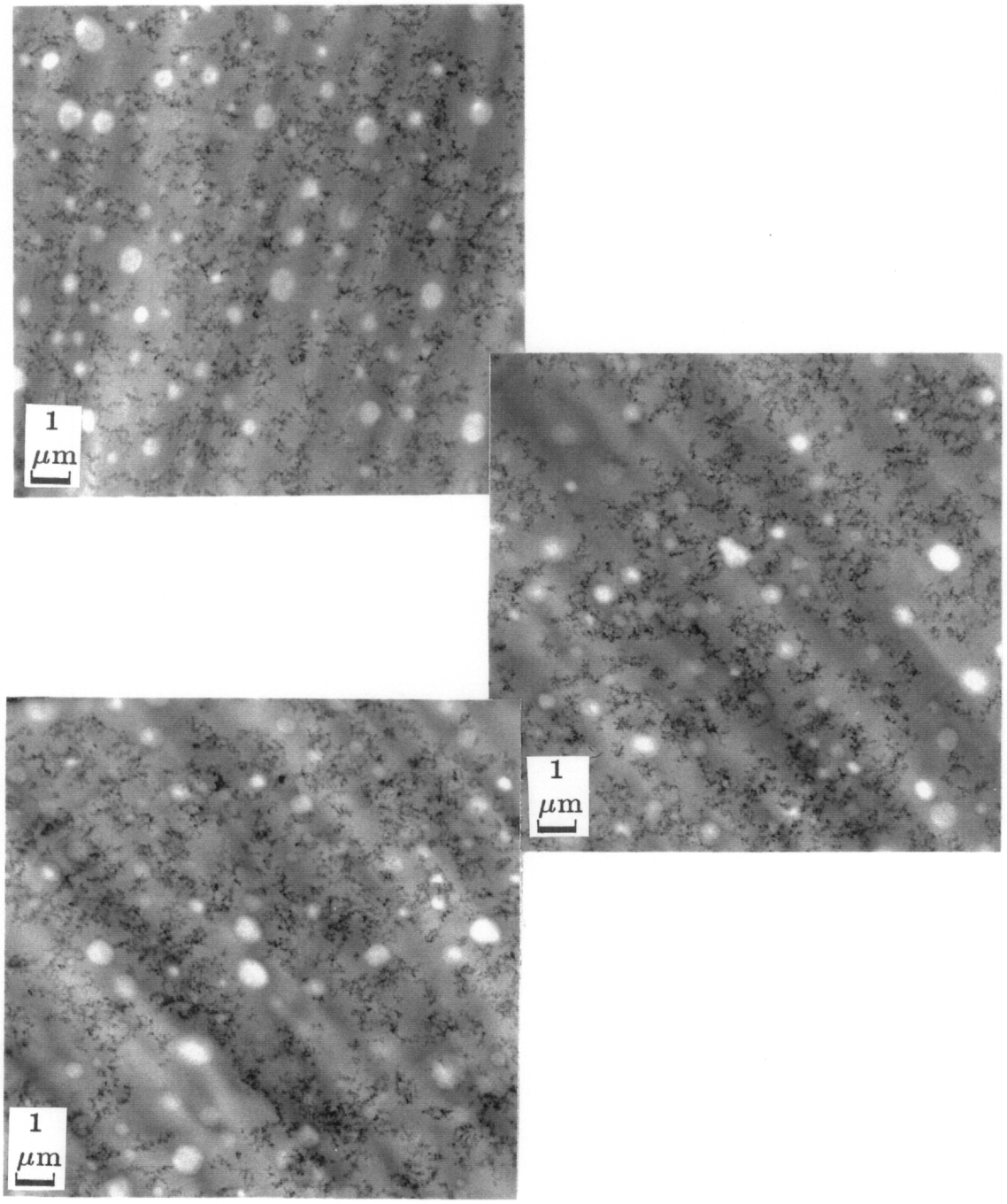

Figure 5.13 Transmission electron micrographs of adhesive C2. From top to bottom, cure temperatures of 130, 150, and 170 °C.

5.3.4 XPS Failure Surface Evaluations

X-ray photoelectron spectroscopy (XPS) studies were conducted to quantify the failure surfaces of the SENB, static DCB, fatigue DCB, and NCA specimens. However, for the purposes of these studies, and due to time and space constraints, only the results of the DCB and SENB analyses will be presented. In addition, these will be limited to the results of the analyses of adhesives A2 and E2 only. Tables 5.2 and 5.3 present a summary of results from the SENB failures, and Tables 5.4-5.7 give the surface results of the static DCB failures.

Table 5.2 Surface compositions (at.%) for the bulk adhesive (SENB) failures as a function of the cure temperature (adhesive A2).

Formulation (Cure Temp)	A2 (130 °C)	A2 (150 °C)	A2 (170 °C)
Carbon	76.2	79.0	77.9
Oxygen	18.0	15.5	17.9
Nitrogen	2.6	3.5	3.1
Iron	<0.2	<0.2	<0.2
Silicon	3.3	2.1	1.1

Table 5.3 Surface compositions (at.%) for the bulk adhesive (SENB) failures as a function of the cure temperature (adhesive E2).

Formulation (Cure Temp)	E2 (130 °C)	E2 (150 °C)	E2 (170 °C)
Carbon	79.3	80.9	78.4
Oxygen	15.0	14.4	16.7
Nitrogen	3.8	4.4	2.5
Iron	<0.2	<0.2	<0.2
Silicon	1.9	<0.2	2.4

Table 5.4 Surface compositions (at.%) for the static DCB failures (adhesive side) as a function of the cure temperature (adhesive A2).

Formulation (Cure Temp)	A2 (130 °C)	A2 (150 °C)	A2 (170 °C)
Carbon	82.1	78.6	77.3
Oxygen	13.7	15.8	15.8
Nitrogen	3.1	4.7	5.3
Iron	<0.2	<0.2	<0.2
Silicon	1.2	0.8	1.6

Table 5.5 Surface compositions (at.%) for the static DCB failures (metal side) as a function of the cure temperature (adhesive A2).

Formulation (Cure Temp)	A2 (130 °C)	A2 (150 °C)	A2 (170 °C)	Steel
Carbon	51.5	61.4	52.9	51.7
Oxygen	34.7	27.1	30.7	37.5
Nitrogen	3.9	4.7	6.8	<0.2
Iron	8.4	5.6	8.6	10.3
Silicon	1.5	1.1	1.0	<0.2

Table 5.6 Surface compositions (at.%) for the static DCB failures (adhesive side) as a function of the cure temperature (adhesive E2).

Formulation (Cure Temp)	E2 (130 °C)	E2 (150 °C)	E2 (170 °C)
Carbon	78.5	79.9	77.0
Oxygen	17.5	16.4	19.0
Nitrogen	2.8	3.2	3.0
Iron	<0.2	<0.2	<0.2
Silicon	1.1	0.5	1.0

Table 5.7 Surface compositions (at.%) for the static DCB failures (metal side) as a function of the cure temperature (adhesive E2).

Formulation (Cure Temp)	E2 (130 °C)	E2 (150 °C)	E2 (170 °C)	Steel
Carbon	51.9	53.7	56.2	51.7
Oxygen	34.9	34.8	34.8	37.5
Nitrogen	1.4	1.6	3.0	<0.2
Iron	10.7	9.9	7.0	10.3
Silicon	1.2	<0.2	0.7	<0.2

The XPS analyses of the bulk (SENB) failures, for adhesives A2 and E2, did not detect any variations in the surface compositions of the specimens as a function of the cure temperature. It was expected that as the cure temperature was increased, and thus the amount of reactive dicyandiamide in the system also increased, a corresponding increase in the failure surface nitrogen level would be noted. This was not the case which further demonstrates that chemical changes in these latent cure systems occur more prominently at the interphase than in the bulk.

To investigate this interesting result, the C 1s and O 1s photopeaks for adhesives A2 and E2 were inspected. These are given in Figures 5.14 and 5.15, for adhesive A2 as a representative case, and clearly demonstrate that the chemical composition of the bulk is influenced by variations in the cure temperature. This is based on the fact that, as the cure temperature is increased, a shoulder in the C1s photopeak appears at approximately 286.5 eV. Detailed explanations of other similar results have already been given in Chapters 3 and 4, and this is most likely indicative of an increased pendant hydroxyl concentration (C-O-H, indicative of the epoxy/dicy reaction), an increased ether concentration (C-O-C, indicative of the etherification side reaction), or

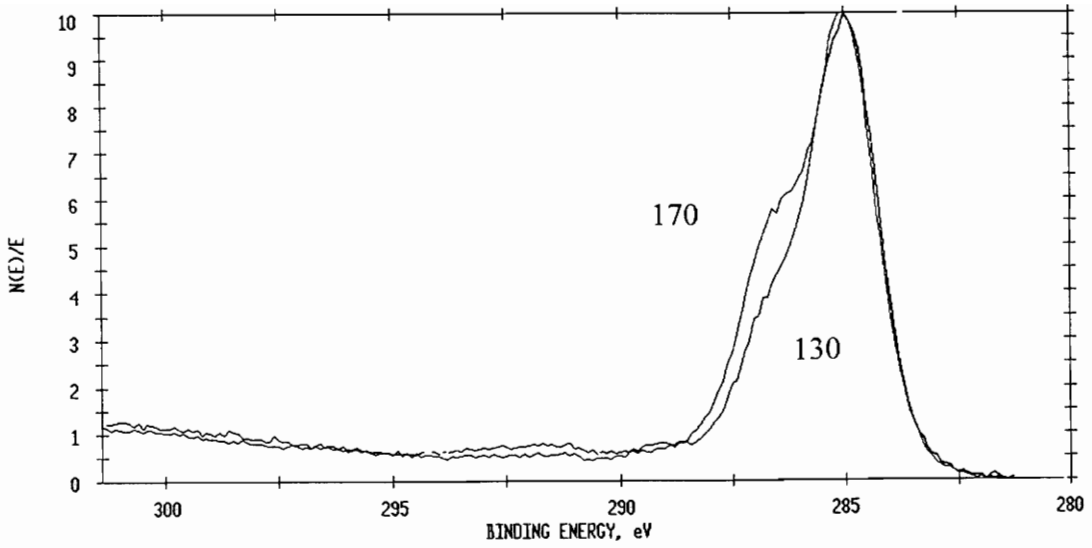

Figure 5.14 Montage of C 1s photopeaks from the bulk (SENB) failure surface analyses as a function of the cure temperature (adhesive A2).

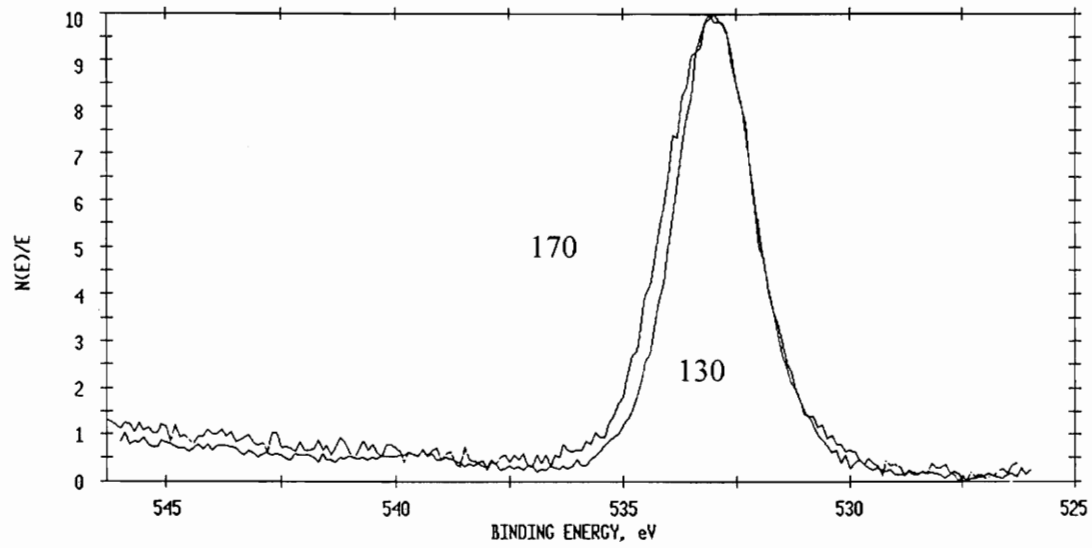

Figure 5.15 Montage of O 1s photopeaks from the bulk (SENB) failure surface analyses as a function of the cure temperature (adhesive A2).

an increased number of carbon-nitrogen linkages (C-N, indicative of reacted or unreacted dicyandiamide). In addition, a small increase in the shoulder of the O 1s photopeak is detectable at 533.5 eV and demonstrates that the change does involve some C-O functionality. However, based on the magnitude of this peak and comparing it with the magnitude of the shoulder in the carbon peak, the change is most likely attributable to the C-N functionality.

As has been the case in all of the studies thus far, the surface analysis results generally support the visual observation that the failures occurred in the region of the epoxy/steel interphase. This conclusion is based on a comparison of the metal side surface iron values, from the failed static DCB specimens, with the nonbonded steel surface iron values. Overall, the former ranged from 5.6 to 10.7 at.%, and the latter was 10.3 at.%. In addition, the adhesive side iron values were all determined to be < 0.02 at.%, which leads to the conclusion that failure did not occur within the metal substrates. Thus, failure is considered to occur very near to the metal surface, but still within the region of the epoxy/metal interphase.

From these results it was also noted that the cure temperature, while significantly influencing the interfacial fracture properties of the bonded systems, did not appear to have any impact on the location of the failures within the interphase. That is, within a given set of tests, failures consistently occurred at one location regardless of the isothermal cure temperature utilized. This result was consistent, as well, with respect to all of the other variables studied in this dissertation research. In no case was it found that toughener content variations, dicyandiamide concentration variations, or cure temperature modifications caused the locale of failure to change.

From this same set of data it was also determined that increases in the isothermal cure temperature resulted in increasing levels of nitrogen on the static DCB metal side failures. In other words, as the cure temperature was increased, it appears that the dicyandiamide concentration at the interphase likewise increased (Tables 5.5 and 5.7).

It is difficult to determine whether the nitrogen increases correspond to reactive dicyandiamide, solid dicyandiamide, or some combination of both. Thus, to gain some additional and more detailed information, the C 1s and O 1s photopeaks were inspected. These photopeaks, for adhesive A2 cured at temperatures of 130 and 170 °C, are given in Figures 5.16 and 5.17. From these plots it is obvious that the chemical composition at the interphase is significantly altered by the isothermal cure temperature variations. As the cure temperature is increased, shoulders appear in the interphase C 1s and O 1s curves at approximately 286.5 and 533.5 eV. It has been discussed extensively that these shoulders correspond to chemical functionalities present in dicyandiamide and dicy/epoxy reaction products. Thus, it will simply be stated that the results seem to indicate an increased dicyandiamide concentration at the interphase, much of which has been involved in curing reactions.

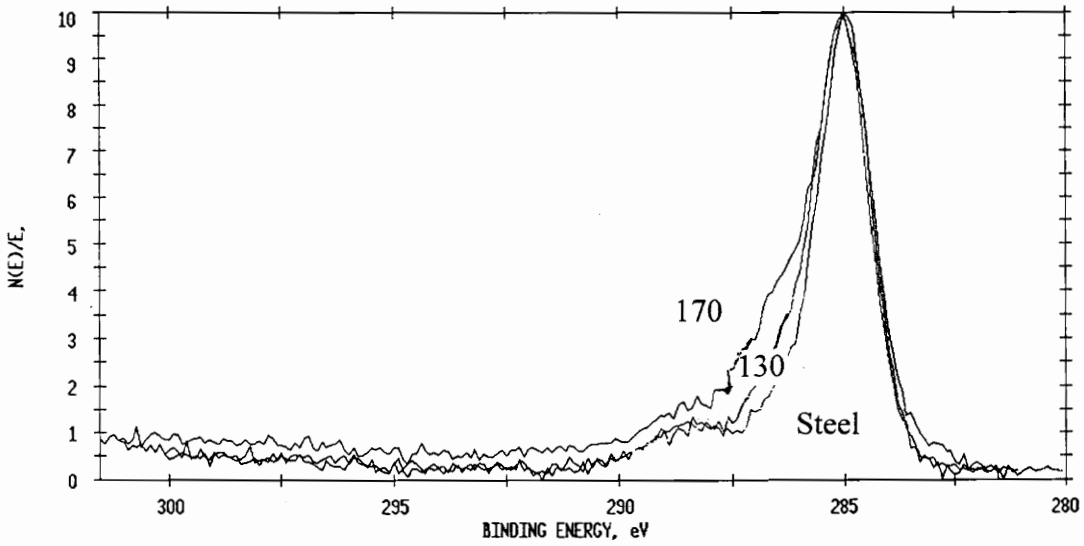

Figure 5.16 Montage of C 1s photopeaks from the static DCB failure surface analyses (adhesive side) as a function of the cure temperature (adhesive A2).

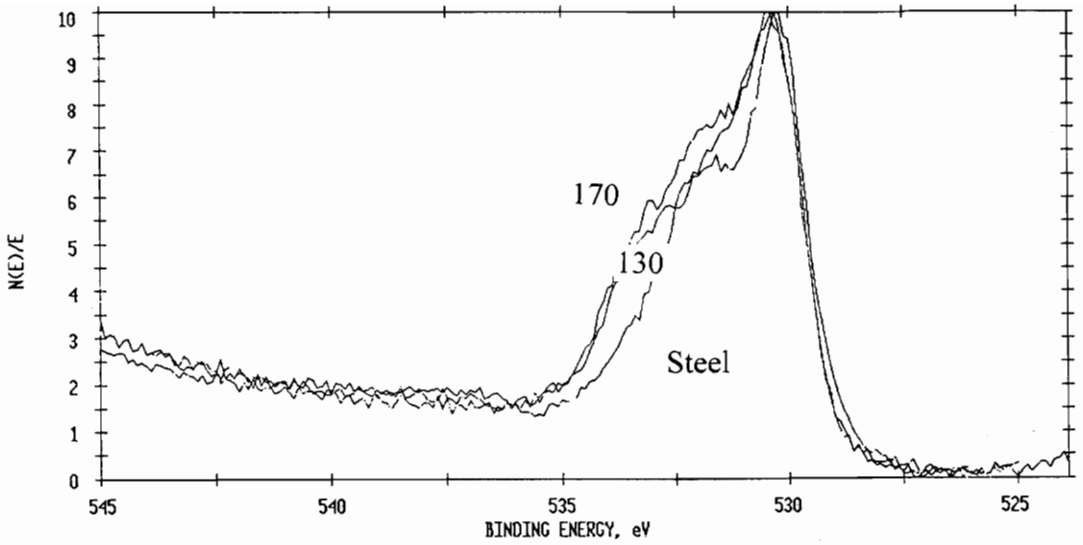

Figure 5.17 Montage of O 1s photopeaks from the static DCB failure surface analyses (metal side) as a function of the cure temperature (adhesive A2).

Together with the results from Chapters 3 and 4, the results of the research conducted in Chapter 5 leads to some very significant conclusions. Specifically, for these latent cure epoxy systems it is clearly demonstrated that as the dicyandiamide concentration increases, interfacial fracture performance decreases. Furthermore, increases in the cure temperature result in increases in the interfacial fracture performance. This dependence on cure temperature, however, decreases with increasing dicyandiamide content. Thus, it is very clear that, overall, the interfacial fracture performance depends highly upon minimization of the sedimentation of solid dicyandiamide to the interphase. This can be accomplished through either decreases in dicyandiamide content, or increases in the cure temperature. It should be noted, however, that by increasing the cure temperature and thus the concentration of reactive dicyandiamide, the reaction mechanisms and crosslinking scenario may be altered.

Chapter 6
An Evaluation of Contrasting Interphases

6.1 Introduction

In all of the bonded system fracture analyses conducted up to this point, the focus was maintained on the bottom interphase. That is, care was taken to ensure that crack initiation and propagation occurred in the epoxy/steel interphase region that was on the *bottom* of the hot press during the cure cycle. This provided a uniquely well suited system for evaluation of the effects of curing agent sedimentation on the interfacial fracture performance of epoxy/steel assemblies. Figure 2.2 (page 82) gives a schematic representation of the DCB curing arrangement and a designation of the *top* and *bottom* interphases.

The results of much of this dissertation research (Chapters 3-5) give support to the theory of dicyandiamide sedimentation. They have agreed with the limited research findings reported in the scientific literature, such as resultant chemical and mechanical variations, as well. From these concepts came the idea of studying the *top* interphase. If the overabundance of dicyandiamide at the bottom interphase caused such drastic changes in performance, it was proposed that the top interphase should also possess some unique properties due to a dicyandiamide deficiency. Also, it has been suggested independently by many researchers that the curing reactions of dicy/epoxy systems produce, and depend upon the emission of, gaseous reaction byproducts (e.g., methylamine). Thus, it was also proposed that limitations in the ability of the system to emit these volatiles, because of the bonded system geometry, could result in measurable fluctuations. As well, byproducts trapped at the top interphase could cause voids in the cured assembly (stress concentrators).

In the studies of Chapter 6 emphasis is placed on the top interphase. It is evaluated as a function of the cure temperature for adhesives A2 and E2, unmodified and toughened formulations, respectively. Static DCB specimens are utilized for data collection and the analyses, outlined previously in Chapters 1 and 2, are employed to

quantify crack growth at the top interphase. Surface analyses are conducted, as well, and the fracture and surface data are compared with the bottom interphase results.

6.2 Experimental

Static DCB evaluations were conducted on the top interphase in exactly the same manner as the bottom interphase analyses of Chapters 3-5. The specimens were prepared as described in Chapter 2, utilizing adhesives A2 and E2, and curing was carried out at temperatures of 130, 150, and 170 °C. Mechanical testing and analysis were conducted in an identical fashion to the evaluations of Chapters 3-5, but the precracks were carefully initiated at the top interphase rather than at the bottom. A small saw, wedge, and razor blades were used to position the precracks appropriately.

6.3 Results and Discussion

6.3.1 Adhesive Evaluations (Static)

The results of the static DCB tests demonstrate that there are no measurable differences in the interfacial fracture properties of the two opposing interphases. In the evaluations of either the toughened or untoughened formulations, at fixed isothermal cure temperatures, the SERR values were found to be statistically equivalent. In addition, the effects of temperature, as discussed in Chapter 5 for the bottom interphase region, were not present in the fracture properties of the top interphase. That is, for increasing isothermal cure temperature variations, the SERR values for the bottom interphase increase (in general), whereas the SERR values for the top interphase remain unchanged. These results are depicted graphically in Figures 6.1 and 6.2.

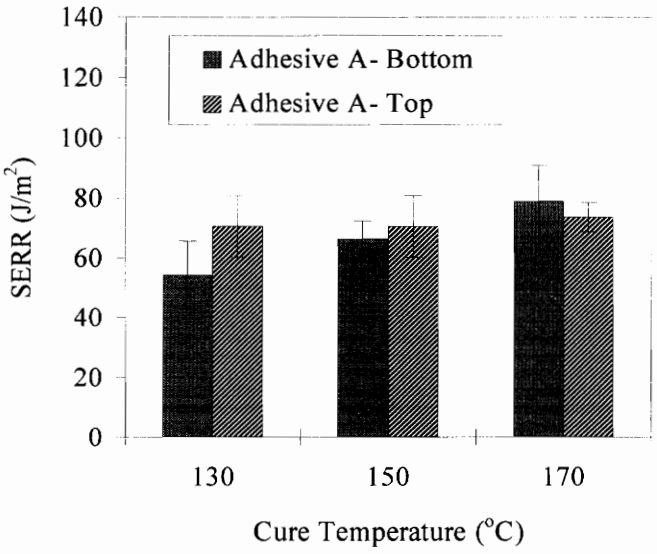

Figure 6.1 SERR values for the top and bottom interphases as a function of the isothermal cure temperature (adhesive A2).

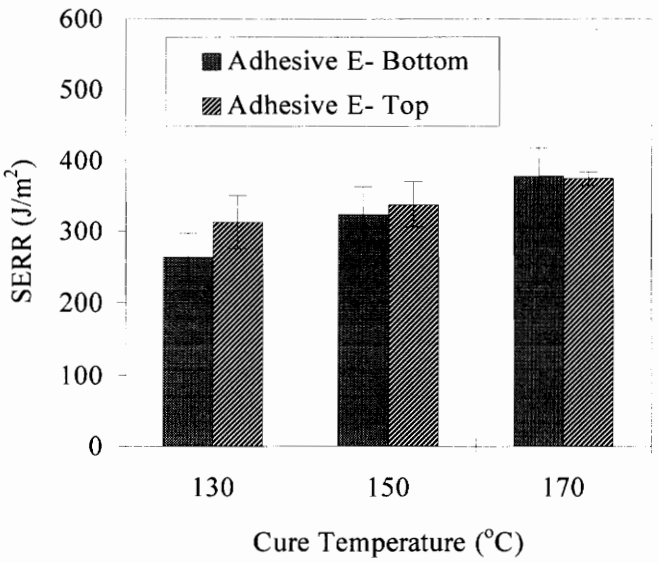

Figure 6.2 SERR values for the top and bottom interphases as a function of the isothermal cure temperature (adhesive E2).

6.3.2 TEM Studies

As stated previously, there are many microstructural features in 2-phase materials which can be correlated with fracture performance. For the screening purposes of this work, the elastomer particle size, particle size distribution, and system morphology were of particular interest. Transmission electron micrographs were utilized to characterize these adhesive features at both the top and bottom interphases, and one representative set of data is given here as an example. E2 is the adhesive system and 170 °C is the cure temperature utilized in this example.

The interphase morphology of the material was found to be independent of the orientation, or location, during the cure process (i.e., whether it was at the top epoxy/steel region or at the bottom epoxy/steel region). As is clearly shown in Figure 6.3, the large, nearly co-continuous rubber domains were found to be present in each of the samples analyzed.

6.3.3 XPS Failure Surface Evaluations

X-ray photoelectron spectroscopy (XPS) studies were conducted to quantify the failure surfaces of the static DCB specimens. Since the bonded specimens *appeared* to fail in an interfacial manner, the two sides of the DCB specimens are denoted in the tables as the "metal" and "adhesive" sides corresponding to their appearances. A sample of the cold rolled steel was also cut from a pretreated plate, prior to bonding, and analyzed to provide background information. This is represented in the tables as "steel".

The results of the XPS evaluations, for adhesives A2 and E2 cured at 130, 150, and 170 °C, are summarized in Tables 6.1-6.4.

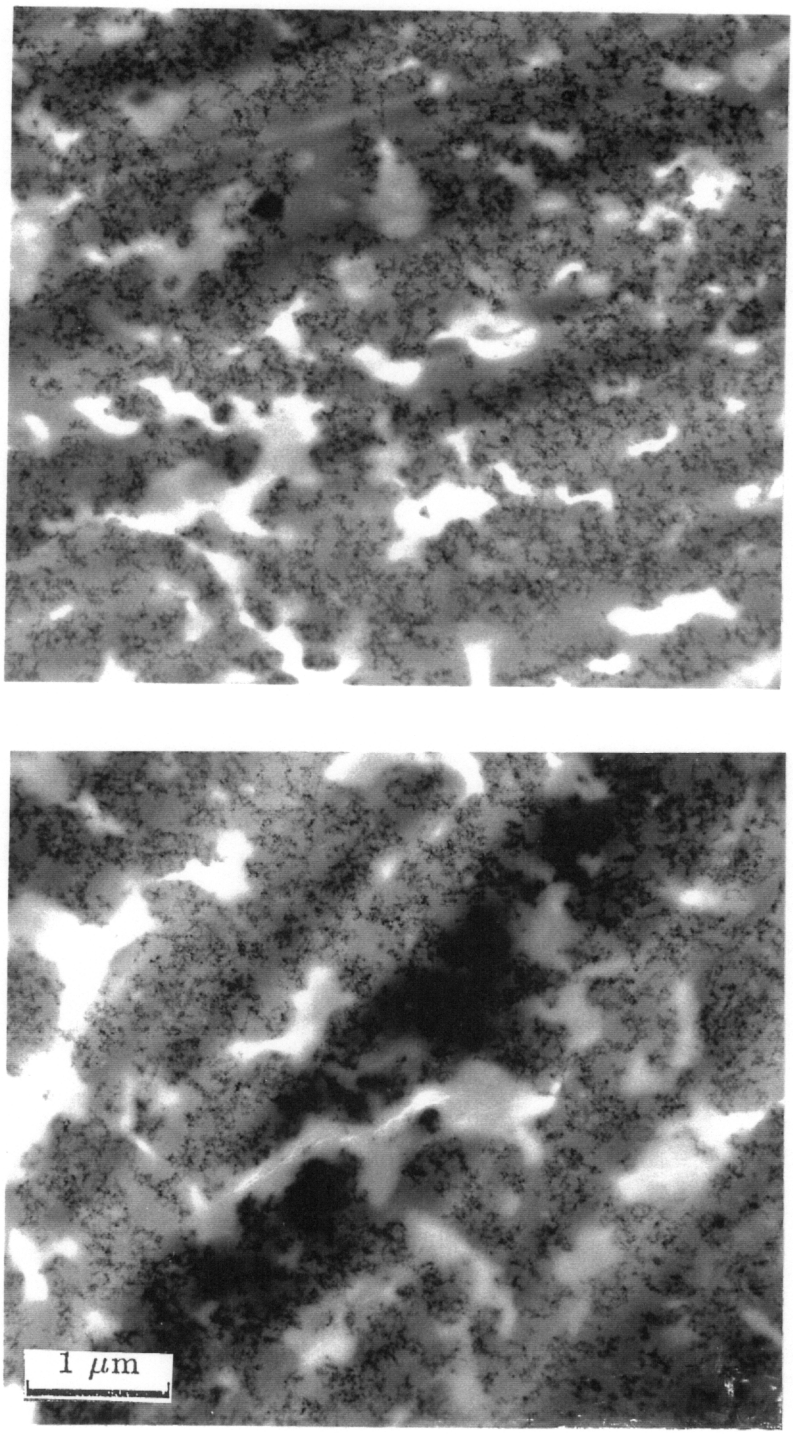

Figure 6.3 TEM images of the opposing interphases. From the top of the page, specimens from the top and bottom interphases, respectively.

Table 6.1 Surface compositions (at.%) for the static DCB failures (adhesive side, top interphase) as a function of the cure temperature.

Formulation (Cure Temp)	A2 (130 °C)	A2 (150 °C)	A2 (170 °C)
Carbon	82.5	86.6	87.6
Oxygen	15.8	11.8	10.6
Nitrogen	0.8	1.3	<0.2
Iron	<0.2	<0.2	<0.2
Silicon	0.9	0.3	1.9

Table 6.2 Surface compositions (at.%) for the static DCB failures (metal side, top interphase) as a function of the cure temperature.

Formulation (Cure Temp)	A2 (130 °C)	A2 (150 °C)	A2 (170 °C)	Steel
Carbon	54.9	58.4	78.7	51.7
Oxygen	34.9	32.9	17.1	37.5
Nitrogen	1.2	1.3	0.5	<0.2
Iron	8.2	7.4	2.3	10.3
Silicon	0.8	<0.2	1.4	<0.2

Table 6.3 Surface compositions (at.%) for the static DCB failures (adhesive side, top interphase) as a function of the cure temperature.

Formulation (Cure Temp)	E2 (130 °C)	E2 (150 °C)	E2 (170 °C)
Carbon	80.2	80.1	79.5
Oxygen	17.2	16.8	17.9
Nitrogen	2.5	2.8	2.0
Iron	<0.2	<0.2	<0.2
Silicon	<0.2	0.3	0.5

Table 6.4 Surface compositions (at.%) for the static DCB failures (metal side, top interphase) as a function of the cure temperature.

Formulation (Cure Temp)	E2 (130 °C)	E2 (150 °C)	E2 (170 °C)	Steel
Carbon	44.0	45.8	45.0	51.7
Oxygen	42.3	41.7	42.5	37.5
Nitrogen	1.3	1.6	1.2	<0.2
Iron	12.3	11.0	11.5	10.3
Silicon	<0.2	<0.2	0.7	<0.2

The results of the static DCB failure surface analyses indicated that the top interphase fractures occurred in a fashion similar to the fractures of the bottom interphase. Thus, many of the key findings are identical or similar to those already discussed in Chapters 3-5. For the sake of completeness, however, and to reinforce the most important results, these will be briefly discussed. Additionally, for the properties which are unique to the top interphase, a more detailed discussion is given.

The surface analysis results generally support the visual observation that the failures occurred in the region of the epoxy/steel interphase. This conclusion is based on a comparison of the DCB top interphase metal side surface iron values to the nonbonded steel surface iron values. Overall, the former ranged from 2.3 to 12.3 at.% and the latter was 10.3 at.%. In addition, the adhesive side iron values were all determined to be < 0.02 at.%. Thus, the failures were interfacial in nature and close to the metal surface in most cases.

For the systems based on adhesive E2, it was observed that the location of the failure within the top interphase region was not dependent on the isothermal cure temperature. That is, within a given set of tests, failures consistently occurred at the same location regardless of the isothermal cure temperature utilized. For the systems based on adhesive A2, however, a dependence was observed. As the cure temperature was increased, the locale of crack growth moved more into the interphase region and away from the steel. This was an isolated observation and it appears to have been due to the brittle nature of the fractures occurring in the untoughened systems. Although the interfacial SERR values for both the top and bottom interphases were statistically equivalent, with the untoughened adhesive it was visually obvious that the cracks frequently tended to bridge and shift toward the bottom interphase. In addition, it was often difficult to get slow, controlled crack propagation in these materials.

Evaluations of the bottom interphase (Chapters 3-5) determined that increases in the isothermal cure temperature resulted in increasing levels of nitrogen on the static DCB metal side failures, and this was most likely caused by sedimentation. In support of this idea, the top interphase analyses showed no measurable differences in the nitrogen

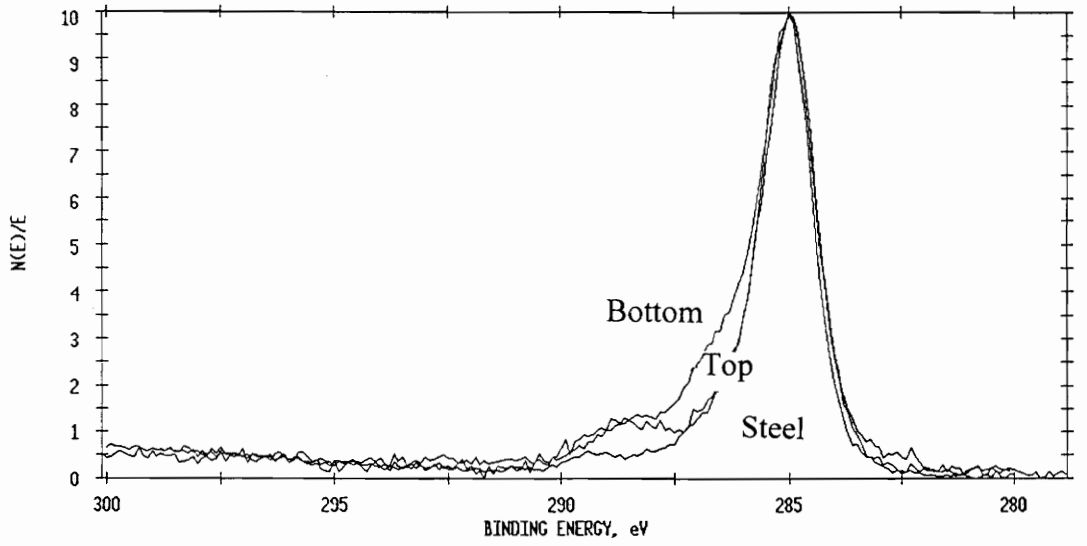

Figure 6.4 Montage of C 1s photopeaks from the static DCB (metal side) failure surface analyses as a function of location (adhesive A2).

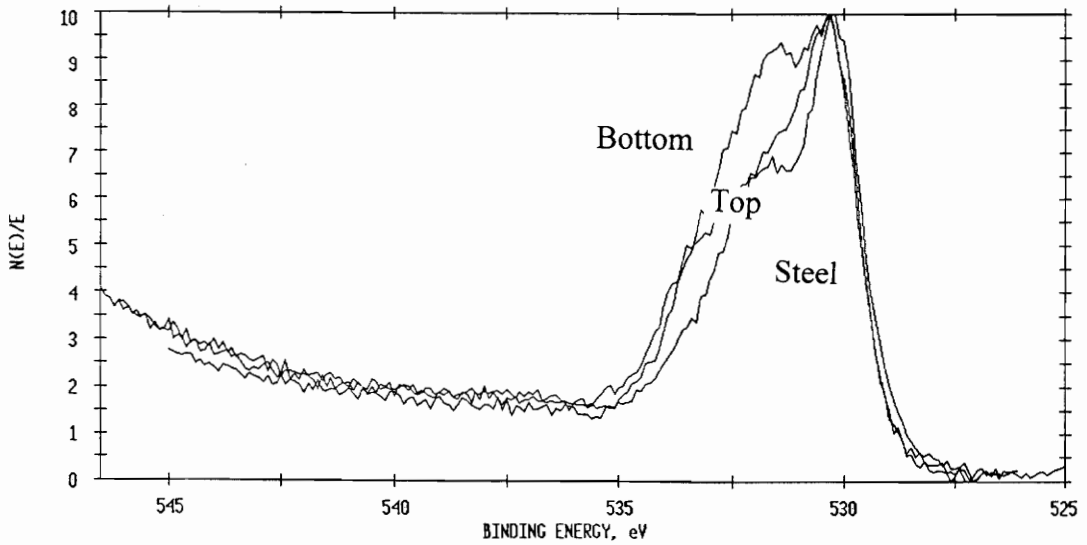

Figure 6.5 Montage of O 1s photopeaks from the static DCB (metal side) failure surface analyses as a function of location (adhesive A2).

content as the cure temperature was increased. Thus, it is apparent that the composition of the top interphase is independent of both dicyandiamide concentration and isothermal cure temperature.

To gain more detailed information on the chemical functionalities present on the top interphase failure surfaces, the C 1s and O 1s photopeaks were evaluated. These photopeaks, for adhesive A2 cured at temperatures of 130 and 170 °C, are given in Figures 6.4 and 6.5 along with the bottom interphase and nonbonded steel photopeaks. From these results it is obvious that the chemical composition at the top interphase is significantly different than that of the bottom interphase. For the bottom interphase shoulders appear in the C 1s and O 1s curves at approximately 286.5 and 533.5 eV. For the top interphase, however, only minimal changes are observed, and the photopeaks more closely resemble those for the nonbonded steel. It has been discussed extensively that these shoulders correspond to chemical functionalities present in dicyandiamide and dicy/epoxy reaction products. It is therefore sufficient to simply state that these results indicate an increased dicyandiamide concentration at the bottom interphase, and a decreased dicyandiamide concentration at the top interphase.

Chapter 7
Overall Summary and Conclusions

The focus of this dissertation research was directed toward the chemical and mechanical evaluation of fracture behavior in latent cure epoxy structural adhesives. Specifically, the studies focused upon the interfacial fracture of dicyandiamide cured epoxy/steel adhesive assemblies. Through a combination of concepts from chemistry, fracture mechanics, spectroscopy, and microscopy, these studies provided a unique contribution to the science and technology of adhesion.

The first step in the progression of this work involved the development of a testing and data analysis methodology. The basic requirement imposed was that this method be capable of reliably detecting and quantifying changes in the performance properties of adhesively bonded structures. Fracture mechanics was chosen as the basis, since the concepts have been applied successfully in the assessment of adhesive toughness, determination of bond failure mechanisms, and estimation of the service life of flawed structures. In addition, fracture mechanics based tests have been proven to be highly sensitive to performance variations, and thus are ideally suited for this type of analysis. A collaborative effort was therefore undertaken by the Departments of Chemistry and Engineering Science and Mechanics (ESM), and it was determined that the DCB fracture specimen matched the necessary requirements. However, the available methods of data analysis for the DCB were not adequate, and this resulted in the research and subsequent development of the *compliance-beam theory* method. This method is a detailed mathematical model of the specimen behavior and provides accurate predictions of the applied SERR. It is equally applicable in the analysis of either fatigue or static test results.

As mentioned previously, dicyandiamide cured epoxies were utilized in the adhesive performance evaluations. They are commonly used in the automotive and aerospace industries for the structural bonding of metals. Accordingly, much effort has been exerted to evaluate the bulk mechanical properties as a function of formulation and

cure condition variations. Almost no published research exists, however, on evaluations of these parameters in bonded systems (e.g., epoxy/steel assemblies). And of the studies that have been conducted, most have looked only at materials that failed in a cohesive manner. Thus, the influence of formulation and cure condition variations on the adhesive/substrate interphase region were neglected. The need for an extensive interfacial assessment of this type was emphasized since the failure of structural adhesives often occurs at the interphase (especially under adverse conditions). In particular, this dissertation evaluated the influence of toughener content, curing agent content, and cure temperature on the interfacial fracture performance of epoxy/steel adhesively bonded assemblies.

The addition of a reactive liquid toughener to the resin was found to drastically change the morphological, bulk mechanical, and adhesive properties. Modulus values decreased and bulk fracture toughness values increased with increasing toughener content. Static DCB, fatigue DCB, and NCA interfacial fracture performances all increased with increasing toughener content. XPS analyses were conducted on the failed bulk and bonded specimens, as well, and it was determined that the resultant chemical changes were more prominent at the epoxy/steel interphase than in the bulk. It was hypothesized that the changes were due to sedimentation of dicyandiamide, and this concept was further investigated.

A series of elastomer modified model epoxy systems were cured with varying amounts of dicyandiamide, and evaluated. The modulus and bulk fracture toughness values were found to be independent of dicyandiamide content, whereas the adhesive performance was shown to be greatly influenced. For increases in dicyandiamide content, SLS failure values increased, while quasi-static DCB and NCA test performances were decreased. Fatigue DCB results showed an initial increase followed by a decrease in the adhesive performance as the dicyandiamide content was increased. XPS surface evaluations were conducted and demonstrated that the dicyandiamide variations produced significant chemical changes only in the epoxy/steel interphase

region, and not in the bulk. Again, this occurred due to the sedimentation of solid curing agent to the interphase.

Analyses were conducted, as discussed in the previous studies, using two additional cure temperatures. The purpose of this work was to alter the dicyandiamide solubility in the resin, and hopefully the reaction mechanisms, and to determine what influence these changes had on the bonded joint performance. In general it was found that as the cure temperature was increased, bonded joint performance increased. This result is reasonable, as it is believed that by increasing the dicyandiamide solubility, more of it is utilized in the dicy/epoxy reactions and less remains to participate in sedimentation to the interphase.

In general it should also be noted that the DCB and NCA results were consistently in excellent agreement. In fact, only in the case of the highly toughened material (E2) was there a statistically significant difference. This was postulated to be the result of plastic deformations within the adhesive layer. The SLS studies, on the other hand, were not in good agreement with the fracture test results. Actually, the SLS results consistently demonstrated opposite trends to the fracture trends. This difference was addressed in Chapter 3, and arises due to gross plastic deformation, this time of the substrates.

Overall, this dissertation research has clearly demonstrated that the combination of fracture mechanics with surface analytical techniques can provide a valid and useful method for quantitatively evaluating the mechanics of interfacial fracture. In these studies, the double cantilever beam and NCA fracture test geometries (SLS for comparison purposes) were utilized in association with XPS and TEM. While the time required to obtain results from the double cantilever beam and single lap shear tests were about the same, substantially more information was available from the fracture mechanics based tests. The NCA test provided an added bonus of requiring less fabrication, testing, and analysis time. Furthermore, *the controlled interfacial failures* which were exhibited by the NCA and DCB tests allowed for a more fundamental understanding of the failure processes to be obtained.

Chapter 8
Future Studies

The research conducted for this dissertation was initiated as more of a mechanics project than a chemistry project. However, due to the tremendously sensitive detection capabilities of the fracture evaluations (in assessing chemical changes in adhesive systems), a multitude of relevant chemical research ideas have arisen along with the standard mechanics ideas. Most of these focus on the region of the adhesive/substrate interphase since it was shown to be of critical importance in the determination of bonded structure strength and performance. However, some fundamental studies in the mechanics area must also be conducted, as they inherently promote understanding of the interrelationships between adhesive chemistry and bonded system performance.

Since understanding interfacial failures was a main focus of this work, some of the future work will continue in this area. Specifically, to help decipher the durability problem (for adhesives, in general), three areas of fracture testing will be utilized. First, data will need to be collected for specimens which have been environmentally conditioned. Second, data will need to be collected from specimens while they are being subjected to various environmental conditions. And lastly, rate dependent failures will be investigated as a potential means for durability prediction.

For the chemical side of this work, it is obvious that there needs to be more quantifiable bulk and suffice data. That is, in the studies where the XPS could not resolve C-O-C from C-N, an additional method should have been employed. It is proposed that the XPS information could be combined with any surface sensitive IR technique to decipher the findings. In addition, more quantitative information is needed on the interrelationships between dicyandiamide solubility, temperature, total concentration, and accelerator (PDMU) concentration. With this information, test formulations could be more carefully designed so as to isolate the system variables (e.g., amount of dicyandiamide that is dissolved).

In general, this combination of new fracture mechanics methodologies and surface evaluations provides a very thorough means by which to assess interfacial fracture performance. Thus, these should be exhaustively evaluated and implemented in future studies of any new polymeric materials. One such area would be the characterization of the interfacial fracture performance of water-borne epoxy films and coatings. Although environmentally friendly, these materials are known to have a limited durability in the presence of moisture. Thus, by working to enhance the interfacial adhesion of these systems, durability improvements could be realized.

Chapter 9

References

1. S. R. Hartshorn, *Structural Adhesives-Chemistry and Technology;* S. R. Hartshorn, Ed.; Plenum Press: New York, 1986, Chapter 1.

2. A. J. Kinloch, *Adhesion and Adhesives-Science and Technology;* Chapman and Hall: London, 1987.

3. D. J. Zalucha, *Engineered Materials Handbook, Volume 3, Adhesives and Sealants;* H. F. Brinson, Technical Chairman; ASM International: 1990; p. 39.

4. *American Adhesive Index*; E. P. McGuire, Ed.; Padric Publishing Co.: New Jersey, 1967.

5. *Annual Book of ASTM Standards, Volume 15.06 Adhesives;* ASTM D907-89.

6. L. H. Sharpe, *Engineered Materials Handbook, Volume 3, Adhesives and Sealants;* H. F. Brinson, Technical Chairman; ASM International: 1990, p. 33.

7. *Handbook of Adhesives, 3rd ed.;* I. Skeist, Ed.; van Nostrand-Reinhold: New York, 1990.

8. J. Shields, *Adhesives Handbook;* Butterworth: London, 1970.

9. C. V. Cagle, *Handbook of Adhesive Bonding;* C. V. Cagle, Ed.; McGraw-Hill: New York, 1983, Chapter 1.

10. R. C. Snogren, *Mech. Eng.* **1970,** May, 33.

11. T. J. Reinhart, Jr., *Adhesives Age* **1973,** 16, 35.

12. J. Schultz, M. Nardin, *Handbook of Adhesive Technology;* A. Pizzi, K. L. Mittal, Ed.; Marcel Dekker, Inc.: New York, 1994, Chapter 2.

13. A. J. Kinloch, *Durability of Structural Adhesives;* Applied Sci. Pub.: London, 1983.

14. K. W. Allen, *J. Adhesion* **1987,** 29, 265.

15. L. H. Sharpe, *J. Adhesion* **1989,** 29, 1.

16. *Adhesive Bonding;* L. H. Lee, Ed.; Plenum Press: New York, 1991.

17. J. W. McBain, D. G. Hopkins, *J. Phys. Chem* **1925,** 29, 88.

18. E. M. Borroff, W. C. Wake, *Trans. Inst. Rubber Ind.* **1949,** 25, 190.

19. W. C. Wake, Adhesion and the Formulation of Adhesives; Applied Science Publishers: London, 1982, Chapter 5.

20. B. V. Deryaguin, N. A. Krotova, *Dokl. Akad. Nauk SSSR* **1948,** 61, 843.

21. C. L. Weidner, *Adhesives Age* **1963,** 6, 30.

22. J. J. Bikerman, *The Science of Adhesive Joints;* Academic Press: New York, 1961.

23. W. D. Bascom, C. O. Timmons, R. L. Jones, *J. Mater. Sci* **1975,** 19, 1037.

24. R. J. Good, *J. Adhesion* **1972,** 4, 133.

25. L. H. Sharpe, *Proc. 162nd ACS Meeting* **1971,** 31, 201.

26. J. Schultz, A. Carre, C. Mazeau, *Intern. J. Adhesion Adhesives* **1984,** 4, 163.

27. J. Schultz, L. Lavielle, A. Carre, P. Comien, *J. Mater. Sci* **1989,** 24, 4363.

28. M. Nardin, E. M. Asloun, f. Muller, J. Schultz, *Polymer Adv. Technol.* **1991,** 1, 161.

29. M. Nardin, A. El Maliki, J. Schultz, *J. Adhesion* **1993,** 40, 93.

30. J. Schultz, a. Carre, *J. Appl. Polymer Sci. Appl. Polyer Symp.* **1984,** 39, 103.

31. L. H. Sharpe, H. Schonhhorn, *Chem. Eng. News* **1963,** 15, 67.

32. H. W. Fox, W. A. Zisman, *J. Colloid Sci.* **1950,** 5, 514; **1952,** 109, 428.

33. A. Dupre, *Theorie Mecanique de la Chaleur;* Gauthier-Villars: Paris, 1869, p. 369.

34. F. M. Fowkes, *J. Phys. Chem.* **1963,** 67, 2538.

35. J. Schultz, K. Tsutsumi, J. B. Donnet, *J. Colloid Interface Sci.* **1977,** 59, 277.

36. F. M. Fowkes, *Ind. Eng. Chem* **1964,** 56, 40.

37. D. K. Owens, R. C. Wendt, *J. Appl. Polymer Sci* **1969,** 13, 1740.

38. F. M. Fowkes, S. Maruchi, *Org. Coatings Plastics Chem.* **1977,** 37, 605.

39. F. M. Fowkes, M. A. Mostafa, *Ind. Eng. Chem. Prod. Res. Dev.* **1978,** 17, 3.

40. R. S. Drago, G. C. Vogel, T. E. Needham, *J. Am. Chem. Soc.* **1971,** 93, 6014.

41. F. M. Fowkes, *J. Adhesion Sci. Technol.* **1987,** 1, 7.

42. V. Gutmann, *The Donor-Acceptor Approach to Molecular Interactions;* Plenum Press: New York, 1978.

43. C. Saint-Flour, E. Papirer, *Ind. Eng. Chem. Prod. Res. Dev.* **1982,** 21, 337.

44. M. Levine, G. Ilkka, P. Weiss, *J. Polymer Sci* **1964,** B2, 215.

45. E. H. Andrews, A. J. Kinloch, *Proc. Roy. Soc.* **1973,** A332, 385.

46. S. S. Voyutskii, *Autohesion and Adhesion of High Polymers;* Wiley Interscience: New York, 1963.

47. R. M. Vasenin, *Adheison, Fundamentals and Practice;* McLaren and Son: London, 1969, p. 29.

48. J. N. Anand, H. J. Karam, *J. Adhesion* **1969,** 1, 16.

49. S. Buchan, W. D. Rae, *Trans. Inst. Rubber Ind.* **1946,** 20, 205.

50. E. P. Plueddeman, *Silane Coupling Agents;* Plenum Press: New York, 1982.

51. A. N. Gent, A. Ahagon, *J. Polymer Sci. Polymer Phys. Ed.* **1975,** 13, 1285.

52. T. M. Goulding, *Handbook of Adhesive Technology;* A. Pizzi, K. L. Mittal, Ed.; Marcel Dekker, Inc.: New York, 1994, Chapter 33.

53. C. D. Wright, J. M. Muggee, *Structural Adhesives-Chemistry and Technology;* S. R. Hartshorn, Ed.; Plenum Press: New York, 1986, Chapter 3.

54. G. L. Hagnauer, D. A. Dunn, *J. Appl. Pol. Sci.* **1981,** 26, 1837.

55. T. Guthner, B. Hammer, *J. Appl. Pol. Sci.* **1993,** 50, 1453.

56. S. A. Zahir, *Adv. Org. Coat. Sci. Technol. Ser.* **1982,** 4, 83.

57. M. Fedtke, A. Rudolf, G. Thiele, W. Tanzer, *Z. Chem.* **1985,** 25, 177.

58. M. Fedtke, F. Domaratius, A. Pfitzmann, *Polym. Bull.* **1990,** 23, 381.

59. E. Sacher, *Polymer* **1973,** 14, 91.

60. Y. G. Lin, J. Galy, H. Sautereau, J. P. Pascault, *Cross-linked Epoxies;* W. deGruyter: Berlin, 1987, p. 148.

61. M. D. Gilbert, N. S. Schneider, W. J. MacKnight, *Macromolecules* **1991,** 24, 360.

62. B. C. Ennis, R. G. Davidson, P. J. Pearce, C. E. M. Morris, *J. Adhesion.* **1992,** 37, 131.

63. H. Lee, K. Neville, *Handbook of Epoxy Resins;* McGraw-Hill: New York, 1966.

64. P. Eyerer, *J. Appl. Polym. Sci.* **1971,** 15, 3067.

65. T. F. Saunders, M. F. Levy, J. F. Serino, *J. Polym. Sci. Part A-1* **1967,** 5, 1609.

66. P. Son, C. D. Weber, *J. Appl. Polym. Sci.* **1973,** 17, 1305.

67. R. B. Prime, *Thermal Characteization of Polymeric Materials;* R. Turi, Ed.; 1981, Chapter 5.

68. R. D. Adams, *Engineered Materials Handbook, Volume 3, Adhesives and Sealants;* H. F. Brinson, Technical Chairman; ASM International: 1990, p. 325.

69. Y. G. Lin, H. Saunterau, J. P. Pascault, *J. Appl. Polym. Sci.* **1987,** 33, 685.

70. M. A. Markevitch, V. I. Irzhak, *Brit. Polym. J.* **1986**, 18.

71. M. D. Rakestraw, M. A Vrana, T. Chang, D. A. Dillard, T. C. Ward, J. G. Dillard, *Evaluation of Adhesive Performance Using Static, Fatigue, and Environmental Fracture Testing (CASS/MESc/94-2);* Center for Adhesive and Sealant Science: Blacksburg, VA, 1994.

72. G. Zeppenfeld, L. Matejka, P. Specek, K. Dusek, *Die Angew. Makromol. Chem.* **1989,** 172, 185.

73. N. Amoudini, H. Sauterau, J. F. Gerard, J. P. Pascault, *Polymer* **1990,** 31, 1245.

74. B. R. LaLiberte, R. E. Sacher, J. Bornstein, AMMRC TR 81-30 AD A105870, 1981.

75. G. B. Portelli, *Structural Adhesives-Chemistry and Technology;* S. R. Hartshorn, Ed.; Plenum Press: New York, 1986, Chapter 9.

76. *Annual Book of ASTM Standards, Part 22;* American Society for Testing and Materials: Philadelphia, PA, 1982.

77. C. V. Cagle, *Adhesive Bonding;* McGraw-Hill: New York, 1968.

78. R. Chait, E. T. Clegg, *Adhesives in Manufacturing;* G. L. Schneberger, Ed.; Marcel Dekker: New York, 1983, p. 649.

79. *Specifications for Adhesives;* Cordura: San Diego, 1979.

80. H. Koski, G. L. Schneberger, *Adhesives in Manufacturing;* G. L. Schneberger, Ed.; Marcel Dekker: New York, 1983, p. 551.

81. K. L. DeVries, P. R. Borgmeier, *Handbook of Adhesive Technology;* A. Pizzi, K. L. Mittal, Ed.; Marcel Dekker, Inc.: New York, 1994, Chapter 5.

82. A. Kinloch, R. Young, *Fracture Behavior of Polymers;* Elsevier Applied Science: London, 1983.

83. R. Kambour, *Encyclopedia of Polymer Science and Engineering, Vol. 4;* 1987.

84. L. Sperling, *Introduction to Physical Polymer Science;* John Wiley & Sons: New York, 1986.

85. C. Hsial, J. Sauer, *J. Appl. Phys.* **1950,** 21, 1071.

86. E. Kramer, *Crazing in Polymers, Advances in Polymer Science, Vol. 52/53;* H. Kausch, Ed.; Springer Verlag: 1983.

87. H. Kausch, J. Williams, *Encyclopedia of Polymer Science and Engineering Vol. 7., 2nd ed.;* 1987.

88. A. A. Griffith, *Phil. Trans. Roy. Soc.* **1920,** A221, 163.

89. E. Orowan, *Rept. Prog. Phys.* **1948,** 12, 185.

90. R. S. Rivlin, A. G. Thomas, *J. Polymer Sci.* **1953,** 10, 291.

91. J. P. Berry, *J. Polymer Sci.* **1961,** 50, 107.

92. H. M. Westergaard, *J. Appl. Mech.* **1939,** A-June, 46.

93. G. R. Irwin, *Appl. Mater. Res.* **1973,** 3, 65.

94. Kenneth M. Liechti, *Engineered Materials Handbook, Volume 3, Adhesives and Sealants;* H. F. Brinson, Technical Chairman; ASM International: 1990, p. 335.

95. J. R. Rice, G. C. Sih, *J. Appl. Mech.* **1964,** 31, 477.

96. M. Comninou, *J. Appl. Mech.* **1977,** 44, 631.

97. J. R. Rice, G. C. Sih, *J. Appl. Mech.* **1965,** 32, 418.

98. R. T. Fenner, A. J. Kinloch, E. Thrusabanjong, J. G. Williams, *unpublished work*; 1986.

99. S. S. Wang, J. F. Mandell, F. J. McGarry, *Int. J. Fract.* **1978,** 14, 39.

100. H. T. Corten, *Fracture, An Advanced Treatise, Vol. 7;* H. Leiebowitz, Ed.; Academic Press: New York, 1972, p. 675.

101. B. M. Malyshev, R. L. Salganik, *Int. J. Fracture Mech.* **1966,** 1, 114.

102. B. Blackman, J. P. Dear, A. J. Kinloch, S. Osiyemi, *J. Mat. Sci. Lett.* **1991,** 10, 253.

103. S. Hashemi, A. J. Kinloch, J. G. Williams, *Proc. R. Soc. Lond.,* A **1990,** 427, 173.

104. S. Mostovoy, E. J. Ripling, *Fracturing Characteristics of Adhesive Joints;* Materials Research Laboratory, Inc.: 1972.

105. J. G. Williams, *Comp. Sci. and Tech.* **1989,** 35, 367.

106. J. G. Williams, *J. of Comp. Mat.* **1987,** 21, 330.

107. S. Hashemi, A. J. Kinloch, J. G. Williams, *J. Mat. Sci. Lett.* **1989,** 8, 125.

108. R. Olsson, *Comp. Sci. and Tech.* **1992,** 43, 329.

109. D. R. Lefebvre, D. A. Dillard, H. F. Brinson, *Exp. Mech.* **1988,** 28, 38.

110. M. F. Kanninen, *Int. J. of Fract.* **1973,** 9, 83.

111. M. B. Ouezdou, A. Chudnovsky, *J. Adhesion* **1988,** 25, 169.

112. M. D. Rakestraw, M. A. Vrana, D. A. Dillard, J. G. Dillard, T. C. Ward, *Durability and Damage Tolerance, AD-Vol. 43;* ASME WAM **1994,** 65.

113. P. C. Paris, F. Erdogan, *ASME Trans., J. Basic Eng.* **1963,** 85D (4), 528.

114. A. J. Kinloch, S. O. Osiyemi, *J. Adhesion* **1993,** 43, 79.

115. R. H. Martin, G. B. Murri, *ASTM STP* **1990,** 1059, 251.

116. H. W. Liu, *Theor. and App. Fract. Mech.* **1991,** 16, 91.

117. J. Luckyram, A. E. Vardy, *J. Adhesion* **1988,** 26, 273.

118. R. Joseph, J. P. Bell, A. J. McEvily, J. L. Liang, *J. Adhesion* **1993,** 41, 169.

119. S. Mall, W. S. Johnson, R. A. Everett, Jr., *Adhesive Joints;* K.L. Mittal, Ed.; Plenum Press: New York, 1984; p. 639.

120. S. Mall, K. T. Yun, *J. Adhesion* **1987,** 23, 215.

121. Y. H. Lai, D. A. Dillard, *J. Adhesion* **1994,** in print.

122. Y. H. Lai, D. A. Dillard, *A Study of Blister Test...;* Virginia Polytechnic Institute: Blacksburg, Virgina, 1994.

123. T. Chang, E. A. Sproat, Y. Lai, N. E. Shephard, D. A. Dillard, *J. Adhesion* **1995,** in print.

124. *Annual Book of ASTM Standards, Volume 15.06 Adhesives;* ASTM D638.

125. *Annual Book of ASTM Standards, Volume 15.06 Adhesives;* ASTM D5045.

126. *Annual Book of ASTM Standards, Volume 15.06 Adhesives;* ASTM D1002.

127. C. Lin, K. M. Liechti, *J. Adhesion* **1987,** 21, 1.

128. D. W. Schmueser, *J. Adhesion* **1991,** 36, 1.

129. E. H. Rowe, A. R. Siebert, R. S. Drake, *Modern Plastics* **1970,** 110.

130. F. J. Mc Garry, *Proc. Roy. Soc. Lond.* **1970,** 59, A 319.

131. W. D. Bascom, R. L. Cottington, R. L. Jones, P. Peyser, *J. Appl. Polym. Sci.* **1975,** 19, 2545.

132. G. T. Beckwith, D. J. Crabtree, *13th National SAMPE Technical Conference*, October 13-15, 1981.

133. J. Odorico, J. N. Dewas, Aerospatiale, Laboratoire Central, Report No. 47/378 (1987).

134. E. Sancaktar, H. Jozavi, R. M. Klein, *J. Adhesion* **1983,** 15, 241.

135. Cuntz, Cavedon, Villatte, Aerospatiale, Report DCR/I-03357-90 (1190).

136. T. R. Guess, R. E. Allred, F. P. Gerstle, Jr., *J. Test Eval.* **1984,** 5, 84.

137. E. Sancaktar, S. Padgilwar, *Mech. Des.* **1982,** 104, 643.

138. F. Schmit, J. M. Ranson, R. Pauliard, J. C. Crasson, Arcueil Research Center, 89-R-107 (1989).

139. A. J. Kinloch, Structural Adhesives: *Developments in Resins and Primers;* A. J. Kinloch, Ed.; Elsevier Applied Science: London, 1986, p. 127.

140. J. N. Goodier, *Trans. Amer. Soc. Mech. Eng.* **1933,** 55, 39.

141. A. J. Kinloch, S. J. Shaw, D. A. Tod, *Polymer* **1983,** 24, 1341.

142. J. N. Sultan, F. J. McGarry, *Polym. Eng. Sci.* **1973,** 13, 29.

143. J. E. deVries, J. W. Holubka, R. A. Dickie, *J. Adhesion Sci. Technol.* **1989,** 3, 189.

144. J. E. deVries, L. P. Haack, J. W. Holubka, R. A. Dickie, *J. Adhesion Sci. Technol.* **1989,** 3, 203.

145. A. J. Kinloch, S. J. Shaw, *Polymer* **1983,** 24, 1355.

146. V. B. Gupta, L. T. Drzal, C. Y. Lee, *Polym. Engineering Sci.* **1985,** 25, 812.

147. A. F. Yee, R. A. Pearson, *J. Mater. Sci.* **1986,** 21, 2462.

148. R. A. Pearson, A. F. Yee, *J. Mater. Sci.* **1986,** 21, 2475.

149. G. Cancelli, A. Pavan, T. Ricco, *Looking Ahead for Materials and Processes;* Elsevier Science Pub.: Amsterdam, 1987.

150. D. Verchere, H. Sautereau, J. P. Pascault, S. M. Moschiar, C. C. Ricciardi, R. J. J. Williams, *J. Appl. Polym. Sci.* **1990,** 41, 467.

151. D. Verchere, H. Sautereau, J. P. Pascault, S. M. Moschiar, C. C. Ricciardi, R. J. J. Williams, *J. Appl. Polym. Sci.* **1991,** 43, 293.

152. M. A. Vrana, M. D. Rakestraw, D. A. Dillard, J. G. Dillard, T. C. Ward, *J. Adhesion* **1995,** in print.

Chapter 10
Vitae

Mark A. Vrana was born on February 26, 1968, in Spangler, Pennsylvania, to Nancy L. and Kenneth P. Vrana. For the next eighteen years he resided with his parents and sister, Valerie, in the small, rural town of Westover, PA. Mark graduated senior class Valedictorian from Harmony High School in May 1986.

In August 1986, Mark began his undergraduate studies in Chemistry at The Indiana University of Pennsylvania (IUP), in Indiana, PA. As part of his program of study, Mark participated in an industrial internship after his junior year. He worked as a QC/QA chemist with The Witco Chemical Corp., Petrolia, PA, in their specialty petoleum products group. During his senior year, Mark participated in two independent research projects. Under the direction of Professor Robert Patsiga, Mark studied the synthesis of novel, polystyrene containing polymers. Under the direction of Professor Augusta Syty, Mark studied methodology development in the area of trace metal (Cr VI) extraction and quantification. He presented the latter work at the Intercollegiate Student Chemists Convention in 1990 and was awarded second place in the analytical division. During his four years of study at IUP, Mark was awarded several academic honors from the Department of Chemistry. He graduated with a Bachelor of Science degree in Chemistry in May 1990.

In May, 1990, Mark moved to Blacksburg, Virginia. There he began conducting polymer related research, under the direction of Professor Thomas C. Ward, at Virginia Polytechnic Institute and State University. In August of that year, he began his formal graduate studies in the Materials Engineering Science program, with a program of study emphasis on polymeric materials and adhesion. In May of 1991, Mark accepted an offer to participate in a VPI/Dow Chemical Co. joint research effort. He spent 16 weeks in the Central Research-Advanced Polymeric Systems Lab at the Dow facility in Midland, Michigan. This was the beginning of the work which lead to this dissertation. During the next four years of study, Mark was actively involved with The Center for Adhesive

and Sealant Science at VPI & SU. In each of these years he was awarded a CASS Fellowship, based on an original research proposal, to continue with his dissertation work. In July of 1995, Mark successfully defended his research and received a Ph.D. in Materials Engineering Science.

In August of 1995 Mark will be moving to Columbus, Ohio, where he will begin employment with Franklin International, Inc., a manufacturer of specialty adhesives. He will be working as a Product/Technology Development Chemist. Lisa Vogler will be accompanying Mark on the move to Ohio, and will be seeking employment in a research related field as well. The couple is planning their engagement and marriage in the near future.